U.PORTO

Doutoramento

Biologia Molecular e Celular

Uncover the duality of neuronal and glial dysfunctions in the neuropathogenesis of plasmalogen deficiency

Ana Rita Alves Malheiro

D

2019

Ana Malheiro

Uncover the duality of neuronal and glial dysfunctions in the neuropathologies of plasmalogen deficiency

D.ICBAS 2019

Uncover the duality of neuronal and glial dysfunctions in the neuropathologies of plasmalogen deficiency

Ana Rita Alves Malheiro

SEDE ADMINISTRATIVA INSTITUTO DE CIÊNCIAS BIOMÉDICAS ABEL SALAZAR
FACULDADE DE CIÊNCIAS

Ana Rita Alves Malheiro

UNCOVER THE DUALITY OF NEURONAL AND GLIAL DYSFUNCTIONS IN THE NEUROPATHOGENESIS OF PLASMALOGEN DEFICIENCY

Tese de Candidatura ao grau de Doutor em Biologia Molecular e Celular submetida ao Instituto de Ciências Biomédicas Abel Salazar da Universidade do Porto.

Orientador – Doutor Pedro Miguel Brites

Categoria – Investigador Principal

Afiliação – Instituto de Biologia Molecular e Celular, Instituto de Investigação e Inovação em Saúde - Porto

Este trabalho foi financiado pela Fundação para a Ciência e Tecnologia (FCT), Portugal, através de uma bolsa de doutoramento (FRH/BD/93110/2013).

The work presented in this thesis was funded by Fundação para a Ciência e Tecnologia (FCT), Portugal, through a doctoral fellowship (FRH/BD/93110/2013).

Foi utilizado nesta tese o artigo publicado:

Malheiro AR, Correia B, Ferreira da Silva T, Bessa-Neto D, Van Veldhoven PP, Brites P. (2019) "Leukodystrophy caused by plasmalogen deficiency rescued by glyceryl 1-myristyl ether treatment" Brain Pathol, Jan 22. doi: 10.1111/bpa.12710

This thesis was written based on the published manuscript:

Malheiro AR, Correia B, Ferreira da Silva T, Bessa-Neto D, Van Veldhoven PP, Brites P. (2019) "Leukodystrophy caused by plasmalogen deficiency rescued by glyceryl 1-myristyl ether treatment" Brain Pathol, Jan 22. doi: 10.1111/bpa.12710

À minha família e amigos que de forma positiva contribuíram para o meu crescimento pessoal e profissional.

Table of contents

Acknowledgements / Agradecimentos

Tendo chegado o culminar desta etapa resta agradecer a todas as pessoas que tornaram esta tarefa possível.

Ao meu orientador Pedro Brites, gostaria de agradecer antes de mais, a oportunidade que me deu em fazer parte de um grupo de pessoas inspiradoras. Tendo sido recebida inicialmente enquanto aluna de mestrado e mais tarde aluna de doutoramento, estou-lhe grata pelo voto de confiança e pela constante partilha de conhecimento. É um grande investigador e alguém pela qual nutro grande admiração. Obrigada por todo este percurso de constante aprendizagem.

Como a investigação é um trabalho de equipa, gostaria de agradecer a todas as pessoas com as quais trabalhei e travei amizade ao longo destes anos, e que tornaram toda esta aventura mais prazerosa. Por isso, agradeço a todos os elementos, presentes e passados, do grupo Neurolipid Biology, Nerve Regeneration e Neurodegeneration. Dos mais antigos aos mais novos e sem ordem de preferência, agradeço a todos a amizade, o companheirismo, a partilha de conhecimento, os convívios, os abraços, sorrisos e lágrimas. É um grande prazer e orgulho conviver e aprender com vocês. Aos vizinhos do GCB, um obrigado por toda a partilha de conhecimento e reagentes.

À FCT por financiar este trabalho, ao ICBAS e a todas as pessoas envolvidas no PDBMC, nomeadamente ao diretor Professor Doutor Claudio Sunkel e à Catarina Carona, por toda a disponibilidade e ajuda na realização dos PADs.

E porque a vida é muito mais do que trabalho, quero agradecer à minha família: aos meus pais, às irmãs Ana's, ao meu marido e companheiro de todos os momentos, e aos amigos de vida. Foi graças a vocês que cheguei até aqui e, é a vocês que dedico esta conquista. A vocês devo tudo! A vocês irei desejar sempre o melhor! Obrigada!

Summary

Plasmalogens are a special class of phospholipids characterized by a vinyl-ether linkage at the *sn*-1 position of the glycerol backbone. Plasmalogens were found to be highly enriched in the nervous tissue, kidneys, lung, testis, and skeletal muscle making up for more than 50% of the ethanolamine phospholipid content of specialized membranes such as myelin. The importance of plasmalogens to human health is highlighted by the severe clinical presentation of rhizomelic chondrodysplasia puntacta (RCDP), a severe developmental disorder caused by impairment in the biosynthesis of plasmalogens. A better understanding of the physiological consequences of a plasmalogen deficiency on RCDP but also in other neurodegenerative disorders that display abnormal levels of plasmalogens (e.g. Alzheimer's disease and Parkinson's disease), will be extremely relevant.

Using the *Gnpat* knockout (KO) mouse, a mouse model of RCDP characterized by a complete impairment in the biosynthesis of plasmalogens, we determined the consequences of a plasmalogen deficiency during myelination and myelin homeostasis in the central nervous system (CNS). We unraveled that the lack of plasmalogens causes a generalized hypomyelination in several CNS regions including the optic nerve, corpus callosum and spinal cord. The defect in myelin content evolved to a progressive demyelination concomitant with generalized astrocytosis and white matter-selective microgliosis. Oligodendrocyte precursor cells (OPC) and mature oligodendrocytes were abundant in the CNS of *Gnpat* KO mice during the active period of demyelination. Axonal loss was minimal in plasmalogen-deficient mice, although axonal damage was observed in spinal cords from aged *Gnpat* KO mice. Characterization of the plasmalogen-deficient myelin identified myelin basic protein and septin 7 as early markers of dysmyelination, whereas myelin-associated glycoprotein was associated with the active demyelination phase. Using *in vitro* myelination assays, we unraveled that the

intrinsic capacity of oligodendrocytes to ensheath and initiate membrane wrapping requires plasmalogens. The defect in plasmalogens was rescued with glyceryl 1-myristyl ether [1-*O*-tetradecyl glycerol (1-O-TDG)], a novel alternative precursor in the plasmalogen biosynthesis pathway. 1-O-TDG treatment rescued myelination in plasmalogen-deficient oligodendrocytes and in mutant mice.

In summary, our results demonstrate the importance of plasmalogens for oligodendrocyte function and myelin assembly and identified a novel strategy to promote myelination in nervous tissue, which combined, may contribute to a better understanding of the human disease.

Sumário

Os plasmalogénios representam uma classe especial de fosfolípidos caracterizados por uma ligação éter-vinílica na posição *sn*-1 do esqueleto do glicerol. Encontram-se enriquecidos no tecido nervoso, nos rins, pulmões, testículos e no músculo esquelético, e constituem mais de 50% do conteúdo total em fosfolípidos de etanolamina em membranas, nomeadamente na bainha de mielina. A importância dos plasmalogénios na saúde humana é realçada pela apresentação clínica da condrodisplasia puntacta rizomélica (CDPR), uma doença severa do desenvolvimento causada por um defeito na biossíntese dos plasmalogénios. Uma melhor compreensão das consequências fisiológicas da deficiência em plasmalogénios no CDPR, mas também em outras doenças neurodegenerativas que apresentam níveis anormais de plasmalogénios (p. ex., a doença de Alzheimer e a doença de Parkinson), será extremamente relevante.

Utilizando o murganho *Gnpat* knockout (KO), um modelo da doença CDRP caracterizado por uma deficiência total na biossíntese de plasmalogénios, determinamos as consequências de uma deficiência de plasmalogénios durante a mielinização e a manutenção da mielina no sistema nervoso central (SNC). Os nossos resultados demonstraram que a ausência de plasmalogénios causa uma hipomielinização generalizada em várias regiões do SNC, nomeadamente no nervo ótico, corpo caloso e espinal medula. O defeito inicial na mielinização agrava-se para uma desmielinização progressiva, concomitantemente com uma astrocitose generalizada e uma microgliose circunscrita à matéria branca da espinal medula. Surpreendentemente, células precursoras de oligodendrócitos e oligodendrócitos maduros foram detetados em abundância no SNC do murganho *Gnpat* KO durante o período ativo de desmielinização. Embora sinais de dano axonal tenham sido detetados na espinal medula de murganhos *Gnpat* KO, não foi observado uma perda significativa de axónios. Uma caracterização detalhada da mielina deficiente

em plasmalogénios identificou alterações nos níveis da proteína básica de mielina e da septina 7, sugerindo que estas proteínas possam ser marcadores da hipomielinização que precede o início do período ativo de desmielinização. Por sua vez, a glicoproteína associada à mielina foi associada à fase de desmielinização ativa. Utilizando ensaios de mielinização *in vitro*, desvendamos que a capacidade intrínseca dos oligodendrócitos para envolver os axónios e iniciar o processo de formação da bainha de mielina requer plasmalogénios. Também mostramos que o defeito em plasmalogénios pode ser restaurado com 1-*O*-tetradecil glicerol (1-O-TDG), um novo precursor alternativo na via de biossíntese dos plasmalogénios. O tratamento com 1-O-TDG restaurou a mielinização em oligodendrócitos deficientes em plasmalogénios e em murganhos *Gnpat* KO.

Em resumo, este trabalho demonstrou a importância dos plasmalogénios para a função dos oligodendrócitos e formação da bainha de mielina; identificou uma nova estratégia para promover a mielinização no tecido nervoso, e poderá contribuir para uma melhor compreensão da CDPR.

Abbreviations list

AA – arachidonic acid

ACAA1– acetyl-Coenzyme A acyltransferase 1

AD – Alzheimer disease

AG – alkyl glycerols

AGPS – alkylglycerone phosphate synthase

ALD – X-linked adrenoleukodystrophy

AKT – Protein kinase B

BA– batyl alcohol

BBB – blood brain barrier

CA – chimyl alcohol

CNP – cyclic nucleotide phosphodiesterase

CNS – central nervous system

DBP – D-bifunctional protein

DHA – docohexanoic acid

ECM – extracellular matrix

ER – endoplasmic reticulum

FAR1 or FAR2– fatty acyl-CoA reductase 1 and 2

GFAP – glial fibrillary acidic protein

GNPAT – glyceronephosphate O-acyltransferase

GPA – 1-O-alkyl-2-hydroxy-*sn*-glycerophosphate

GSK3β – glycogen synthase kinase-3β

Iba-1– ionized calcium binding adaptor molecule 1

IPL – intraperiod line

KO – knockout

LiCl – Lithium chloride

MDL – major dense line

MBP – myelin basic protein

MOG – myelin oligodendrocyte glycoprotein

OLGs – oligodendrocytes

OPC – oligodendrocyte progenitor cell

PD – Parkinson's disease

PC-plasmalogens – choline plasmalogens

PE-plasmalogens – ethanolamine plasmalogens

Pex – peroxin

PEX – peroxisomal protein transporter

PexRAP – peroxisomal reductase activating PPARγ

PHYH – phytanic acid Co-A hydrolase

PLP – proteolipid protein

PNS – peripheral nervous system

PTS – peroxisomal targeting signal

PTMs – posttranslational modifications

PUFAS– polyunsaturated fatty acids

RCDP – rhizomelic chondrodysplasia puntacta

ROS – reactive oxygen species

1-O-TDG – glyceryl 1-myristyl ether (1-*O*-tetradecyl-*sn*-glycerol)

SIRT2 – Sirtuin 2

SOD1– superoxide dismutase 1

TEM – transmission electron microscopy

VLCFA – very-long-chain fatty-acids

WT – wild type

YFP – yellow fluorescent protein

ZS – Zellweger spectrum

General Introduction

Lipids and the nervous system

Lipids are important components of cell membranes. Being vital for all cells, lipids have a preponderant impact on biology of nervous tissue [1]. From embryonic development to aging, lipids are essential for the various phases of the nervous system development [1]. Consequently, alterations in the nervous system lipidome are associated with a wide spectrum of neurological disorders [1]. Lipids in the nervous system accomplish a great number of key functions, from axonal extension and axonal guidance during embryonic development, passing through to myelination, synaptogenesis and impulse conduction [2-5]. Importantly, lipids are essential parts of the myelin sheath that coats and protects the axons [6]. During the active phase of myelination, an enormous amount of lipids are necessary for proper myelin production [7, 8]. This work was focused in the physiological relevance of a particular class of ether-phospholipids, called plasmalogens, for the central nervous system myelination.

Plasmalogens

Plasmalogens are a special type of membrane phospholipids firstly described by Feulgen *et al* in 1924. However, it was only in 1957 that, through the work of Marinetti *et al*, the structure of plasmalogens was described [9]. Specifically, plasmalogens are the most abundant class of ether glycerophospholipids, characterized by the presence of a vinyl-ether bond at the *sn*-1 position of the glycerol backbone (Fig. 1A) [9]. Compared to diacyl glycerophospholipids that contain two fatty acids linked to glycerol backbone (at the *sn*-1 and -2 positions) (Fig. 1B) via ester bonds, ether glycerophospholipids present one of two types of ether bonds at the *sn*-1 position of the glycerol

backbone: (1) an alkyl bond (present in plasmanyl-phospholipids, namely the platelet activating factor) or (2) an alkenyl-bond (present in plasmenylphospholipids, also known as plasmalogens) [10].

In plasmalogens, the aliphatic moieties at the *sn*-1 position consist in palmitic acid (C16:0), stearic acid (C18:0) or oleic acid (C18:1). The *sn*-2 position is preferentially occupied by polyunsaturated fatty acids (PUFAS), namely arachidonic acid (AA; C20:4, w-6) or docohexanoic acid (DHA; C22:6, w-3), and the head group is ethanolamine (ethanolamine plasmalogens) or choline (choline plasmalogens) (Fig. 1A) [9].

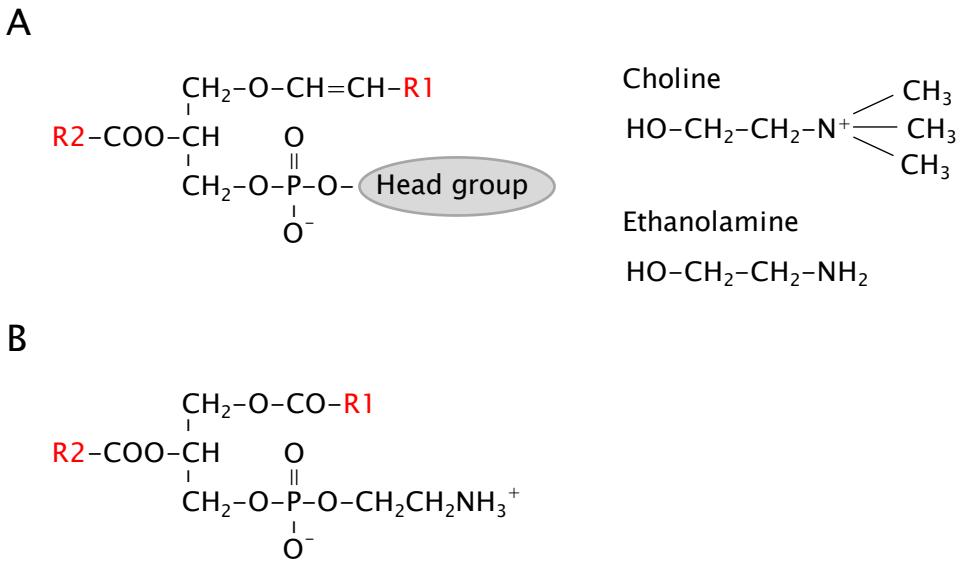

Figure 1. Chemical structure of two phospholipids. **A** Schematic representation of a plasmalogen, highlighting the position R1 where a fatty alcohol is linked to the glycerol backbone via a vinyl-ether bond, and the position R2, in which a polyunsaturated fatty acid is linked via an ester bond. The head group can be either choline (PC-plasmalogens) or ethanolamine (PE-plasmalogens). **B** Ethanolamine diacylphospholipid showing that the two fatty acids - R1 and R2 - are linked to the glycerol backbone via ester bonds.

In humans, plasmalogens make up to 20% of the total phospholipid content, although having variable amounts, depending on cell or tissue analyzed [10]. High levels of ethanolamine plasmalogens (PE-plasmalogens) are present in nervous

tissue, particularly in myelin. Ethanolamine plasmalogens can also be found in other specialized structures such as synaptic vesicles and lipid rafts, being both specialized in cell-to-cell signaling [11]. In its turn, cardiac muscle is rich in choline plasmalogens (PC-plasmalogens). Kidney, skeletal muscle and spleen have moderate amounts of plasmalogens, whilst liver has the lowest level of plasmalogens [12]. In addition to the fact that the amount of plasmalogens varies depending on the tissue, plasmalogen levels also change temporally. Particularly, increasing levels are observed during development, a steady plateau during adulthood, and then a decrease with aging [13].

Peroxisomes and peroxisomal protein import

Peroxisomes are small and single-membrane organelles that provide a subcellular compartment for a wide variety of metabolic processes. Initially described, in 1954 by Rhodin *et al*, as organelles involved in production and protection of reactive oxygen species (ROS), peroxisomes are now considered organelles responsible for many metabolic and biosynthetic processes [14]. Particularly, peroxisomes are able to perform a wide variety of enzymatic processes, namely β-oxidation of very-long-chain fatty acid (VLCFA), ether-phospholipid synthesis, α-oxidation of branched chain fatty acids, docosahexaenoic acid synthesis, glyoxylate detoxification, bile acid synthesis, amino acid metabolism, and ROS/RNS metabolism [15]. However, to accomplish all these processes, a correct localization of the involved enzymes is needed [16].

The biogenesis of peroxisomes involves a high number of proteins, named peroxins (PEX) [15, 17]. These proteins control a variety of different processes including the formation of peroxisomal membranes, import of peroxisomal membrane and matrix proteins, division and inheritance [18]. Moreover, peroxisomes contain a complex, but efficient, machinery of protein import, in

which in mammals, more than 100 peroxisomal matrix proteins are described being involved in different metabolic pathways [12, 19]. The import of peroxisomal matrix proteins can be accomplished through three routes: (A) peroxisome targeting signal (PTS) type 1-mediated import, (B) PTS2-mediated import, and (C) piggyback-mediated import [19, 20].

PTS-mediated import

Peroxisomes are eukaryotic organelles that posttranslationally import matrix proteins via one of two conserved peroxisomal targeting signal (PTS1 or PTS2) mediated pathways. The PTS-mediated import is a four-step cycling process: (1) recognition of the PTS-sequence by an adaptor protein, (2) transport and binding of the cargo/adaptor complex to the docking complex, (3) formation of a transient protein-pore capable of translocation of proteins, (4) and recycling of the adaptor protein to the cytoplasm for a new import cycle [21].

In mammals, the majority of the PTS-mediated import is accomplished through a PTS1-sequence. One of the enzymes containing a PTS-1 signal is the glyceronephosphate O-acyltransferase (GNPAT), involved in the first step of biosynthesis of plasmalogens. The PTS1 is a C-terminal tripeptide with a consensus sequence (S/A/C)-(K/H/R)-(L/M). Proteins containing a PTS1 signal are recognized by the seven tetratricopeptide repeats (TPR) of peroxin 5 (Pex5) adaptor protein in the cytosol [12]. The formed complex is then capable to interact with the docking-complex protein Pex14p. In mammal cells, two functional splicing isoforms of PEX5 have been identified [15]. The longer form, Pex5L, contains an extra exon relatively to the shorter form Pex5S. Both forms are involved in the import of PTS1 proteins but Pex5L is also involved in the import of PTS2 proteins (Fig. 2A).

Far fewer peroxisomal proteins are known to contain a PTS2-sequence: the alkylglycerone phosphate synthase (AGPS), involved in the second step of biosynthesis of plasmalogens; the acetyl-Coenzyme A acyltransferase 1 (ACAA1), involved in the β-oxidation of very-long-chain fatty-acids (VLCFA); and the phytanic acid Co-A hydrolase (PHYH), involved in the α-oxidation of phytanic acid [22, 23]. The PTS2 is a N-terminal nonapeptide sequence -(R/K)(L/V/I/Q)XX(L/V/I/H/Q)(L/S/G/A/K) X(H/Q)(L/A/F)- recognized by the cytosolic receptor Pex7 [23]. However, by itself, Pex7 is not capable of interacting with the docking complex. In mammals, Pex7 interacts specifically with the long isoform of Pex5 (Pex5L), and this interaction allows the Pex7-cargo complex to be targeted to the docking complex and, consequently, for a normal PTS2 import (see Fig. 2B) [24, 25].

Piggyback-mediated import

Besides the import of peroxisomal matrix proteins via peroxisome targeting signals, some proteins lacking a PTS are imported by piggy-backing onto PTS-containing proteins. Due to the capacity of peroxisomes to import fully folded proteins and complexed oligomers, some proteins associate with PTS-containing proteins and are co-imported to the peroxisomal matrix. So far, few proteins are described as using the piggyback-mediated import: the co-import of lactate dehydrogenase (LDH) subunit A and B, in association with the predicted PTS1-bearing LDHx; the superoxide dismutase 1 (SOD1), that is co-import with the PTS1-bearing copper chaperon of SOD1 (CCS); and the nicotinamidase Pnc1, that is co-imported with the PTS2-containing enzyme glycerol-3-phosphate dehydrogenase 1, Gpd [26-28].

Plasmalogen biosynthesis, regulation and transport

Biosynthesis

The biosynthesis of plasmalogens is initiated in peroxisomes and completed in the endoplasmic reticulum (ER), resulting in a perfect metabolic interplay between these two organelles (Fig. 2C) [12].

The initial reaction step is the acylation of dihydroxyacetone phosphate (DHAP) by the enzyme glyceronephosphate O-acyltransferase (GNPAT), a PTS1-containing protein. The second reaction step is carried out by the alkylglycerone phosphate synthase (AGPS; a PTS2-carrying protein), by the exchange of the fatty acid for a fatty alcohol, forming 1-alkyl-DHAP. The topology and proper localization of the peroxisomal enzymes involved in the biosynthesis of plasmalogens, is crucial for their biosynthesis. Specifically, GNPAT and AGPS need to be localized in close association at the inner surface of the peroxisomal membrane. In addition, it was demonstrated that GNPAT and AGPS physically interact, forming a complex, with two AGPS to one GNPAT molecule [29]. The reaction performed by AGPS follows a double placement reaction, in which acyl-DHAP is converted in DHAP, which is then converted in alkyl-DHAP [30]. This bisubstrate reaction follows a “ping-pong”-like mechanism rather than a sequential reaction as it is believed that AGPS undergoes an intermediate form [30]. In addition, the complex GNPAT-AGPS is thought to be essential for the enzymatic activity of GNPAT, given that the mistargeting of AGPS to the cytosol, affects the protein levels of GNPAT and its enzymatic activity [29]. The fatty alcohol necessary for the formation of the ether-bond derives from the reduction of long-chain acyl-CoAs through the action of the enzymes fatty acyl-CoA reductase 1 and 2 (FAR1 or FAR2) localized in the outer surface of the peroxisomal membrane [31]. Finally, the reduction of the ketone group at the *sn*-2 position of the 1-alkyl-DHAP by an

acyl/alkyl-DHAP reductase, located in both peroxisomal and ER membranes, results in the formation of 1-O-alkyl-2-hydroxy-*sn*-glycerophosphate (GPA). The reductase responsible for this enzymatic step, dehydrogenase/reductase (SDR family) member 7B (DHRS7B), was recently characterized and renamed as the peroxisomal reductase activating PPARγ (PexRAP), by Lodhi *et al*. [32]. All subsequent steps to form mature plasmalogens take place in the ER (Fig. 2C). Within these steps that occur in the endoplasmic reticulum one is very specific, which is the conversion of plasmanylethanolamine into plasmenylethanolamine, by the introduction of the vinyl-ether bond (the double bond characteristic of plasmalogens), by the plasmanylethanolamine desaturase (Δ1′-alkyl desaturase). This step is extremely relevant, since if the enzyme is disrupted, no ether lipids with a vinyl double bond (i.e. no plasmalogens) can be formed in the cell [33]. Depending on the head-group endorsed, plasmalogens are classified in two major classes: ethanolamine plasmalogens (PE-plasmalogens) and choline plasmalogens (PC-plasmalogens) [13].

Despite the essential role of the endoplasmic reticulum in the plasmalogen biosynthesis, disorders characterized by deficiencies in plasmalogens are described as being caused only by defects within the peroxisomal steps [12]. Since some of the ER enzymes involved in the plasmalogen biosynthesis are also involved in the biosynthesis of diacyl-glycerophospholipids, mutations in such enzymes are set to severely affect the formation of membranes, which is likely not viable, making its clinical study impossible [34].

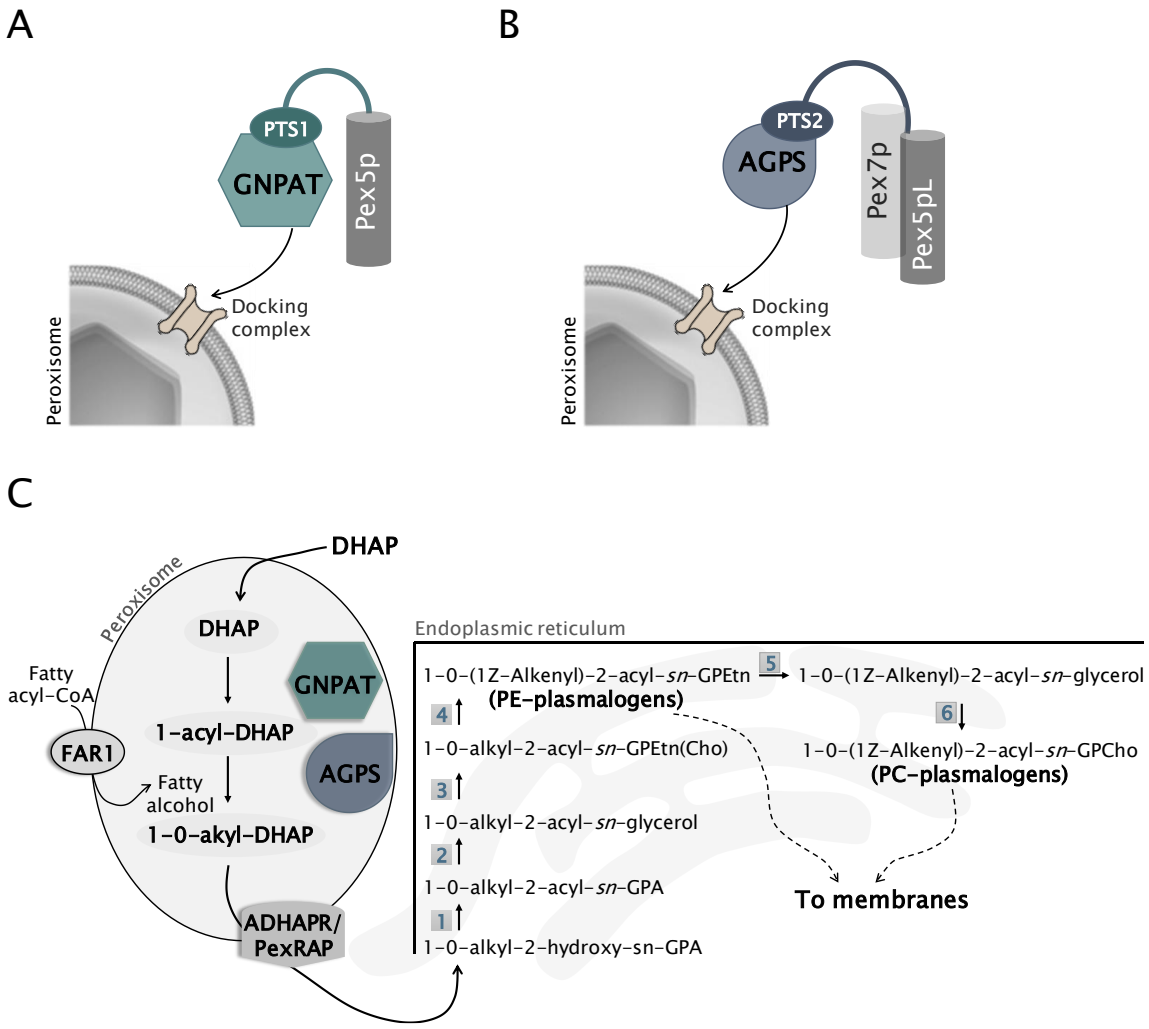

Figure 2. Peroxisomal protein import and the biosynthesis of plasmalogens. A Proteins containing a PTS1-import sequence, such as, glyceronephosphate O-acyltransferase (GNPAT) are recognized and translocated into the peroxisomal matrix via a Pex5-dependent way. **B** PTS2-containing proteins, namely AGPS, are imported through Pex7 recognition. **C** Schematic representation of the steps involved in the biosynthesis of plasmalogens. The two first steps of the biosynthetic pathway take place in peroxisomes through the action of GNPAT and AGPS enzymes. In the third step the alkyl-DHAP is converted into 1-O-alkyl-2- hydroxy-*sn*-glycerophosphate (GPA), and may occur both in peroxisomes and in the endoplasmic reticulum (ER). Finally, all the remaining steps are carried in the ER by the sequential action of: (1) alkyl/acyl-glycerophosphate acyltransferase, (2) phosphatidic acid phosphatase, (3) ethanolamine phosphotransferase, (4) plasmenylethanolamine desaturase, (5) phospholipase C, (6) choline phosphotransferase.

Regulation

The regulation of the biosynthetic pathway of plasmalogens is intrinsically dependent on the generation of the fatty alcohol by FAR1 and FAR2, the fatty alcohol reductases that reduce fatty acyl-CoAs [35]. Localized on the cytosolic face of the peroxisome, it was proposed that FAR enzymes are subject to feedback regulation by cellular plasmalogen levels, which induce FAR protein degradation [31, 36]. Although having a broadly distribution in mice, FAR1 is highly expressed in brain, kidney and testis, whereas liver and small intestine have the lowest expression levels [35]. In contrast, FAR2 is highly expressed in skin, eye lid, brain, and small intestine, whereas liver, kidney, and lung have the lowest expression levels, suggesting a unique role in the biosynthesis of plasmalogens in these tissues [35]. More interestingly, both FAR1 and FAR2 are highly expressed in brain where large amounts of ether lipids are synthesized. As presented in a following section, the importance of FAR proteins in the biosynthesis of plasmalogens is highlighted by the identification of FAR1 mutations in a subset of patients with intellectual disability and epilepsy [37].

Transport

Produced in the endoplasmic reticulum, plasmalogens must undergo transport/movement to organelles and plasma membranes. However, the processes and mechanisms behind the distribution of plasmalogens within the cells are not understood. Currently, the proposed processes involved in the transport of plasmalogens may include the vesicular pathway (involving the Golgi), non-vesicular pathways (using lipid transporter proteins), or the exchange of lipids at ER-plasma membrane contact sites [38, 39]. In addition, the nascent lipids are asymmetrically distributed to the inner or outer plasma membrane leaflet of plasma

membranes. PE-plasmalogens are concentrated and founded predominantly in the inner leaflet, and PC-plasmalogens are enriched on the external leaflet [40, 41].

Biological roles attributed to plasmalogens

Many functions have been proposed for plasmalogens. Due to their physico-chemical properties, namely the specific vinyl-ether bond at the *sn*-1 position, as well as, the distribution in the cell, these ether-phospholipids have been associated with important biological processes. Plasmalogens have been implicated as important scavengers of reactive oxygen species (ROS), structural organizers of membranes, regulators of membrane fluidity, mediators of membrane dynamics and storages of polyunsaturated fatty acid (PUFAs), lipid mediators and regulators of membrane and cell signaling.

Structural attributes

Phospholipids are fundamental biological building blocks maintaining the proper functioning of membranes. From the biophysical point of view, the various lipids constituting cell membranes directly affect their biophysical properties, such as thickness, stiffness, separation of lateral phases and tendency to fusion. Therefore, plasmalogens, due to their significant content in the total amount of membrane lipids, and by virtue of their vinyl ether bond may play a critical role in cell membranes, providing unique structural attributes and facilitating signaling processes [42].

The structure of a phospholipid can roughly be divided into two parts: the hydrophilic head group and the hydrophobic acyl chains [42]. In diacyl glycerophospholipids, the *sn*-1 acyl chain is oriented perpendicular to the membrane surface. Differently, the *sn*-2 acyl chain contains a bend that increases

the molecular cross sectional area [43]. The vinyl-ether linkage at the *sn*-1 position of plasmalogens may decrease that bend, bringing the proximal portions of the *sn*-1 and *sn*-2 chains closer together and nearly parallel, leading to a smaller cross-sectional area [42, 44]. As possible consequences, plasmalogens have been shown to decrease membrane fluidity, increase order and promote at lower temperatures the formation of non-bilayer phases, which are needed for fusion and fission events (e.g. synaptic vesicle fusion with membrane) [45, 46]. In addition, the lack of the carbonyl oxygen at *sn*-1 position alters the hydrophobicity of the head group affecting the way they interact with other membrane components [42].

Lipid raft microdomains are lateral membrane domains, enriched in cholesterol and sphingomyelin. These domains are less fluid and more compacted regions of the plasma membrane, and are therefore considered extremely important to mediate various physiological processes. In addition, these domains contain proteins required for cell signaling, cell-cell interactions, and endocytosis [47]. Some studies showed that PE-plasmalogens are enriched in lipid rafts [11, 38]. The enrichment of plasmalogens in lipid rafts, if universal, might facilitate membrane phase and signal transduction processes. Moreover, plasmalogen-deficient cells revealed an increase in the concentration of ethanolamine phospholipids in lipid rafts, suggesting an attempt by the cells to maintain the important physicochemical properties that govern these micro-domains and that are essential for several physiological functions.

Recently, using mouse models with defects in plasmalogens new evidences were established regarding the role of plasmalogens in cell signaling [48]. In an attempt to discover what were the mechanisms behind the pathology, the study revealed that plasmalogen-deficient mice had an impairment in the AKT signaling pathway [48]. The work showed that in the PNS, a deficiency in plasmalogens

affects the ability of AKT to be activated by phosphorylation at the plasma membrane. This inability causes a reduction in AKT phosphorylation leading to inactive AKT. AKT is a kinase that when active phosphorylates several targets including glycogen synthase kinase-3β (GSK3β). AKT phosphorylates GSK3β at the serine 9 residue, inhibiting the activity of the kinase. In plasmalogen-deficient mice, the impairment in AKT causes a deficient phosphorylation of GSK3β, which is necessary to induce Schwann cell differentiation and maturation to initiate myelination [49, 50].

Antioxidant potential

A large number of experimental evidences, albeit mostly based on *in vitro* studies, suggested that plasmalogens are important scavengers of reactive species, protecting other lipid components from peroxidation [51]. The presence of a vinyl-ether bond makes plasmalogens more susceptible to oxidative attack. In a simplified way, the hydrogen atoms adjacent to the vinyl-ether bond have relatively low dissociation energies and are oxidized when exposed to free radicals and singlet oxygen [51]. As a consequence of this reaction, plasmalogens are consumed, acting as sacrificial oxidants and protecting polyunsaturated fatty acids and other vulnerable membrane lipids from oxidative attack. It was demonstrated that the oxidative products of plasmalogens are unable to further propagate lipid peroxidation, and so plasmalogens may terminate lipid oxidation [52]. However, it remains unclear if the oxidative products, which include very reactive aldehydes [53], could be harmful and affect other cellular components with negative consequences.

Recently, using mouse models with a deficiency in plasmalogens, new evidences were established regarding the importance of plasmalogens in the protection against oxidative attack. If on the one hand, Brodde *et al.* demonstrated

that plasmalogen-deficient fibroblasts are more susceptible for oxidative attack, Luoma *et al.* revealed that the myelin sheath from sciatic nerves of plasmalogen-deficient animals was more prone to oxidative damage [54, 55]. It is therefore interesting the link between decreased plasmalogen levels and common neurodegenerative disorders such as Alzheimer's and Parkinson's [56, 57]. In these disorders, the defect in plasmalogens is seen as secondary to the primary disease-causing pathology [13, 58, 59]. However, it is unclear if increased neuroinflammation and/or oxidative stress triggers or causes a reduction in the levels of plasmalogens or if a decrease in plasmalogens potentiates the damage caused by neuroinflammation and oxidative damage. Nevertheless, it is thus important to understand the consequences of a primary defect in plasmalogens to then address the outcomes in other disorders.

Storage of PUFAS and reservoirs for second messengers

Plasmalogens are enriched in docosahexaenoic acid (DHA) and arachidonic acid (AA), the most frequent PUFAs at the *sn*-2 position of the glycerol backbone. As so, plasmalogens may function as reservoirs for these biologically active lipid mediators, released by phospholipase A2 hydrolysis [60]. These PUFAs are known to carry important physiological functions. DHA has been linked to cell survival, cell differentiation and ERK-signaling pathway; on its turn AA is an important second messenger, and some of their metabolites, namely prostaglandins, prostacyclin, thromboxane, and leukotrienes, mediate several cellular signaling pathways [61, 62]. Another product obtained from the enzymatic cleavage of plasmalogens is lysoplasmalogen. Lysoplasmalogen is an important mediator of membrane fluidity and permeability, facilitating the extracellular entry of calcium thought transmembrane channel [63].

Plasmalogen deficiency in disease

Inherited disorders of plasmalogen synthesis

The only genetically inherited disorders with defects in the biosynthetic pathway of plasmalogens are the peroxisomal disorders rhizomelic chondrodysplasia puntacta (RCDP) and Zellweger spectrum (ZS). Zellweger spectrum is a severe disorder, characterized by a generalized impairment in peroxisomal functions due to defects in peroxisome biogenesis. The clinical presentation of Zellweger patients shares some features with that of RCDP patients, but the disease severity is greater since all peroxisomal functions are impaired [64, 65]. The clinical presentation of Zellweger patients includes hypotonia, cranial and facial dysmorphism, hepato- and splenomegaly, dysmyelination, and defective neuronal migration [65]. Given the multitude of biochemical abnormalities, it becomes difficult to attribute a given symptom or tissue pathology to one of the biochemical defects. However, although plasmalogens deficiency contributes to pathology in Zellweger spectrum, in RCDP the deficiency in plasmalogens is the direct and primary cause of pathology.

Rhizomelic chondrodysplasia puntacta (RCDP)

RCDP is an autosomal recessive disorder, with an overall incidence of 1/100,000. At present, five different forms of the disorder have been identified. The most frequent form of the disorder is caused by mutations in the gene encoding the peroxisomal protein transporter, PEX7 (RCDP type 1) and the remainder are caused by defects in the genes encoding peroxisomal enzymes required for plasmalogen biosynthesis (RCDP type 2 to 5) [13, 66, 67].

As a consequence of mutations in the gene encoding PEX7, RCDP type 1 patients has impaired PTS2-mediated import, affecting the import of 3 proteins:

AGPS (involved in plasmalogen biosynthesis), acetyl-Coenzyme A acyltransferase 1 (ACAA1; involved in β-oxidation of very long chain fatty acids (VLCFA)), and phytanic acid Co-A hydrolase (PHYH; involved in α-oxidation of phytanic acid) [12, 31]. Although the PEX7 transporter is required for peroxisome localization of these 3 proteins, only AGPS deficiency determines RCDP pathology. This is supported because in RCDP type 1 there is no generalized accumulation of VLCFA caused by mistargeting of ACAA1, suggesting the action of other thiolases that allow the normal degradation of VLCFA; the accumulation of phytanic caused by mistargeting of PHYH can be circumvented with a controlled diet containing reduced amounts of phytanic acid [12, 60, 68]. In addition, the indistinguishable pathology amongst RCDP types 1, 2 and 3, and a direct correlation between disease severity and amounts of residual plasmalogens also supports this notion. Classical RCDP patients, with extreme low levels of plasmalogens, present the most severe form of the disorder. Milder patients, representing 10% of RCDP patients, have around 1/3 of normal erythrocyte plasmalogens, which corresponds to an increase of 10 to 40 times over the classical RCDP. Patients with higher or near-normal erythrocyte plasmalogen levels show milder clinical variants that can range from absence of rhizomelia to an adult Refsum disease (ARD)-like presentation (with a primary peripheral neuropathy) or even autistic-like presentations [13, 69-71].

RCDP type 2 is caused by mutations in the *GNPAT* gene, and RCDP type 3 in the *AGPS* gene. Both are single peroxisomal enzyme deficiencies leading to isolated defects of glyceronephosphate O-acyltransferase (GNPAT) and alkylglycerone phosphate synthase (AGPS), respectively, producing an isolated impairment in plasmalogen biosynthesis [72, 73]. The newly described forms of RCDP are caused by mutations in the gene encoding FAR1 - RCDP type 4, and in the exon encoding Pex5 long isoform (PEX5L) - RCDP type 5 [37, 74]. RCDP type 4 patients show decreased levels of plasmalogens, due to the unavailability of fatty alcohols needed

to the initial generation of the ether bond in alkyl-DHAP [37]. Similar to RCDP type 1, RCDP type 5 patients have an impaired PTS2-mediated import [74].

As discussed above, RCDP is a heterogeneous disorder with respect to the genetic cause of the disease, but also in terms of clinical presentation. Patients with classical RCDP have a skeletal dysplasia characterized by rhizomelia, chondrodysplasia punctata (CDP) and abnormal, premature or delayed mineralization of cartilage. Rhizomelia and CDP can be detected as early as 18 weeks of gestation by routine ultrasound [75]. Additionally, RCDP patients exhibit cortical cataracts, hypotonia, congenital heart and renal malformations and profound growth and mental retardation [76, 77]. Central nervous system abnormalities are common and include progressive cerebral atrophy, spinal stenosis and decrease in white matter with gliosis [78, 79]. The combination of all these factors leads to a serious disease state with a high mortality rate, with few patients living for more than 5 years. Specifically, only 50% of RCDP patients are alive at 6 years of age and most succumb by adolescence. Within the most common possible causes of neonatal deaths is the pulmonary hypoplasia [80]; in turn, in older patient's chronic respiratory compromise is often the main cause of death [76]. Taken together, the characteristic defects observed in patients with RCDP revealed that plasmalogens are critical for proper development of various organs or tissues, namely central nervous system, lens and bone. Equally important, the progression and complications of the disease highlight the sustained role of plasmalogens in tissue maintenance throughout life.

Although the genetic and biochemical causes of RCDP are known, there is still a long way to go in understanding how the defect in plasmalogens is associated with cell and tissue pathology, or mechanisms behind the defects. The generation and characterization of several RCDP mouse models is currently contributing to a

better understanding of the role of plasmalogen in affected tissues, as well as the pathogenic mechanisms underlying RCDP.

Secondary plasmalogen deficiency

Reduced plasmalogen levels have also been found in a variety of diseases etiologically unrelated to RCDP [13]. Some examples of secondary plasmalogen deficiency are the X-linked adrenoleukodystrophy (ALD) and D-bifunctional protein (DBP) deficiency [81, 82]. Specifically, active demyelinating areas of the brain from ALD patients revealed low levels of plasmalogens, suggesting that the deficiency in plasmalogens may act synergistically with the accumulation of VLCFA and thereby exacerbate the pathology and accelerate disease progression [81]. In DBP deficiency, a disorder characterized by a defect in peroxisomal β-oxidation with accumulation of VLCFA, lipid analyses in the brain of a DBP patient revealed a decreased amount of plasmalogens in gray matter. In both cases, more investigation is needed to understand if the observed defects are related to an impairment in the biosynthesis of plasmalogens or an increased degradation.

Decreased plasmalogen levels have also been found in non-peroxisomal disorders. The enrichment of plasmalogens in the brain makes the observation of reduced levels of plasmalogens in various neurodegenerative disorders not surprising. Among the diseases with secondary plasmalogen deficiency are found Alzheimer disease (AD), Parkinson's disease (PD), Neimann Pick type C and Down syndrome [83-86]. Although there is a better understanding of the pathogenic mechanisms of these common disorders, it remains to be determined whether plasmalogen loss is a contributing cause or a downstream effect of the pathology. In the case of the X-linked adrenoleukodystrophy (X-ALD), caused by the accumulation of very long chain fatty acids, the dual possibility still stands. The

secondary plasmalogen deficiency could contribute for disease progression, as verified by the finding that a plasmalogen deficiency worsens brain pathology in the X-ALD mouse model [87]. Conversely, decreased levels of PE-plasmalogens have also been linked to increased ROS species [81, 87, 88]. The continued study of the role of plasmalogens in these disorders, will not only contribute to a better understanding of the disease state but also to highlight the role of plasmalogens in neurodegeneration.

The mouse models for human peroxisomal disorders

The complexity of human peroxisomal disorders is emphasized by: i- the multitude of biochemical defects that can affect peroxisome functions, ii- the lack of clear genotype-phenotype correlations or difficulties in assigning correlations, iii- the variety of organs and tissues affected, and iv- the rarity of the diseases combined with extremely reduced access to postmortem materials, makes the study of these disorders a real challenge. The generation of mouse models for human peroxisomal disorders has, to some extent, circumvented some of these problems [89]. For the Zellweger spectrum, the *Pex5*, *Pex2*, *Pex11* and *Pex13* knockout mice are some of the mouse models generated for the study of the disease [90-92]. The phytanoyl-CoA 2-hydroxylase (*PhyH*) knockout mouse was created for the study of Refsum disease, the multifunctional protein 2 (*MFP2*) knockout mouse for the D-bifunctional protein deficiency [93, 94], and X-linked adrenoleukodystrophy is studied in *Abcd1* knockout mice [95, 96].

Additionally, the generation and characterization of mouse models with defects in plasmalogens biosynthesis allows a better understanding of the role and importance of this ether-phospholipid, as well as pathogenic mechanisms underlying RCDP. The *Pex7* knockout mouse was generated for RCDP type 1 and *Gnpat* knockout mouse was generated for RCDP type 2 [68, 97]. The life span of

these mouse models is variable, but both have early lethality. For circumvent the early lethality observed *Pex7* and *Gnpat* knockout, a hypomorphic mouse was also generated. The *Pex7* hypomorphic mouse has *Pex7* transcripts levels reduced by 95% of wild type (WT) levels. The mice present a milder phenotype, mimicking patients with milder disease presentations [98]. Moreover, the blind sterile 2 (bs2) mouse has been characterized. The bs2 mice have reduced expression of *Agps* by 85% of WT levels, representing a model for RCDP type 3 [99].

The *Gnpat* knockout model

The *Gnpat* knockout (KO) mouse is a model for RCDP type 2, in which exons 5 to 7 were deleted through homologous gene recombination, leading to absence of detectable Gnpat activity and the complete absence of plasmalogens in tissues [97]. At birth, mutant mice are alive, but exhibit hypotonia with decreased motility, which, consequently, causes increased lethality during the first week of life. The pups that surpass the difficulties of the first days of live, survive up to 17 months of age [48, 97]. Homozygous mutants are viable but reveal defects in reproduction (males are infertile and females are sub-fertile). The mice also show defects in eye and lens development; compromised myelination in central and peripheral nervous system; defects in paranode organization and Purkinje cell innervation [48, 97, 100]. These findings demonstrate that the *Gnpat* KO mouse serves as a good model for RCDP. The complete absence of plasmalogens results in a severe phenotype, with type and degree of pathology similar to that observed in *Pex7* KO mice [89].

Despite the understanding of genetic and biochemical causes of RCDP, there is relatively less knowledge on how the defect in plasmalogens is associated with cellular defects, tissue pathology or the mechanisms behind known defects. The following sections highlight some of processes that we found dysregulated in the mouse models for RCDP.

The central nervous system

The central nervous system (CNS), composed of the brain (including the optic nerve) and the spinal cord, is a complex system consisting mainly of neurons and glial cells. The axon is the projection of a neuron, whose function is transmitting information to different neurons, muscles or glands, through electrical impulses known as the action potentials [101]. The rapid transduction of electrical impulses is required for the efficient function of the vertebrate nervous system. The maximization of these impulses along axons is reliant on myelin, a specialized structure generated by oligodendrocytes, composed of extended and compacted spirals of the oligodendrocyte plasma membrane around the axon [102]. The myelinated areas of the CNS, called white matter, are composed of myelinated axons, glial cells (myelinating oligodendrocytes and oligodendrocyte progenitor cells [OPCs], NG2-glia, astrocytes and microglia) and blood vessels, all embedded in the extracellular matrix (ECM). CNS white matter is half myelin and half non-myelin on a dry weight basis. The gray matter regions in the CNS are mainly composed of blood vessels, astrocytes, microglia and neuron somas and dendrites [103, 104].

White matter integrity and function: the important role of different cells as a team

Astrocytes

Astrocytes are the most abundant cells in the CNS playing important roles in homeostatic functions. They are an extremely heterogeneous cell type essential for formation and maintenance of the blood brain barrier (BBB), nutrient provision

and maintenance of extracellular homeostasis [105]. Accordingly to their location in grey or white matter, astrocytes may exhibit a branched or a long fiber-like morphology, respectively [105]. They also participate in regulating developmental myelination and myelin maintenance in the brain, playing an active role in OPC survival, oligodendrocytes differentiation, maturation and myelination [106, 107]. On the other hand, in response to many CNS pathologies, such as trauma, hypoxia, and in many neurodegenerative diseases, astrocytes become activated (reactive) leading to astrocytosis. Astrocytosis is characterized by cellular hypertrophy, increased astrocyte numbers, and increased expression of glial fibrillary acidic protein (GFAP) [108]. The functions of reactive astrocytes are not well understood, and both harmful and beneficial activities have been reported. However, the importance of astrocytes is emphasized by the clinical presentation of Alexander disease, a rare fatal leukodystrophy of the central nervous system that causes progressive loss of motor and mental function, and is caused by mutations in the gene encoding GFAP [109, 110].

Microglia

Microglia, firstly described in 1932 by del Rio-Hortega, are the mononuclear resident “macrophages” of CNS tissues. In contrast to oligodendrocytes and astrocytes that originate from neural progenitors within the neuroectoderm, microglia arise from yolk sac (YS)-primitive macrophages, which persist in the CNS into adulthood [103, 111, 112]. Considered the most versatile cells, microglial cells have the capacity to, in response to various signals, morphologically adapt and change from an amoeboid to a more ramified shape [113]. Microglia act as sentinels to detect the first signs of invasion, inflammation or injury, acting as scavengers that remove cell debris, and/or producers of inflammatory signaling

molecules, contributing for supporting and homeostatic functions [114]. In the white matter, microglia are involved in the regulation of myelin maintenance and play a role upon injury and during repair. In homeostatic conditions, microglia promote OPC survival and differentiation, and myelination [115, 116]. Upon injury, microglia can play dual roles: delaying OPC differentiation and inducing oligodendrocyte apoptosis or promoting OPC differentiation and remyelination [103, 117, 118]. Additionally, microglia play an important role in the clearance of myelin debris in the case of white matter damage with myelin loss [119]. This step is crucial in the remyelination process and underscores the importance of microglia during white matter repair [119–121]. Moreover, mutations in genes highly expressed in microglia cause progressive white matter brain diseases. Is the case of dominant loss-of-function mutations in colony-stimulating factor 1 receptor (CSF1R) that cause adult-onset leukoencephalopathy with axonal spheroids and pigmented glia (ALSP), also known as hereditary diffuse leukoencephalopathy with axonal spheroids (HDLS) [122–124]. The CSF1R mutations cause lower microglia numbers and widespread microglia depletion in postmortem brain tissue of ALSP patients, which suggests that microglia loss may be an early pathogenic event contributing to leukodystrophy [122].

Neurons

Neurons and their axons interact with oligodendrocytes bidirectionally and throughout life, being such interaction essential for both (the lack of myelin leads to axonal degeneration and axonal degeneration leads to loss of myelin) [125]. During development, axonal signals participate in: (1) regulating oligodendroglial lineage progression and myelination, (2) controlling myelination, (3) regulating membrane trafficking in oligodendrocytes, (4) and being fundamental for the

establishment of adequate myelin thickness [126-128]. Additionally, by itself, the neuronal activity directly influences myelination [129]. Because of this close interaction between axons and oligodendrocytes, myelination is perturbed when axonal dysfunction and degeneration begin before myelination is complete [103].

Oligodendrocytes

Oligodendrocyte progenitor cells (OPCs) are generated in distinct waves throughout time and space. During development, brain produces an overabundance of OPCs to ensure sufficient cells to achieve proper myelination [130, 131]. In addition, a substantial number of OPCs persist in the adult brain, where are involved in myelin remodeling, de novo myelination of unmyelinated axons and remyelination upon injury [132].

To ensure an adequate number of OPCs at the final sites of myelination, a rigid control of OPC migration, through signals provided by white matter cells other than oligodendrocytes, is essential. Once they have reached their final destination, OPCs terminally differentiate into myelin-forming oligodendrocytes [102, 133]. Modulated by axonal and astrocytic factors, the balance between OPC proliferation and terminal differentiation is tightly regulated to ensure that oligodendrocyte lineage progression takes place in an orderly sequence [103, 134]. OPC terminal differentiation and myelination are almost concurring events in mice, with pre-myelinating oligodendrocytes rapidly progressing to myelination [131]. By contrast, in the human brain, pre-myelinating oligodendrocytes are observed for longer periods, before start to myelinate [135].

The final stage of oligodendrocyte development is myelination. Myelination of axons occurs in a very short time window in the lifetime of the oligodendrocyte, during which myelin sheaths are formed and the number of sheaths is determined

[136]. Modulated by intrinsic and extrinsic regulators, the balance between differentiation and myelination is, in a spatiotemporally specific manner, a tightly regulated process [103, 137]. Being essential for myelin formation, oligodendrocytes are also important for neuronal survival and trophic support [138].

Myelination in the Central Nervous System

Myelin structure and biogenesis

Myelination is an evolutionary adaptation of the mammalian nervous system achieved through the action of oligodendrocytes in the CNS, and Schwann cells in the peripheral nervous system (PNS) [138]. Myelin formation proceeds with outgrowth and retraction of glial cell processes, target axon recognition, stabilization of cellular contacts, rapid biosynthesis and trafficking of lipid and protein constituents of the myelin membrane, and its organization as a multilayered structure around the axon [139]. Once myelinated, axons become dependent on glial support [140]. Each oligodendrocyte is able to extend several protrusions, enwrap and myelinate up to 50 different axonal segments, without an apparent restriction for their caliber [141].

The multilayered plasma membrane stacks of myelin surrounding the axons compose a highly compartmentalized structure (Fig. 3). This compartmentalization is a prerequisite for the proper glial cell-axon communication, the trophic/metabolic support and optimal conduction of action potentials [138]. Myelinating oligodendrocytes enwrap a well-defined length of the axon, called the internode. The extent of myelination and the length of the internodes affect the action potential propagation [142]. The internodes are 150-200μm in length and are separated from each other by the nodes of Ranvier (Fig. 3B). These nodes are short periodical interruptions in myelin sheath and are enriched in voltage sodium

(NaV) channels. As a result of myelination, and because axonal membrane depolarization occurs exclusively at the nodes, conduction velocities are approximately 100 times faster than in unmyelinated axons, where NaV channels are diffused throughout the axon. As so, myelination of axons is essential for the rapid and saltatory conduction of action potentials, which is rapid and energy saving mechanism [143].

Myelin also forms the flanking membrane loops termed the paranodes. Paranodes are composed of non-compact myelin containing cytoplasm of oligodendrocytes, which serves to separate the nodal sodium channels from the potassium channels, enriched in the adjacent juxtaparanodes (Fig. 3B) [143]. Radially, myelinating oligodendrocytes cells possess two distinct plasma membrane surfaces. The inner membrane surface, called inner tongue, is in direct contact with the axon, allowing the establishment of protein interactions between the axon and the oligodendrocyte cell. The outer membrane surface is called outer tongue (Fig. 3C) [143]. Additionally, along the internode, CNS myelin present uncompact regions called radial component [144, 145]. The radial component of CNS myelin was first observed in cross sections of optic nerves where it appears as radially oriented, linear arrays of thickenings of the intraperiod line extending across the myelin sheath [146]. Although not completely understood, this structural specialization within CNS myelin is thought to stabilize the apposition of membranes in the internode and sustain the transport of metabolic substances across the myelin sheath [145, 147].

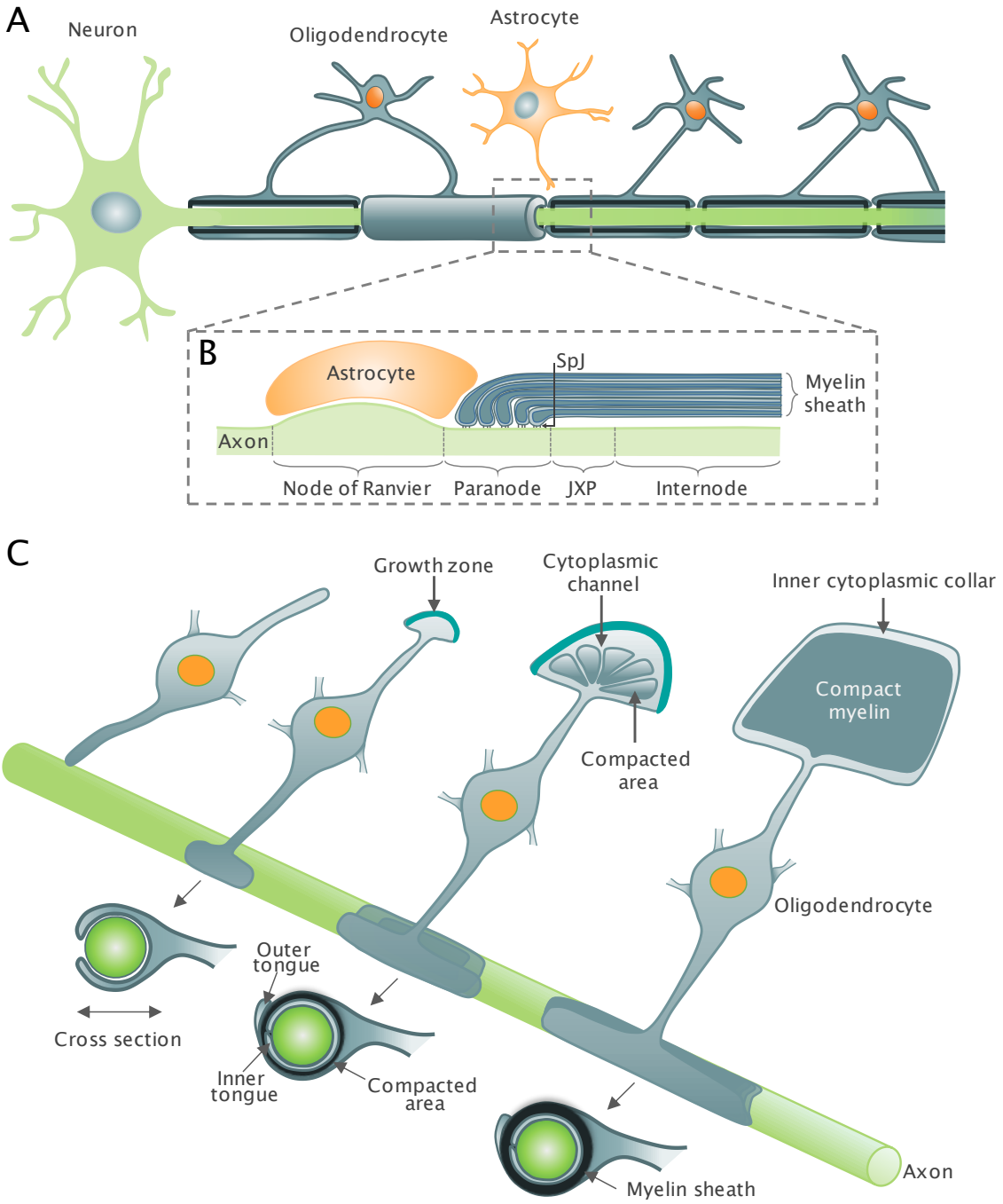

Figure 3. CNS myelin formation and organization. A Oligodendrocytes extend several protrusions and myelinate different axonal segments, by enwrapping their membranes several times around the axon. **B** Schematic longitudinal cut of a myelinated axon showing the node of Ranvier, paranode, juxtaparanode (JXP) and internode. The node is contacted by processes from astrocytes. The paranodal loops form a septate-like junction (SpJ) with the axon. The JXP region resides beneath the compact myelin next to the paranode. The internode extends from the juxtaparanodes and lies under the compact myelin. **C** Schematic representation of the currently accepted model of myelination in the CNS. A differentiated oligodendrocyte extends a protrusion towards an unmyelinated axon and upon contact starts wrapping by spreading its membrane. The myelin membrane extends radially and longitudinally. After several myelin membrane layers are formed, compaction occurs from the outermost to the inner layers.

The current accepted model of how the myelin membrane is formed around axons has been proposed by Snaidero and colleagues [148]. These authors showed that myelin emerges as a single triangle-like shaped membrane that wraps the leading edge around the axon, underneath previously deposited membrane. Simultaneously, lateral extension of myelin membrane layers occurs, towards the nodal regions (Fig. 3C) [148]. Additionally, for a proper myelin compaction, equal expression levels of myelin basic protein (MBP) and cyclic nucleotide phosphodiesterase (CNPase) are needed, occurring first in the outermost layers and moving inwards with time [148].

Myelin composition

Myelin in central nervous system is composed of 70-80% lipids, including cholesterol, phospholipids, galactolipids and plasmalogens; and around 20-30% of proteins, namely proteolipid protein (PLP), myelin basic protein (MBP), cyclic nucleotide phosphodiesterase (CNPase), myelin oligodendrocyte glycoprotein (MOG) and myelin-associated glycoprotein (MAG) [149, 150].

Lipid composition

The myelin sheath is highly enriched in lipids. In relation to the lipid content, myelin of the PNS and the CNS present similar compositions of: cholesterol, cerebroside, sphingomyelin and ethanolamine plasmalogen [149-152]. Interestingly, the lipid composition of myelin varies significantly from other biological membranes. Specifically, the molar ratio of cholesterol, phospholipids and glycosphingolipids is different in the myelin sheath. The molar ratios of these three different components in myelin are 40%:40%:20%, whereas in most of the membranes is in the order of 25%:65%:10% [150]. This specific lipid composition

enables the close packing and tight organization of molecules within the membrane. As so, the composition and structural properties of myelin lipids are important to impose stability for the long-term maintenance of myelin [6].

During the active phase of myelination, myelinating glial cells generate an enormous amount of lipids in a relatively short period of time. In the CNS, when myelination is completed, oligodendrocytes have synthesized ~40% of the total lipids in the human brain [153]. Interestingly, the lipid composition of myelin is not fixed, but modifiable and with the potential to undergo relevant rearrangements. Specifically, in aging or in diseases such as multiple sclerosis or certain leukodystrophies (genetically inherited disorders that affect CNS myelin), alteration on myelin lipidome is observed, which may contribute to myelin destabilization and breakdown. Remarkably, studies in mutant mice targeting various lipid biosynthesis pathways have shown that myelinating glia have a capacity to compensate the lack of individual lipids. However, compensation fails when it comes to maintaining long-term stability of myelin.

As mentioned, a distinguishing feature of myelin lipid composition is the high amount of ethanolamine plasmalogens (PE-plasmalogens), representing 12-15% of total myelin lipid [154]. Interestingly, PE-plasmalogens levels correlate with the degree of myelination. Specifically, there is an eight-fold increase in ethanolamine plasmalogens levels per gram of brain tissue in the white matter during first year of human life, and the highest levels are reached between 30 and 40 years of age when myelination is completed [13]. The various unique structural features that distinguish plasmalogens from other phospholipids (see section: Biological roles attributed to plasmalogens), give to plasmalogens an important role in myelin: (1) membrane stabilization (since the enrichment of plasmalogens in myelin should increase the packing density and with it the stability of the membrane), (2) free radical suppression and (3) immunological modulation.

Interestingly, PE-plasmalogens are concentrated and founded predominantly in the inner leaflet, being in close contact with important myelin-associated proteins (Fig. 4; membrane phospholipids highlighted by the black head) [40, 41].

Whereas the lipid composition of myelin is similar between the CNS and PNS, the protein composition differs substantially [81].

Protein composition

The relative abundance of myelin proteins was investigated over the years, revealing a small number of proteins extraordinarily abundant in CNS myelin. Thus, for a long time the literature described that PLP and its smaller splice isoform DM20 accounted for 30–45% of total myelin protein, MBP for 22–35%, 2′,3′-cyclic nucleotide 3′-phosphodiesterase (CNPase) for 4–15%, and all remaining proteins for 5–25% [155, 156]. However, more accurate techniques have confirmed and extended the previous myelin protein compendia [157]. Specifically, in the study carried out by Jahn and colleagues, 342 proteins associated with CNS myelin were described [157]. Strikingly, PLP, MBP, and CNP constituted only 17%, 8%, and 4% of the total myelin-associated proteins, respectively. MOG, MAG, Sirtuin 2 (SIRT2) and oligodendrocyte-specific protein/Claudin 11 (OSP) account for 1% each. Taken together, all previously known myelin proteins constituted 35%, while newly identified myelin associated proteins accounted for 65% [157].

Myelin basic protein (MBP), the second-most abundant myelin protein is present both in CNS and PNS myelin. The classical MBP gene has seven exons that may undergo alternative splicing. MBP is localized in the cytoplasmic surface of the membrane, specifically in the called major dense line (MDL; formed by the appositions of the cytoplasmic leaflets of the membranes) (Fig. 3) [158]. It is generally assumed that MBP mediates the adhesion of the cytoplasmic surfaces

between the individual layers of myelin, via binding of its basic residues with the negatively charged head groups of membrane lipids, giving rise to compact myelin (Fig. 4) [159]. Indeed, membrane association of MBP is controlled by the membrane lipid phosphatidylinositol-(4,5)-bisphosphate [160]. Being crucial for proper myelin formation, MBP play also an important role on spatial restriction of proteins within myelin membranes [158, 161]. By creating a physical barrier that filters proteins with large cytoplasmic domains, MBP keeps proteins such as CNP and MAG in the right cellular compartment, inducing the polarization of membranes. This extrusion of proteins from the myelin membranes is one of the explanation for the low protein-to-lipid ratio of myelin [157, 161].

Proteolipid protein (PLP) is the most abundant protein of mammalian CNS myelin. It is a very hydrophobic transmembranar protein with 25kDa, showing a high affinity to phospholipids and cholesterol. PLP comprises 276 amino acid residues and four hydrophobic stretches that constitute membrane-spanning domains. A second isoform, termed DM20, is generated by alternative RNA splicing, and lacks 35 residues from an intracellular loop region. PLP acts as a support within the myelin of the CNS, with its extracellular loop regions defining the exact spacing between myelin lamellae at the intraperiod lines (IPL) of the compact myelin (Fig. 4). Although the cell biological function of PLP has been difficult to define, their relevance is highlighted by the severe neurological consequences in patients with Pelizaeus-Merzbacher disease (defined by mutations in the PLP gene) [162, 163].

Myelin-oligodendrocyte glycoprotein (MOG) is a specific membrane protein of the CNS, expressed on the oligodendrocyte cell surface and the outermost surface of myelin sheaths (Fig. 4). Due to this localization, it is a primary target antigen involved in immune-mediated demyelination [164]. Although described for a long time as a myelin protein, its functions are not fully understood, but the

involvement in the completion and maintenance of myelin sheath and cell-cell communication is suggested [150, 165].

Another important protein is the myelin-associated glycoprotein (MAG), a type I transmembrane glycoprotein with 16kDa, localized in periaxonal oligodendrocyte membrane of myelin sheaths (myelin layer opposed to the axon; see Fig. 4). Because of its location, MAG is an important protein to mediate certain glia-axon interactions. In addition, it is also believed to be involved in the process of myelination, functioning both as a ligand for an axonal receptor that is needed for the maintenance of myelinated axons and as a receptor for an axonal signal that promotes the differentiation, maintenance and survival of oligodendrocytes [166].

2',3'-cyclic nucleotide 3'-phosphodiesterase (CNPase) is expressed exclusively by oligodendrocytes, and is located in non-compact myelin regions such as, the inner mesaxon and in the paranodes (Fig. 4). The expression of CNPase seems to be one of the earliest events of oligodendrocyte differentiation, suggesting an important role in oligodendrocytes differentiation but also in the events leading up to myelination [167]. Additionally, CNPase is potentially involved in cytoskeletal dynamics, since can link tubulin to cellular membranes, possibly regulating cytoplasmic microtubule distribution [165, 168].

Among the recently identified myelin proteins, a variety of them are candidates for performing important functions in myelin biogenesis and integrity. Some of them are illustrated in Fig. 4 (more details in [157]).

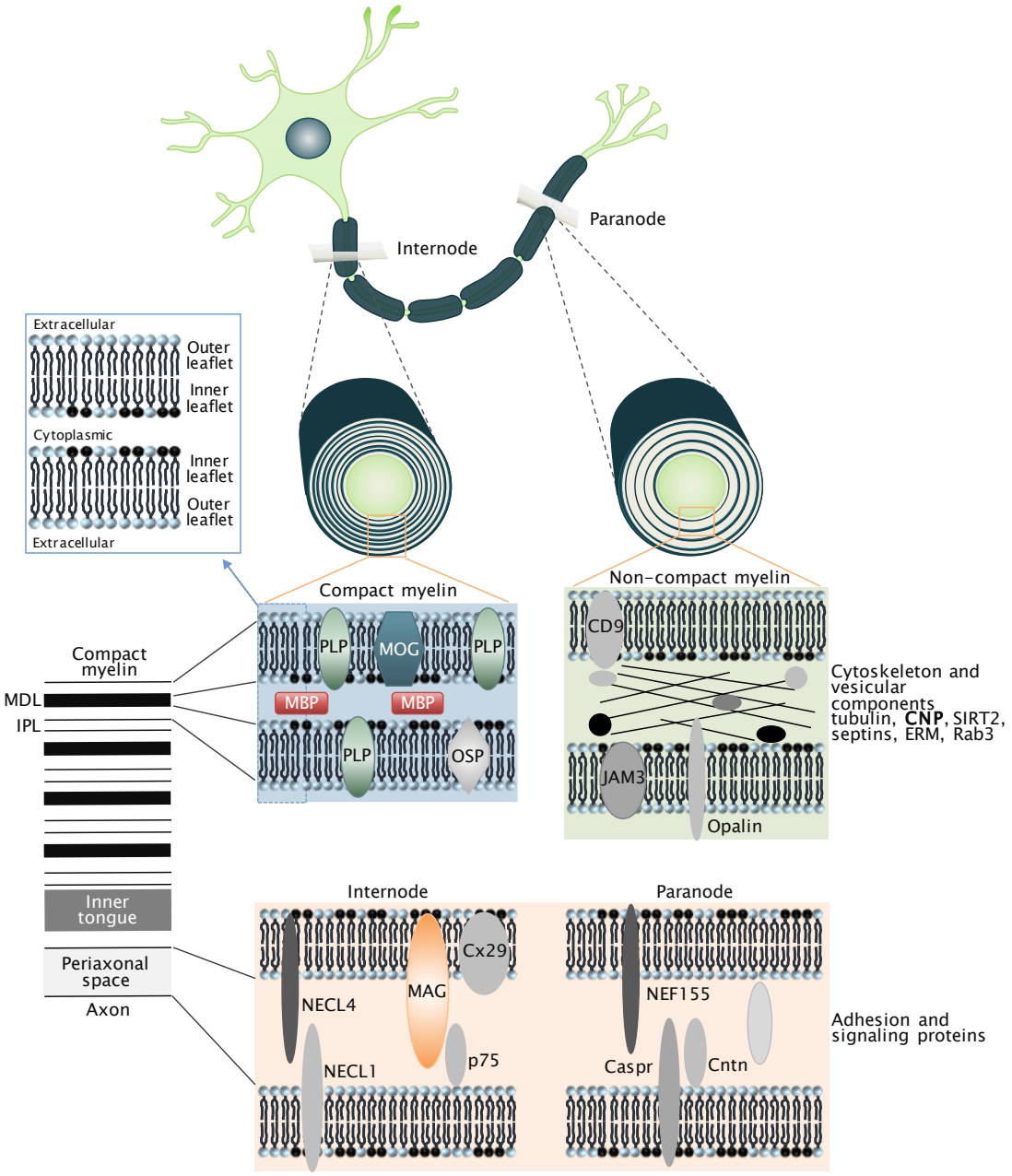

Figure 4. Schematic representation of the myelin sheath structure in the CNS. Cross-sections in the internodal and paranodal segments reveal the subcellular localization of structural proteins of compact myelin (blue box); cytoskeletal and vesicular proteins located in uncompacted regions (green box), and adhesion proteins mediating association with the axon (orange box). Abbreviation list: 2′,3′-cyclic nucleotide phosphodiesterase (CNP,) contactin (Cntn), contactin-associated protein (Caspr), connexin 29 kDa (Cx29), proteolipid protein (PLP,) ezrin (ERM), radixin, moesin, junctional adhesion molecule 3 (JAM3), myelin-associated glycoprotein (MAG), myelin basic protein (MBP), nectin-like protein (Necl), neurofascin 155 kDa (NF155), oligodendrocyte-specific protein/claudin-11 (OSP), Ras-related protein Rab3 (Rab3), sirtuin 2 (SIRT2), intraperiod line (IPL) and major dense line (MDL).

Signaling pathways regulating myelination in the CNS

Several signaling molecules have been implicated in controlling central nervous system myelination. The most commonly described include, the Wnt/β-catenin [169, 170], ERK/MAPK [171] and Akt/mTOR pathways [172, 173]. Although each individual pathway plays important roles in myelination and remyelination, growing evidence shows that none of them are acting alone. Namely, data suggest that the Wnt/β-catenin and Akt/mTOR pathways both play critical roles during OPC differentiation and myelination, while *in vivo* data point to a dominant role for the ERK/MAPK pathway in directly regulating myelin sheath expansion [174].

Signaling, myelination and plasmalogens

Several studies in mouse models with defects in plasmalogens have described abnormalities in myelination. Defects in optic nerve myelination and paranode organization were described in *Gnpat* knockout mice [48, 49]. To study the disease development and progression, as well as, dissect the molecular mechanisms that govern plasmalogen deficiency, our laboratory investigated the role of plasmalogens on peripheral nervous system myelination [50]. In the PNS, plasmalogen-deficient mice have impaired radial sorting and myelination in sciatic nerves, as well as, impaired remyelination after nerve crush. Moreover, the study revealed that plasmalogen-deficient mice had an impairment in the AKT signaling pathway [50]. Specifically, a deficiency in plasmalogens affects the ability of AKT to be activated by phosphorylation at the plasma membrane. This inability causes a reduction in AKT phosphorylation leading to inactive AKT. As a consequence, the impairment in AKT causes a deficient phosphorylation of GSK3β, which is necessary to induce Schwann cell differentiation and maturation to initiate myelination [51, 52].

Myelin in disease

White matter disorders comprise a group of diseases, called leukodystrophies, characterized by failures to properly form myelin or to sustain myelin levels. The term "leukodystrophy" (*leuko*, white and *dystrophy*, wasting) was used for the first time in 1928 [103]. Although the term has been used for a long time, the definition of leukodystrophies has been controversial and the subject of much analysis. Obviously, there is no perfect definition of the word leukodystrophy. Currently, leukodystrophies are defined as all genetically determined disorders primarily affecting central nervous system white matter, irrespective of the structural white matter component involved, the molecular process affected and the disease course [175].

According to the main mechanism of white matter injury, leukodystrophies could be categorized in: hypomyelinating (lack of myelin deposition), demyelinating (loss of previously deposited myelin), dysmyelinating (deposition of structurally or biochemically abnormal myelin) and myelinolytic diseases (myelin vacuolization) [103]. However, taking into account the primary involvement of any white matter component, leukodystrophies are classified into five main categories [103]:

1. White matter disorders in which oligodendrocytes and myelin are primarily or predominantly affected. These are the hypomyelinating disorders, the demyelinating disorders, and the diseases with myelin vacuolization
2. White matter disorders due to defects in astrocyte-specific gene products or in which astrocyte dysfunctions play a major pathogenetic role: the "astrocytopathies".
3. White matter disorders secondary to neuronal or axonal defects: the "leuko-axonopathies". In this category, the white matter degeneration results from an abnormal axo-glia interaction.

4. White matter disorders due to defects in microglia-specific gene products: the “microgliopathies”.
5. Genetic white matter disorders due to vascular pathology: the “leuko-vasculopathies”.

Even so, some leukodystrophies fall into more than one category [103]. In summary, given the complex molecular and cellular interplay underlying white matter pathology, recognition of the cellular pathology behind a disease becomes crucial in addressing possible treatment strategies.

The regenerative response to myelin disruption, characterized by *de novo* synthesis of myelin sheaths on exposed axons – remyelination – is very limited in the adult CNS. Frequently, OPCs in the demyelinated lesion are unable to differentiate and/or mature properly [176-178]. However, even when new myelin is formed, the myelin sheaths are generally thinner and the internodes shorter, features that probably impact neuronal function recovery [179, 180]. Consequently, treatments promoting oligodendrocyte differentiation are a possible strategy to use to stimulate remyelination.

Bibliography

1. Cermenati, G., et al., *Lipids in the nervous system: from biochemistry and molecular biology to patho-physiology.* Biochim Biophys Acta, 2015. **1851**(1): p. 51-60.
2. Wang, T., et al., *Lgl1 activation of rab10 promotes axonal membrane trafficking underlying neuronal polarization.* Dev Cell, 2011. **21**(3): p. 431-44.
3. Ros, O., et al., *Regulation of patterned dynamics of local exocytosis in growth cones by netrin-1.* J Neurosci, 2015. **35**(13): p. 5156-70.
4. Mauch, D.H., et al., *CNS synaptogenesis promoted by glia-derived cholesterol.* Science, 2001. **294**(5545): p. 1354-7.
5. Salzer, J.L., *Axonal regulation of Schwann cell ensheathment and myelination.* J Peripher Nerv Syst, 2012. **17 Suppl 3**: p. 14-9.
6. Schmitt, S., L.C. Castelvetri, and M. Simons, *Metabolism and functions of lipids in myelin.* Biochim Biophys Acta, 2015. **1851**(8): p. 999-1005.
7. Saher, G., et al., *Cholesterol regulates the endoplasmic reticulum exit of the major membrane protein P0 required for peripheral myelin compaction.* J Neurosci, 2009. **29**(19): p. 6094-104.
8. Chrast, R., et al., *Lipid metabolism in myelinating glial cells: lessons from human inherited disorders and mouse models.* J Lipid Res, 2011. **52**(3): p. 419-34.
9. Marinetti, G.V., J. Erbland, and E. Stotz, *The Structure of Pig Heart Plasmalogens.* Journal of the American Chemical Society, 1958. **80**(7): p. 1624-1628.
10. Nagan, N. and R.A. Zoeller, *Plasmalogens: biosynthesis and functions.* Prog Lipid Res, 2001. **40**(3): p. 199-229.

11. Pike, L.J., et al., *Lipid rafts are enriched in arachidonic acid and plasmenylethanolamine and their composition is independent of caveolin-1 expression: a quantitative electrospray ionization/mass spectrometric analysis.* Biochemistry, 2002. **41**(6): p. 2075-88.

12. Wanders, R.J. and H.R. Waterham, *Biochemistry of mammalian peroxisomes revisited.* Annu Rev Biochem, 2006. **75**: p. 295-332.

13. Braverman, N.E. and A.B. Moser, *Functions of plasmalogen lipids in health and disease.* Biochim Biophys Acta, 2012. **1822**(9): p. 1442-52.

14. De Duve, C. and P. Baudhuin, *Peroxisomes (microbodies and related particles).* Physiol Rev, 1966. **46**(2): p. 323-57.

15. Waterham, H.R. and M.S. Ebberink, *Genetics and molecular basis of human peroxisome biogenesis disorders.* Biochim Biophys Acta, 2012. **1822**(9): p. 1430-41.

16. Rucktaschel, R., W. Girzalsky, and R. Erdmann, *Protein import machineries of peroxisomes.* Biochim Biophys Acta, 2011. **1808**(3): p. 892-900.

17. Wanders, R.J., *Peroxisomes, lipid metabolism, and peroxisomal disorders.* Mol Genet Metab, 2004. **83**(1-2): p. 16-27.

18. Ma, C., G. Agrawal, and S. Subramani, *Peroxisome assembly: matrix and membrane protein biogenesis.* J Cell Biol, 2011. **193**(1): p. 7-16.

19. Emmanouilidis, L., et al., *Structural biology of the import pathways of peroxisomal matrix proteins.* Biochim Biophys Acta, 2016. **1863**(5): p. 804-13.

20. Thoms, S., *Import of proteins into peroxisomes: piggybacking to a new home away from home.* Open Biol, 2015. **5**(11).

21. Liu, X., C. Ma, and S. Subramani, *Recent advances in peroxisomal matrix protein import.* Curr Opin Cell Biol, 2012. **24**(4): p. 484-9.

22. Petriv, O.I., et al., *A new definition for the consensus sequence of the peroxisome targeting signal type 2.* J Mol Biol, 2004. **341**(1): p. 119-34.

23. Heiland, I. and R. Erdmann, *Biogenesis of peroxisomes. Topogenesis of the peroxisomal membrane and matrix proteins.* FEBS J, 2005. **272**(10): p. 2362-72.

24. Kunze, M., et al., *Mechanistic insights into PTS2-mediated peroxisomal protein import: the co-receptor PEX5L drastically increases the interaction strength between the cargo protein and the receptor PEX7.* J Biol Chem, 2015. **290**(8): p. 4928-40.

25. Rodrigues, T.A., C.P. Grou, and J.E. Azevedo, *Revisiting the intraperoxisomal pathway of mammalian PEX7.* Sci Rep, 2015. **5**: p. 11806.

26. Islinger, M., et al., *Hitchhiking of Cu/Zn superoxide dismutase to peroxisomes--evidence for a natural piggyback import mechanism in mammals.* Traffic, 2009. **10**(11): p. 1711-21.

27. Schueren, F., et al., *Peroxisomal lactate dehydrogenase is generated by translational readthrough in mammals.* Elife, 2014. **3**: p. e03640.

28. Saryi, N.A., et al., *Pnc1 piggy-back import into peroxisomes relies on Gpd1 homodimerisation.* Sci Rep, 2017. **7**: p. 42579.

29. Biermann, J., et al., *Alkyl-dihydroxyacetone phosphate synthase and dihydroxyacetone phosphate acyltransferase form a protein complex in peroxisomes.* Eur J Biochem, 1999. **261**(2): p. 492-9.

30. Razeto, A., et al., *The crucial step in ether phospholipid biosynthesis: structural basis of a noncanonical reaction associated with a peroxisomal disorder.* Structure, 2007. **15**(6): p. 683-92.

31. Malheiro, A.R., T.F. da Silva, and P. Brites, *Plasmalogens and fatty alcohols in rhizomelic chondrodysplasia punctata and Sjogren-Larsson syndrome.* J Inherit Metab Dis, 2015. **38**(1): p. 111-21.

32. Lodhi, I.J., et al., *Inhibiting adipose tissue lipogenesis reprograms thermogenesis and PPARgamma activation to decrease diet-induced obesity.* Cell Metab, 2012. **16**(2): p. 189-201.

33. Watschinger, K. and E.R. Werner, *Orphan enzymes in ether lipid metabolism.* Biochimie, 2013. **95**(1): p. 59-65.

34. Dorninger, F., et al., *Homeostasis of phospholipids - The level of phosphatidylethanolamine tightly adapts to changes in ethanolamine plasmalogens.* Biochim Biophys Acta, 2015. **1851**(2): p. 117-28.

35. Cheng, J.B. and D.W. Russell, *Mammalian wax biosynthesis. I. Identification of two fatty acyl-Coenzyme A reductases with different substrate specificities and tissue distributions.* J Biol Chem, 2004. **279**(36): p. 37789-97.

36. Honsho, M., S. Asaoku, and Y. Fujiki, *Posttranslational regulation of fatty acyl-CoA reductase 1, Far1, controls ether glycerophospholipid synthesis.* J Biol Chem, 2010. **285**(12): p. 8537-42.

37. Buchert, R., et al., *A peroxisomal disorder of severe intellectual disability, epilepsy, and cataracts due to fatty acyl-CoA reductase 1 deficiency.* Am J Hum Genet, 2014. **95**(5): p. 602-10.

38. Honsho, M., et al., *Isolation and characterization of mutant animal cell line defective in alkyl-dihydroxyacetonephosphate synthase: localization and transport of plasmalogens to post-Golgi compartments.* Biochim Biophys Acta, 2008. **1783**(10): p. 1857-65.

39. Saheki, Y. and P. De Camilli, *Endoplasmic Reticulum-Plasma Membrane Contact Sites.* Annu Rev Biochem, 2017. **86**: p. 659-684.

40. Kirschner, D.A. and A.L. Ganser, *Myelin labeled with mercuric chloride. Asymmetric localization of phosphatidylethanolamine plasmalogen.* J Mol Biol, 1982. **157**(4): p. 635-58.

41. Fellmann, P., P. Herve, and P.F. Devaux, *Transmembrane distribution and translocation of spin-labeled plasmalogens in human red blood cells.* Chem Phys Lipids, 1993. **66**(3): p. 225-30.

42. Koivuniemi, A., *The biophysical properties of plasmalogens originating from their unique molecular architecture.* FEBS Lett, 2017. **591**(18): p. 2700-2713.

43. Han, X.L. and R.W. Gross, *Plasmenylcholine and phosphatidylcholine membrane bilayers possess distinct conformational motifs.* Biochemistry, 1990. **29**(20): p. 4992-6.

44. Paltauf, F., *Ether lipids in biomembranes.* Chem Phys Lipids, 1994. **74**(2): p. 101-39.

45. Hermetter, A., et al., *Influence of plasmalogen deficiency on membrane fluidity of human skin fibroblasts: a fluorescence anisotropy study.* Biochim Biophys Acta, 1989. **978**(1): p. 151-7.

46. Lohner, K., *Is the high propensity of ethanolamine plasmalogens to form non-lamellar lipid structures manifested in the properties of biomembranes?* Chem Phys Lipids, 1996. **81**(2): p. 167-84.

47. Kumar, A., et al., *Cellular traffic cops: the interplay between lipids and proteins regulates vesicular formation, trafficking, and signaling in mammalian cells.* Curr Opin Biotechnol, 2015. **36**: p. 215-21.

48. da Silva, T.F., et al., *Peripheral nervous system plasmalogens regulate Schwann cell differentiation and myelination.* J Clin Invest, 2014. **124**(6): p. 2560-70.

49. Ogata, T., et al., *Opposing extracellular signal-regulated kinase and Akt pathways control Schwann cell myelination.* J Neurosci, 2004. **24**(30): p. 6724-32.

50. Azim, K. and A.M. Butt, *GSK3beta negatively regulates oligodendrocyte differentiation and myelination in vivo.* Glia, 2011. **59**(4): p. 540-53.

51. Broniec, A., et al., *Interactions of plasmalogens and their diacyl analogs with singlet oxygen in selected model systems.* Free Radic Biol Med, 2011. **50**(7): p. 892-8.

52. Sindelar, P.J., et al., *The protective role of plasmalogens in iron-induced lipid peroxidation.* Free Radic Biol Med, 1999. **26**(3-4): p. 318-24.

53. Stadelmann-Ingrand, S., et al., *Plasmalogen degradation by oxidative stress: production and disappearance of specific fatty aldehydes and fatty alpha-hydroxyaldehydes.* Free Radic Biol Med, 2001. **31**(10): p. 1263-71.

54. Brodde, A., et al., *Impaired neurotransmission in ether lipid-deficient nerve terminals.* Hum Mol Genet, 2012. **21**(12): p. 2713-24.

55. Luoma, A.M., et al., *Plasmalogen phospholipids protect internodal myelin from oxidative damage.* Free Radic Biol Med, 2015. **84**: p. 296-310.

56. Kou, J., et al., *Peroxisomal alterations in Alzheimer's disease.* Acta Neuropathol, 2011. **122**(3): p. 271-83.

57. Igarashi, M., et al., *Disturbed choline plasmalogen and phospholipid fatty acid concentrations in Alzheimer's disease prefrontal cortex.* J Alzheimers Dis, 2011. **24**(3): p. 507-17.

58. Spiteller, G., *Peroxyl radicals: inductors of neurodegenerative and other inflammatory diseases. Their origin and how they transform cholesterol, phospholipids, plasmalogens, polyunsaturated fatty acids, sugars, and proteins into deleterious products.* Free Radic Biol Med, 2006. **41**(3): p. 362-87.

59. Dorninger, F., S. Forss-Petter, and J. Berger, *From peroxisomal disorders to common neurodegenerative diseases - the role of ether phospholipids in the nervous system.* FEBS Lett, 2017. **591**(18): p. 2761-2788.

60. Brites, P., H.R. Waterham, and R.J. Wanders, *Functions and biosynthesis of plasmalogens in health and disease.* Biochim Biophys Acta, 2004. **1636**(2-3): p. 219-31.

61. German, O.L., et al., *Docosahexaenoic acid prevents apoptosis of retina photoreceptors by activating the ERK/MAPK pathway.* J Neurochem, 2006. **98**(5): p. 1507-20.

62. Poorani, R., et al., *COX-2, aspirin and metabolism of arachidonic, eicosapentaenoic and docosahexaenoic acids and their physiological and clinical significance.* Eur J Pharmacol, 2016. **785**: p. 116-132.

63. Farooqui, A.A. and L.A. Horrocks, *Plasmalogens, phospholipase A2, and docosahexaenoic acid turnover in brain tissue.* J Mol Neurosci, 2001. **16**(2-3): p. 263-72; discussion 279-84.

64. Wilson, G.N., et al., *Zellweger syndrome: diagnostic assays, syndrome delineation, and potential therapy.* Am J Med Genet, 1986. **24**(1): p. 69-82.

65. Crane, D.I., *Revisiting the neuropathogenesis of Zellweger syndrome.* Neurochem Int, 2014. **69**: p. 1-8.

66. Braverman, N., et al., *Human PEX7 encodes the peroxisomal PTS2 receptor and is responsible for rhizomelic chondrodysplasia punctata.* Nat Genet, 1997. **15**(4): p. 369-76.

67. Motley, A.M., et al., *Rhizomelic chondrodysplasia punctata is a peroxisomal protein targeting disease caused by a non-functional PTS2 receptor.* Nat Genet, 1997. **15**(4): p. 377-80.

68. Brites, P., et al., *Impaired neuronal migration and endochondral ossification in Pex7 knockout mice: a model for rhizomelic chondrodysplasia punctata.* Hum Mol Genet, 2003. **12**(18): p. 2255-67.

69. Braverman, N., et al., *Mutation analysis of PEX7 in 60 probands with rhizomelic chondrodysplasia punctata and functional correlations of genotype with phenotype.* Hum Mutat, 2002. **20**(4): p. 284-97.

70. Yu, T.W., et al., *Using whole-exome sequencing to identify inherited causes of autism.* Neuron, 2013. **77**(2): p. 259-73.

71. Van den Brink, D.M., et al., *Identification of PEX7 as the second gene involved in Refsum disease.* Adv Exp Med Biol, 2003. **544**: p. 69-70.

72. Wanders, R.J., et al., *Human alkyldihydroxyacetonephosphate synthase deficiency: a new peroxisomal disorder.* J Inherit Metab Dis, 1994. **17**(3): p. 315-8.

73. Wanders, R.J., et al., *Human dihydroxyacetonephosphate acyltransferase deficiency: a new peroxisomal disorder.* J Inherit Metab Dis, 1992. **15**(3): p. 389-91.

74. Baroy, T., et al., *A novel type of rhizomelic chondrodysplasia punctata, RCDP5, is caused by loss of the PEX5 long isoform.* Hum Mol Genet, 2015. **24**(20): p. 5845-54.

75. Krakow, D., et al., *Use of three-dimensional ultrasound imaging in the diagnosis of prenatal-onset skeletal dysplasias.* Ultrasound Obstet Gynecol, 2003. **21**(5): p. 467-72.

76. White, A.L., et al., *Natural history of rhizomelic chondrodysplasia punctata.* Am J Med Genet A, 2003. **118A**(4): p. 332-42.

77. Poll-The, B.T. and J. Gartner, *Clinical diagnosis, biochemical findings and MRI spectrum of peroxisomal disorders.* Biochim Biophys Acta, 2012. **1822**(9): p. 1421-9.

78. Poulos, A., et al., *Rhizomelic chondrodysplasia punctata: clinical, pathologic, and biochemical findings in two patients.* J Pediatr, 1988. **113**(4): p. 685-90.

79. Khanna, A.J., et al., *Cervical stenosis secondary to rhizomelic chondrodysplasia punctata.* Am J Med Genet, 2001. **99**(1): p. 63-6.

80. Oswald, G., et al., *Rhizomelic chondrodysplasia punctata type 1 and fulminant neonatal respiratory failure, a case report and discussion of pathophysiology.* Am J Med Genet A, 2011. **155A**(12): p. 3160-3.

81. Khan, M., J. Singh, and I. Singh, *Plasmalogen deficiency in cerebral adrenoleukodystrophy and its modulation by lovastatin.* J Neurochem, 2008. **106**(4): p. 1766-79.

82. Saitoh, M., et al., *Changes in the amounts of myelin lipids and molecular species of plasmalogen PE in the brain of an autopsy case with D-bifunctional protein deficiency.* Neurosci Lett, 2008. **442**(1): p. 4-9.

83. Han, X., D.M. Holtzman, and D.W. McKeel, Jr., *Plasmalogen deficiency in early Alzheimer's disease subjects and in animal models: molecular characterization using electrospray ionization mass spectrometry.* J Neurochem, 2001. **77**(4): p. 1168-80.

84. Fabelo, N., et al., *Severe alterations in lipid composition of frontal cortex lipid rafts from Parkinson's disease and incidental Parkinson's disease.* Mol Med, 2011. **17**(9-10): p. 1107-18.

85. Schedin, S., et al., *Peroxisomal impairment in Niemann-Pick type C disease.* J Biol Chem, 1997. **272**(10): p. 6245-51.

86. Murphy, E.J., et al., *Phospholipid composition and levels are altered in Down syndrome brain.* Brain Res, 2000. **867**(1-2): p. 9-18.

87. Brites, P., et al., *Plasmalogens participate in very-long-chain fatty acid-induced pathology.* Brain, 2009. **132**(Pt 2): p. 482-92.

88. Singh, I., et al., *Impaired peroxisomal function in the central nervous system with inflammatory disease of experimental autoimmune encephalomyelitis*

animals and protection by lovastatin treatment. Brain Res, 2004. **1022**(1-2): p. 1-11.

89. da Silva, T.F., et al., *The importance of ether-phospholipids: a view from the perspective of mouse models.* Biochim Biophys Acta, 2012. **1822**(9): p. 1501-8.
90. Baes, M., et al., *A mouse model for Zellweger syndrome.* Nat Genet, 1997. **17**(1): p. 49-57.
91. Maxwell, M., et al., *Pex13 inactivation in the mouse disrupts peroxisome biogenesis and leads to a Zellweger syndrome phenotype.* Mol Cell Biol, 2003. **23**(16): p. 5947-57.
92. Faust, P.L., et al., *The peroxisome deficient PEX2 Zellweger mouse: pathologic and biochemical correlates of lipid dysfunction.* J Mol Neurosci, 2001. **16**(2-3): p. 289-97; discussion 317-21.
93. Ferdinandusse, S., et al., *Ataxia with loss of Purkinje cells in a mouse model for Refsum disease.* Proc Natl Acad Sci U S A, 2008. **105**(46): p. 17712-7.
94. Baes, M., et al., *Inactivation of the peroxisomal multifunctional protein-2 in mice impedes the degradation of not only 2-methyl-branched fatty acids and bile acid intermediates but also of very long chain fatty acids.* J Biol Chem, 2000. **275**(21): p. 16329-36.
95. Heinzer, A.K., et al., *Mouse models and genetic modifiers in X-linked adrenoleukodystrophy.* Adv Exp Med Biol, 2003. **544**: p. 75-93.
96. Pujol, A., et al., *Late onset neurological phenotype of the X-ALD gene inactivation in mice: a mouse model for adrenomyeloneuropathy.* Hum Mol Genet, 2002. **11**(5): p. 499-505.
97. Rodemer, C., et al., *Inactivation of ether lipid biosynthesis causes male infertility, defects in eye development and optic nerve hypoplasia in mice.* Hum Mol Genet, 2003. **12**(15): p. 1881-95.

98. Braverman, N., et al., *A Pex7 hypomorphic mouse model for plasmalogen deficiency affecting the lens and skeleton.* Mol Genet Metab, 2010. **99**(4): p. 408-16.

99. Liegel, R., et al., *Blind sterile 2 (bs2), a hypomorphic mutation in Agps, results in cataracts and male sterility in mice.* Mol Genet Metab, 2011. **103**(1): p. 51-9.

100. Teigler, A., et al., *Defects in myelination, paranode organization and Purkinje cell innervation in the ether lipid-deficient mouse cerebellum.* Hum Mol Genet, 2009. **18**(11): p. 1897-908.

101. Edgar, J.M. and K.A. Nave, *The role of CNS glia in preserving axon function.* Curr Opin Neurobiol, 2009. **19**(5): p. 498-504.

102. Emery, B., *Regulation of oligodendrocyte differentiation and myelination.* Science, 2010. **330**(6005): p. 779-82.

103. van der Knaap, M.S. and M. Bugiani, *Leukodystrophies: a proposed classification system based on pathological changes and pathogenetic mechanisms.* Acta Neuropathol, 2017. **134**(3): p. 351-382.

104. Geren, B.B. and J. Raskind, *Development of the Fine Structure of the Myelin Sheath in Sciatic Nerves of Chick Embryos.* Proc Natl Acad Sci U S A, 1953. **39**(8): p. 880-4.

105. Sofroniew, M.V. and H.V. Vinters, *Astrocytes: biology and pathology.* Acta Neuropathol, 2010. **119**(1): p. 7-35.

106. Barnett, S.C. and C. Linington, *Myelination: do astrocytes play a role?* Neuroscientist, 2013. **19**(5): p. 442-50.

107. Harlow, D.E. and W.B. Macklin, *Inhibitors of myelination: ECM changes, CSPGs and PTPs.* Exp Neurol, 2014. **251**: p. 39-46.

108. Pekny, M. and M. Nilsson, *Astrocyte activation and reactive gliosis.* Glia, 2005. **50**(4): p. 427-34.

109. Johnson, A.B., *Alexander disease: a leukodystrophy caused by a mutation in GFAP.* Neurochem Res, 2004. **29**(5): p. 961-4.

110. Quinlan, R.A., et al., *GFAP and its role in Alexander disease.* Exp Cell Res, 2007. **313**(10): p. 2077-87.

111. Ginhoux, F. and M. Prinz, *Origin of microglia: current concepts and past controversies.* Cold Spring Harb Perspect Biol, 2015. **7**(8): p. a020537.

112. Li, Q. and B.A. Barres, *Microglia and macrophages in brain homeostasis and disease.* Nat Rev Immunol, 2018. **18**(4): p. 225-242.

113. Nimmerjahn, A., F. Kirchhoff, and F. Helmchen, *Resting microglial cells are highly dynamic surveillants of brain parenchyma in vivo.* Science, 2005. **308**(5726): p. 1314-8.

114. Mosley, R.L., et al., *Neuroinflammation, Oxidative Stress and the Pathogenesis of Parkinson's Disease.* Clin Neurosci Res, 2006. **6**(5): p. 261-281.

115. Nicholas, R.S., M.G. Wing, and A. Compston, *Nonactivated microglia promote oligodendrocyte precursor survival and maturation through the transcription factor NF-kappa B.* Eur J Neurosci, 2001. **13**(5): p. 959-67.

116. Hamilton, S.P. and L.H. Rome, *Stimulation of in vitro myelin synthesis by microglia.* Glia, 1994. **11**(4): p. 326-35.

117. Miron, V.E., et al., *M2 microglia and macrophages drive oligodendrocyte differentiation during CNS remyelination.* Nat Neurosci, 2013. **16**(9): p. 1211-1218.

118. Yeo, Y.A., et al., *CD137 ligand activated microglia induces oligodendrocyte apoptosis via reactive oxygen species.* J Neuroinflammation, 2012. **9**: p. 173.

119. Neumann, H., M.R. Kotter, and R.J. Franklin, *Debris clearance by microglia: an essential link between degeneration and regeneration.* Brain, 2009. **132**(Pt 2): p. 288-95.

120. Kierdorf, K. and M. Prinz, *Microglia in steady state.* J Clin Invest, 2017. **127**(9): p. 3201-3209.

121. Hagemeyer, N., et al., *Microglia contribute to normal myelinogenesis and to oligodendrocyte progenitor maintenance during adulthood.* Acta Neuropathol, 2017. **134**(3): p. 441-458.

122. Oosterhof, N., et al., *Colony-Stimulating Factor 1 Receptor (CSF1R) Regulates Microglia Density and Distribution, but Not Microglia Differentiation In Vivo.* Cell Rep, 2018. **24**(5): p. 1203-1217 e6.

123. Knopman, D., J.H. Sung, and D. Davis, *Progressive familial leukodystrophy of late onset.* Neurology, 1996. **46**(2): p. 429-34.

124. Kim, S.I., et al., *An Autopsy Proven Case of CSF1R-mutant Adult-onset Leukoencephalopathy with Axonal Spheroids and Pigmented Glia (ALSP) with Premature Ovarian Failure.* Exp Neurobiol, 2019. **28**(1): p. 119-129.

125. Bjartmar, C., X. Yin, and B.D. Trapp, *Axonal pathology in myelin disorders.* J Neurocytol, 1999. **28**(4-5): p. 383-95.

126. Zuchero, J.B. and B.A. Barres, *Intrinsic and extrinsic control of oligodendrocyte development.* Curr Opin Neurobiol, 2013. **23**(6): p. 914-20.

127. Trajkovic, K., et al., *Neuron to glia signaling triggers myelin membrane exocytosis from endosomal storage sites.* J Cell Biol, 2006. **172**(6): p. 937-48.

128. Taveggia, C., et al., *Type III neuregulin-1 promotes oligodendrocyte myelination.* Glia, 2008. **56**(3): p. 284-93.

129. Demerens, C., et al., *Induction of myelination in the central nervous system by electrical activity.* Proc Natl Acad Sci U S A, 1996. **93**(18): p. 9887-92.

130. Barres, B.A. and M.C. Raff, *Proliferation of oligodendrocyte precursor cells depends on electrical activity in axons.* Nature, 1993. **361**(6409): p. 258-60.

131. Trapp, B.D., et al., *Differentiation and death of premyelinating oligodendrocytes in developing rodent brain.* J Cell Biol, 1997. **137**(2): p. 459-68.

132. Young, K.M., et al., *Oligodendrocyte dynamics in the healthy adult CNS: evidence for myelin remodeling.* Neuron, 2013. **77**(5): p. 873-85.

133. Mitew, S., et al., *Mechanisms regulating the development of oligodendrocytes and central nervous system myelin.* Neuroscience, 2014. **276**: p. 29-47.

134. Hughes, E.G., et al., *Oligodendrocyte progenitors balance growth with self-repulsion to achieve homeostasis in the adult brain.* Nat Neurosci, 2013. **16**(6): p. 668-76.

135. Back, S.A., et al., *Arrested oligodendrocyte lineage progression during human cerebral white matter development: dissociation between the timing of progenitor differentiation and myelinogenesis.* J Neuropathol Exp Neurol, 2002. **61**(2): p. 197-211.

136. Czopka, T., C. Ffrench-Constant, and D.A. Lyons, *Individual oligodendrocytes have only a few hours in which to generate new myelin sheaths in vivo.* Dev Cell, 2013. **25**(6): p. 599-609.

137. Yang, Y., R. Lewis, and R.H. Miller, *Interactions between oligodendrocyte precursors control the onset of CNS myelination.* Dev Biol, 2011. **350**(1): p. 127-38.

138. Nave, K.A., *Myelination and the trophic support of long axons.* Nat Rev Neurosci, 2010. **11**(4): p. 275-83.

139. Sherman, D.L. and P.J. Brophy, *Mechanisms of axon ensheathment and myelin growth.* Nat Rev Neurosci, 2005. **6**(9): p. 683-90.

140. Nave, K.A. and B.D. Trapp, *Axon-glial signaling and the glial support of axon function.* Annu Rev Neurosci, 2008. **31**: p. 535-61.

141. Edgar, N. and E. Sibille, *A putative functional role for oligodendrocytes in mood regulation.* Transl Psychiatry, 2012. **2**: p. e109.

142. Waxman, S.G., *Axon-glia interactions: building a smart nerve fiber.* Curr Biol, 1997. **7**(7): p. R406-10.

143. Poliak, S. and E. Peles, *The local differentiation of myelinated axons at nodes of Ranvier.* Nat Rev Neurosci, 2003. **4**(12): p. 968-80.

144. Kosaras, B. and D.A. Kirschner, *Radial component of CNS myelin: junctional subunit structure and supramolecular assembly.* J Neurocytol, 1990. **19**(2): p. 187-99.

145. Karthigasan, J., et al., *Protein and lipid composition of radial component-enriched CNS myelin.* J Neurochem, 1994. **62**(3): p. 1203-13.

146. Peters, A., *A radial component of central myelin sheaths.* J Biophys Biochem Cytol, 1961. **11**: p. 733-5.

147. Denninger, A.R., et al., *Claudin-11 Tight Junctions in Myelin Are a Barrier to Diffusion and Lack Strong Adhesive Properties.* Biophys J, 2015. **109**(7): p. 1387-97.

148. Snaidero, N., et al., *Myelin membrane wrapping of CNS axons by PI(3,4,5)P3-dependent polarized growth at the inner tongue.* Cell, 2014. **156**(1-2): p. 277-90.

149. Aggarwal, S., L. Yurlova, and M. Simons, *Central nervous system myelin: structure, synthesis and assembly.* Trends Cell Biol, 2011. **21**(10): p. 585-93.

150. Quarles, P.M.a.R., *Myelin Formation, Structure and Biochemistry*, in *Basic Neurochemistry: Molecular, Cellular, and Medical Aspects*, A.B. Siegel GJ, Albers RW, Editor. 2005. p. 51-71.

151. Saher, G. and S.K. Stumpf, *Cholesterol in myelin biogenesis and hypomyelinating disorders.* Biochim Biophys Acta, 2015. **1851**(8): p. 1083-94.

152. Jana, A. and K. Pahan, *Sphingolipids in multiple sclerosis.* Neuromolecular Med, 2010. **12**(4): p. 351-61.

153. Norton, W.T., *Biochemistry of myelin.* Adv Neurol, 1981. **31**: p. 93-121.

154. Norton, W.T. and S.E. Poduslo, *Myelination in rat brain: method of myelin isolation.* J Neurochem, 1973. **21**(4): p. 749-57.

155. Morell, P., et al., *Changes in the protein composition of mouse brain myelin during development.* J Neurochem, 1972. **19**(11): p. 2545-54.

156. Banik, N.L. and M.E. Smith, *Protein determinants of myelination in different regions of developing rat central nervous system.* Biochem J, 1977. **162**(2): p. 247-55.

157. Jahn, O., S. Tenzer, and H.B. Werner, *Myelin proteomics: molecular anatomy of an insulating sheath.* Mol Neurobiol, 2009. **40**(1): p. 55-72.

158. Omlin, F.X., et al., *Immunocytochemical localization of basic protein in major dense line regions of central and peripheral myelin.* J Cell Biol, 1982. **95**(1): p. 242-8.

159. Boggs, J.M., *Myelin basic protein: a multifunctional protein.* Cell Mol Life Sci, 2006. **63**(17): p. 1945-61.

160. Nawaz, S., et al., *Phosphatidylinositol 4,5-bisphosphate-dependent interaction of myelin basic protein with the plasma membrane in oligodendroglial cells and its rapid perturbation by elevated calcium.* J Neurosci, 2009. **29**(15): p. 4794-807.

161. Aggarwal, S., et al., *A size barrier limits protein diffusion at the cell surface to generate lipid-rich myelin-membrane sheets.* Dev Cell, 2011. **21**(3): p. 445-56.

162. Simons, M., et al., *Assembly of myelin by association of proteolipid protein with cholesterol- and galactosylceramide-rich membrane domains.* J Cell Biol, 2000. **151**(1): p. 143-54.

163. Koeppen, A.H. and Y. Robitaille, *Pelizaeus-Merzbacher disease.* J Neuropathol Exp Neurol, 2002. **61**(9): p. 747-59.

164. Yannakakis, M.P., et al., *Molecular dynamics at the receptor level of immunodominant myelin oligodendrocyte glycoprotein 35-55 epitope implicated in multiple sclerosis.* J Mol Graph Model, 2016. **68**: p. 78-86.

165. Quarles, R.H., *Comparison of CNS and PNS myelin proteins in the pathology of myelin disorders.* J Neurol Sci, 2005. **228**(2): p. 187-9.

166. Quarles, R.H., *Myelin-associated glycoprotein (MAG): past, present and beyond.* J Neurochem, 2007. **100**(6): p. 1431-48.

167. Gravel, M., et al., *Overexpression of 2',3'-cyclic nucleotide 3'-phosphodiesterase in transgenic mice alters oligodendrocyte development and produces aberrant myelination.* Mol Cell Neurosci, 1996. **7**(6): p. 453-66.

168. Bifulco, M., et al., *2',3'-Cyclic nucleotide 3'-phosphodiesterase: a membrane-bound, microtubule-associated protein and membrane anchor for tubulin.* Proc Natl Acad Sci U S A, 2002. **99**(4): p. 1807-12.

169. Guo, F., et al., *Canonical Wnt signaling in the oligodendroglial lineage--puzzles remain.* Glia, 2015. **63**(10): p. 1671-93.

170. Xie, C., et al., *Wnt signaling in remyelination in multiple sclerosis: friend or foe?* Mol Neurobiol, 2014. **49**(3): p. 1117-25.

171. Gonsalvez, D., et al., *The roles of extracellular related-kinases 1 and 2 signaling in CNS myelination.* Neuropharmacology, 2016. **110**(Pt B): p. 586-593.

172. Norrmen, C. and U. Suter, *Akt/mTOR signalling in myelination.* Biochem Soc Trans, 2013. **41**(4): p. 944-50.

173. Wood, T.L., et al., *mTOR: a link from the extracellular milieu to transcriptional regulation of oligodendrocyte development.* ASN Neuro, 2013. **5**(1): p. e00108.

174. Gaesser, J.M. and S.L. Fyffe-Maricich, *Intracellular signaling pathway regulation of myelination and remyelination in the CNS.* Exp Neurol, 2016. **283**(Pt B): p. 501-11.

175. Kevelam, S.H., et al., *Update on Leukodystrophies: A Historical Perspective and Adapted Definition.* Neuropediatrics, 2016. **47**(6): p. 349-354.

176. Chang, A., et al., *NG2-positive oligodendrocyte progenitor cells in adult human brain and multiple sclerosis lesions.* J Neurosci, 2000. **20**(17): p. 6404-12.

177. Chang, A., et al., *Premyelinating oligodendrocytes in chronic lesions of multiple sclerosis.* N Engl J Med, 2002. **346**(3): p. 165-73.

178. Kuhlmann, T., et al., *Differentiation block of oligodendroglial progenitor cells as a cause for remyelination failure in chronic multiple sclerosis.* Brain, 2008. **131**(Pt 7): p. 1749-58.

179. Duncan, I.D., et al., *Thin myelin sheaths as the hallmark of remyelination persist over time and preserve axon function.* Proc Natl Acad Sci U S A, 2017. **114**(45): p. E9685-E9691.

180. Blakemore, W.F., *Pattern of remyelination in the CNS.* Nature, 1974. **249**(457): p. 577-8.

Aims of the work

Plasmalogens, the most abundant form of ether-phospholipids in neurons and myelin have their importance to human health emphasized by the severe clinical presentation of RCDP. The neurological involvement in RCDP, combined with the observation of plasmalogen deficiencies in several neurodegenerative disorders underscores the role and function of these phospholipids in neurons and myelinating glia. As such, it becomes crucial to know and understand the neuropathogenesis behind defects in the biosynthesis of plasmalogens.

This work had as main objectives:

1- Delineate the neuropathogenesis behind a deficiency in plasmalogens. In order to address the function of plasmalogens in nervous tissue, we investigated the consequences of their deficiency to neurons and oligodendrocytes. Studies involved the usage of homozygous *Gnpat* knockout mice with a complete deficiency in plasmalogens, which serve as a model for RCDP.

2- Assessment of therapeutic strategies. Two strategies were delineated to perform *in vivo* therapeutic interventions. A) Rescue the biochemical defect in the biosynthesis of plasmalogens, using alternative substrates. B) From the knowledge gathered from understanding the molecular and cellular basis of the disease, we manipulated specific pathways affected by the deficiency in plasmalogens, to achieve restoration of cell and tissue homeostasis independently of the plasmalogen defect.

Combined, we elucidate crucial aspects of the disease: what is the nature of the myelin defect (i.e., dysmyelination vs. demyelination); how does the pathology progresses; what is the extent of oligodendrocyte-dependent axonal and neuronal defects; are neurons and their processes a prime target of a deficiency in plasmalogens; can we rescue a plasmalogen deficiency in nervous tissue.

Chapter 1

Myelin and myelination defects in plasmalogen-deficient mice highlights a complex leukodystrophy

Myelin and myelination defects in plasmalogen-deficient mice highlights a complex leukodystrophy

Ana R. Malheiro[1,2], Barbara Correia[1], Tiago Ferreira da Silva[1], Pedro Brites[1]

[1]Neurolipid Biology group, Instituto de Biologia Molecular e Celular – IBMC e Instituto de Investigação e Inovação em Saúde - i3S, Universidade do Porto, Rua Alfredo Allen 208 4200-135, Porto, Portugal, [2]ICBAS, Instituto Ciências Biomédicas Abel Salazar, Rua Jorge Viterbo Ferreira 228, 4050-223 Porto, Portugal,

Introduction

Leukodystrophies are a complex group of genetically distinct disorders characterized by the pathological involvement of CNS white matter due to abnormalities in myelination or in myelin homeostasis [1]. Heterogeneous and diverse cellular deficiencies mediate complex mechanisms that ultimately cause myelin defects. The myelin sheath is the extended and modified plasma membrane of oligodendrocytes in the CNS, wrapped in multilayered stacks around axons [2]. In addition to its unique architecture, the distinctive lipid-rich composition of myelin sets it apart from other membranes. Myelin contains high amounts of plasmalogens, a membrane phospholipid that can account for up to 70% of the pool of ethanolamine glycerophospholipids in myelin [3].

Plasmalogens are a class of ether-phospholipids characterized by a vinyl-ether bond at the *sn*-1 position of the glycerol backbone [4]. The biosynthesis of plasmalogens initiates in peroxisomes through the activity of two peroxisomal enzymes, namely glyceronephosphate O-acyltransferase (GNPAT) and alkylglycerophosphate synthase (AGPS), and the subsequent steps take place in the endoplasmic reticulum [5]. Impairments in the biosynthesis of plasmalogens are the hallmark of Rhizomelic Chondrodysplasia Punctata (RCDP). RCDP is a

genetically heterogeneous autosomal recessive disorder, with an estimated incidence of 1:100000 newborns. Mutations in five different genes (i.e., *PEX7*, *GNPAT*, *AGPS*, *FAR1* and *PEX5L*), involved in the biosynthesis of ether-phospholipids characterize the five types of RCDP (RCDP type 1 to 5, respectively) [6-8]. The impaired biosynthesis of plasmalogens leads to multiple developmental malformations, including congenital cataracts, shortening of proximal limbs, profound growth deficiency and intellectual disability [9]. Abnormal signal intensities on magnetic resonance imaging (MRI) are suggestive of dys- and/or hypomyelination [10-12] but the generalized lack of histopathological analysis has hindered the characterization of myelin defects [13]. The occurrence of seizures in RCDP patients, the development of epilepsy and the increased latencies of evoked potentials have also been proposed to correlate with impaired CNS myelination [14]. The neurological involvement in RCDP patients combined with the observation of plasmalogen deficiencies in several neurodegenerative disorders underscores the role and function of these phospholipids in myelinating glia [7]. The understanding of the pathology and disease mechanisms caused by the deficiency in plasmalogens has been powered by the characterization of mouse models for RCDP [15]. Using the *Gnpat* knockout (KO) mice [16] as a model of RCDP type 2, we analyzed the consequences of a plasmalogen deficiency in the CNS.

Here we unravel how a plasmalogen deficiency compromises myelination and myelin content throughout the CNS. The disease progression in a murine model of RCDP is complex with an initial generalized hypomyelination that evolves into active demyelination. Our results demonstrate that a plasmalogen defect affects the intrinsic ability of oligodendrocytes to myelinate.

Results

Lack of plasmalogens causes generalized myelin deficits to highlight a complex myelin disorder

Our phenotypic analyses showed that from the age of 9 months *Gnpat* KO mice started developing a severe and progressive neurological condition that included tremors and generalized ataxia that worsened with time and culminated in hindlimb paralysis. To determine if plasmalogens play a role on myelination and myelin maintenance within the central nervous system (CNS), different regions were analyzed during the end-stages of the disorder in 1.5 years old *Gnpat* KO mice, and in age-matched wild type (WT) mice. Ultrastructural analysis using electron microscopy revealed that a plasmalogen deficiency caused generalized reduction in myelin in several CNS regions (Fig. 1). Nevertheless, different regions were obviously more affected than others. Optic nerves, the corpus callosum and spinal cord were the most affected regions in the *Gnpat* KO mice. In these regions we observed an extreme loss of myelin as many axons were devoid of myelin (Fig. 1 asterisks) and the vast majority of myelinated axons contained thinner myelin sheaths (Fig. 1 arrowheads). The cerebellar white matter tracts were the least affected regions as axons devoid of myelin were not frequent, despite the generalized occurrence of thinner myelin sheaths. The internal capsule of *Gnpat* KO mice displayed an intermediate pathology with severe features when compared to cerebellar white matter (i.e., presence of axons devoid of myelin) and milder features when compared to the corpus callosum and optic nerves (i.e., increased number of axons that still contain a myelin sheath).

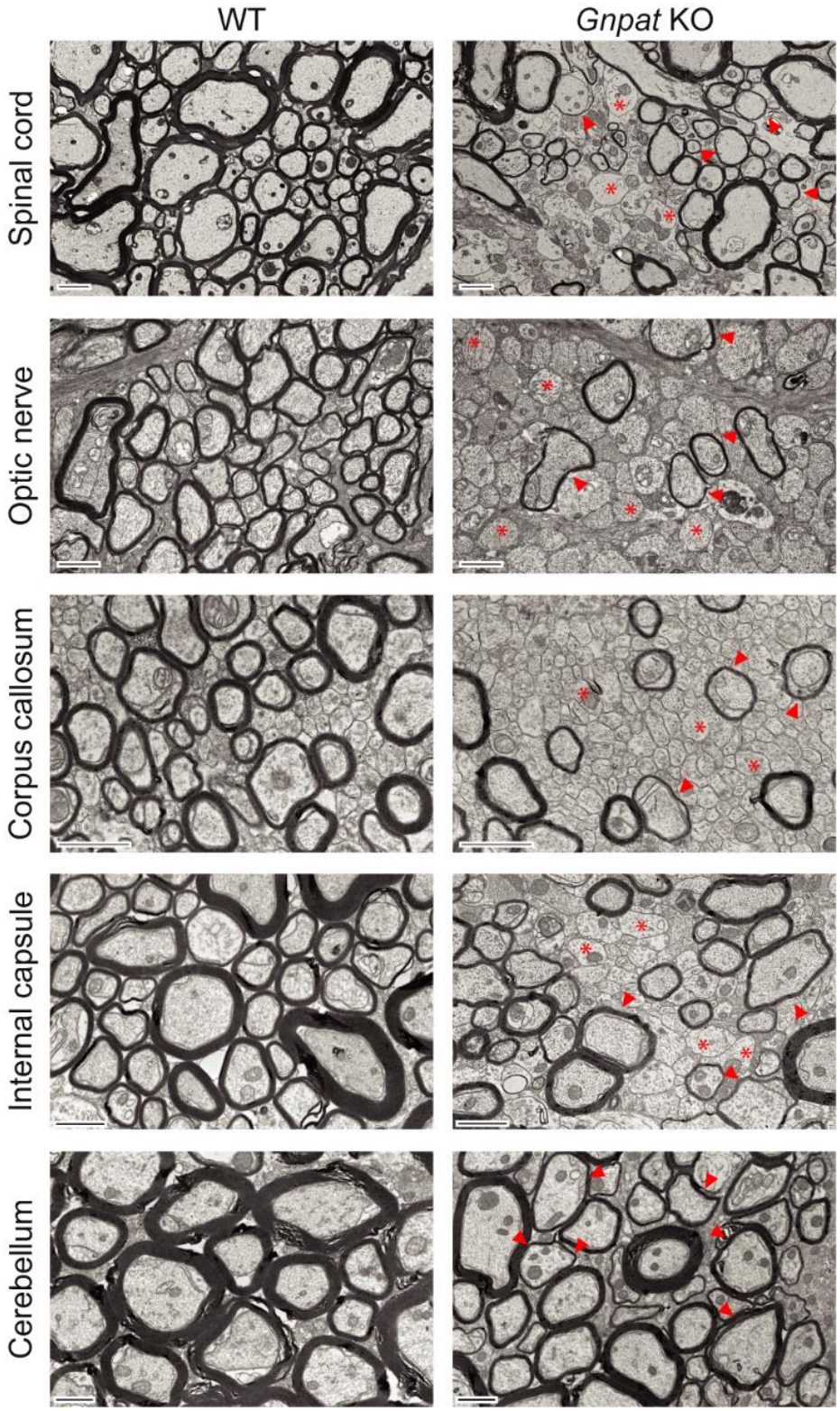

Figure 1. Plasmalogen-deficiency impairs myelination throughout the CNS. Electron microscopy images of spinal cord (n=6 per genotype), optic nerve (n=7 per genotype), corpus callosum (n=3 per genotype), internal capsule (n=3 per genotype) and cerebellum (n=3 per genotype) from 1.5 years old WT and *Gnpat* KO mice. Examples of axons devoid of myelin are highlighted with asterisks and axons with thinner myelin sheaths are highlighted with arrowheads. Scale bars are 2µm in spinal cord and 1µm in the remaining CNS regions.

Combined, these results highlight that a deficiency in plasmalogens causes a complex myelin disorder. To understand the role of plasmalogens in oligodendrocytes and myelin pathology we set out to perform a detailed characterization of optic nerve and spinal cord in *Gnpat* KO mice.

Complex defects in myelinogenesis are aggravated by active demyelination

The previous results, revealing that the lack of plasmalogens affects myelin maintenance throughout the CNS, prompted us to evaluate the process of myelination from the early postnatal period until 1.5 years of age. Focusing on spinal cord and optic nerve, we characterized in detail the myelination defects present in plasmalogens deficient mice. The qualitative analysis of myelination in spinal cords from 2 months and 1.5 years old *Gnpat* KO mice highlighted the progressive worsening of myelin defects (Fig. 2A). Spinal cords from aged plasmalogen-deficient mice had a notable hypoplasia, with a decrease in the white matter area (Fig. 2A). The generalized loss of myelin was detected in several white mater tracts including the ventral and lateral funiculus, and the corticospinal and dorsal column tracts (Fig. 2B). Additionally, in spinal cords from aged *Gnpat* KO mice we observed myelin debris (Fig. 2C), as well as, the presence of myelin-laden cells (Fig. 2 D and E). These cells, presumably macrophages were frequently found close to naked axons and contained lipid accumulations and whorls of myelin.

The morphometric analysis of spinal cords from WT and *Gnpat* KO mice was performed in the ventral funiculus, which encompasses descending tracts. Plasmalogen-deficient mice were characterized by decreased density of myelinated fibers at 21 days (P21), 9 months (9M) and 1.5 years of age (Fig. 3A and C).

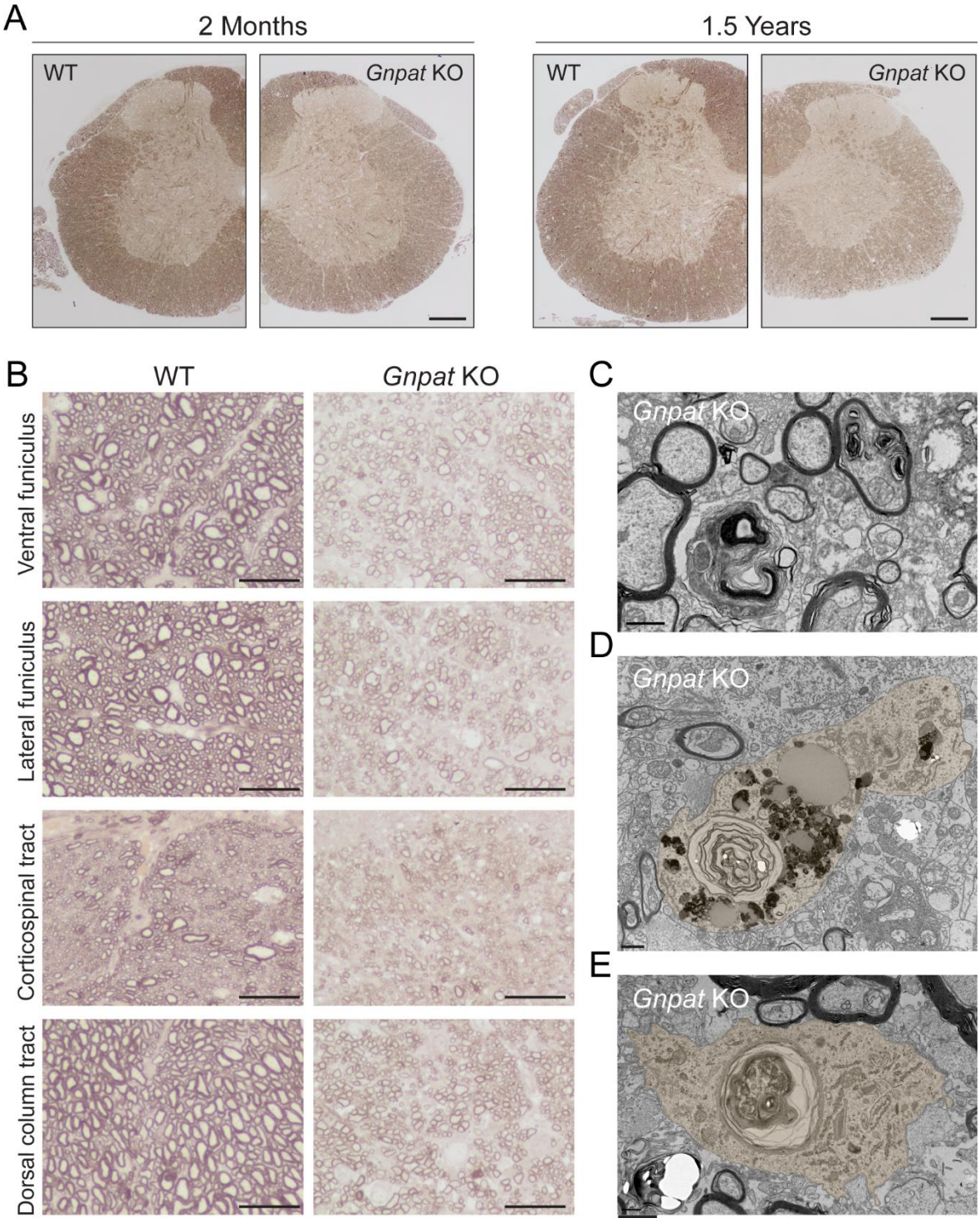

Figure 2. Plasmalogen-deficiency affects myelination in all spinal cord tracts. A Representative images of lumbar spinal cords from WT and *Gnpat* KO mice stained with PPD at 2 months and 1.5 years old mice. **B** Higher magnification of four spinal cord tracts from 1.5 years old mice stained with PPD: ventral funiculus, lateral funiculus, corticospinal tract and dorsal column tract. **C** Electron micrographs of myelin debris in spinal cords from *Gnpat* KO animals. **D** and **E** Electron micrographs of typical phagocytic macrophages (false colored) in *Gnpat* KO spinal cords at 1.5 years old mice. Whorls of myelin, indicative of prior engulfment of myelin, as well as lipid droplets are observed within the cytoplasm of the macrophages. Scale bars are 150µm in A, 25µm in B, 1µm in C, 2µm in D, and 1µm in E.

Surprisingly, at 2 months of age the density of myelinated fibers was normal suggesting that at younger ages there was a delay in the process of myelination (Fig. 3B). However, the determination of the g-ratio revealed that at 2 months of age spinal cords from *Gnpat* KO mice contained less myelin when compared to WT mice (Fig. 3C). Thus, despite reaching a normal density of myelinated axons, the extent of myelination was defective. The analysis also revealed a progressive loss of myelin since higher g-ratios were observed in *Gnpat* KO mice at 1.5 years of age (Fig. 3D). To distinguish if the demyelination observed in spinal cords from aged *Gnpat* KO mice, was due to loss of myelinated axons and/or due to loss of myelin, we performed a detailed ultrastructural analysis. The morphometric analysis (Fig. 3B and E) revealed decreased density of myelinated fibers (MF) and a significant increase of axons completely lacking myelin (un-myelinated fibers (un-MF)) and axons with visible reductions in myelin thickness (hypo-myelinated fibers (hypo-MF)). Given that the total number of axons did not differ between WT and *Gnpat* KO spinal cords, these results indicate that a deficiency in plasmalogens causes a severe loss of myelin, without causing major axonal loss (Fig. 3E). The ultrastructural analysis was crucial for the validation of an active period of myelin loss. Combined, these results demonstrate that a deficiency in plasmalogens causes an initial hypomyelination that progress to a late onset demyelination.

The ultrastructural analysis of optic nerves from WT and *Gnpat* KO mice also revealed the severe consequences of plasmalogen deficiency. Optic nerves from mutant mice at 21 days of age contained axons devoid of myelin (un-myelinated fibers) and axons with reduced amounts of myelin (Fig. 4A). Similarly to what was observed in spinal cord, the morphometric analysis revealed a progressive loss of myelinated fibers with the concomitant increase in axons lacking myelin sheaths (Fig. 4B and C).

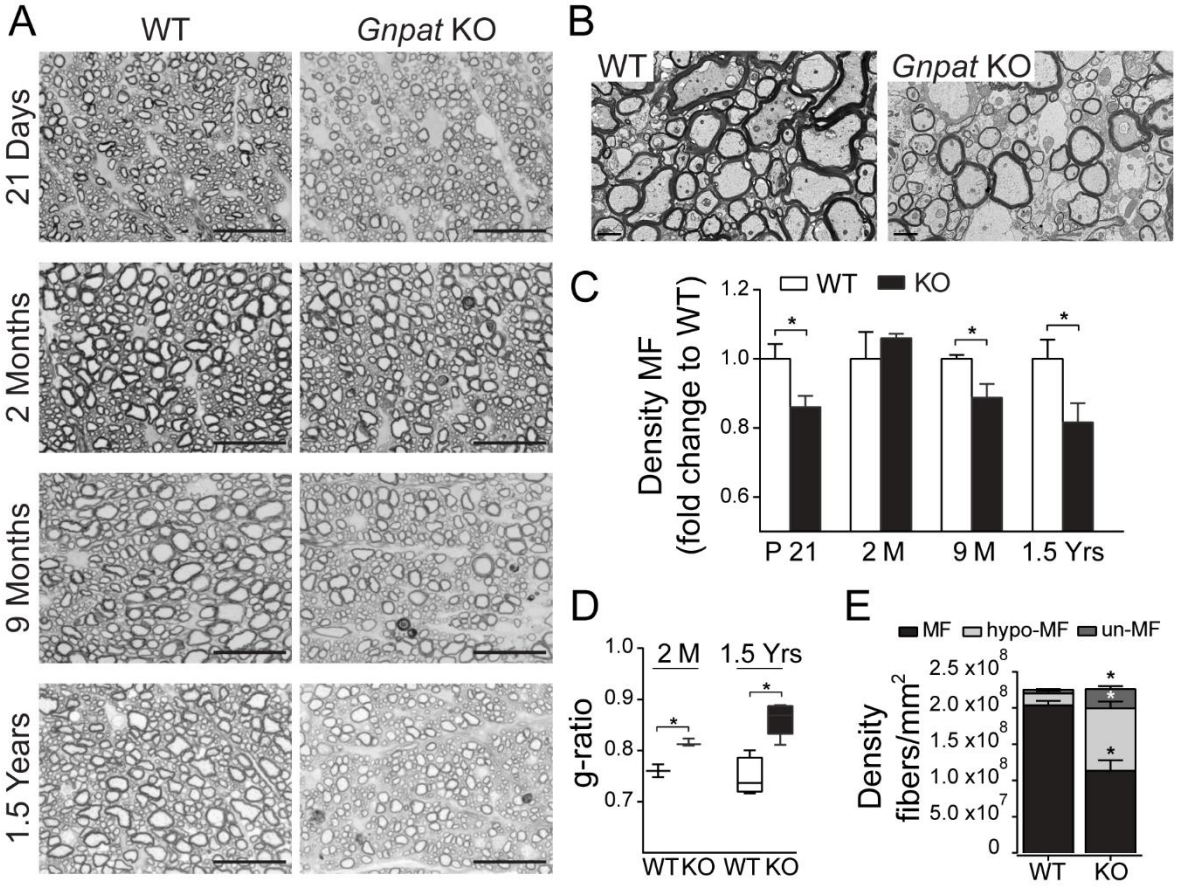

Fig. 3. Morphometric analysis of spinal cord from plasmalogen-deficient mice. A Semi-thin sections of spinal cords stained with PPD in ventral funiculus at 21 days (P21); 2 months (2M) 9 months (9M) and 1.5 years (1.5Yrs) old animals. **B** Electron micrographs of spinal cords of aged mice, revealed that the deficiency in plasmalogens caused a reduced number of myelinated fibers, accompanied with a severe demyelination with drastic reduction in myelin thickness, although un-myelinated axons were present and seemed to be spared. **C** Quantification of density of myelinated fibers (MF) in the ventral funiculus of spinal cords from WT and *Gnpat* KO mice at P21; 2M, 9M and 1.5Yrs. **D** Determination of g-ratio in spinal cords of 2 months and 1.5 years old WT and *Gnpat* KO mice revealed thinner myelin sheaths in mutant mice. **E** Determination of density of myelinated fibers (MF), hypo-myelinated fibers (hypo-MF) and un-myelinated fibers (un-MF), in spinal cord electron micrographs. Student's *T* test in C-E. *$P<0.05$. Scale bars are 25µm in A and 2µm in B.

Measurements of g-ratio confirmed the hypomyelinated status of axons in 2 months old *Gnpat* KO optic nerves and the progressive loss of myelin in aged mice (Fig. 4D). When compared to spinal cord, the optic nerve from *Gnpat* KO mice was more severely affected in terms of myelin loss (Fig. 1 and Fig. 4C). However, the general appearance of axons was better in optic nerves when compared to spinal cords. Completely demyelinated optic nerve axons lacked evident signs of

axonal damage, whereas in spinal cord some axonal damage could be detected (Fig. 3B).

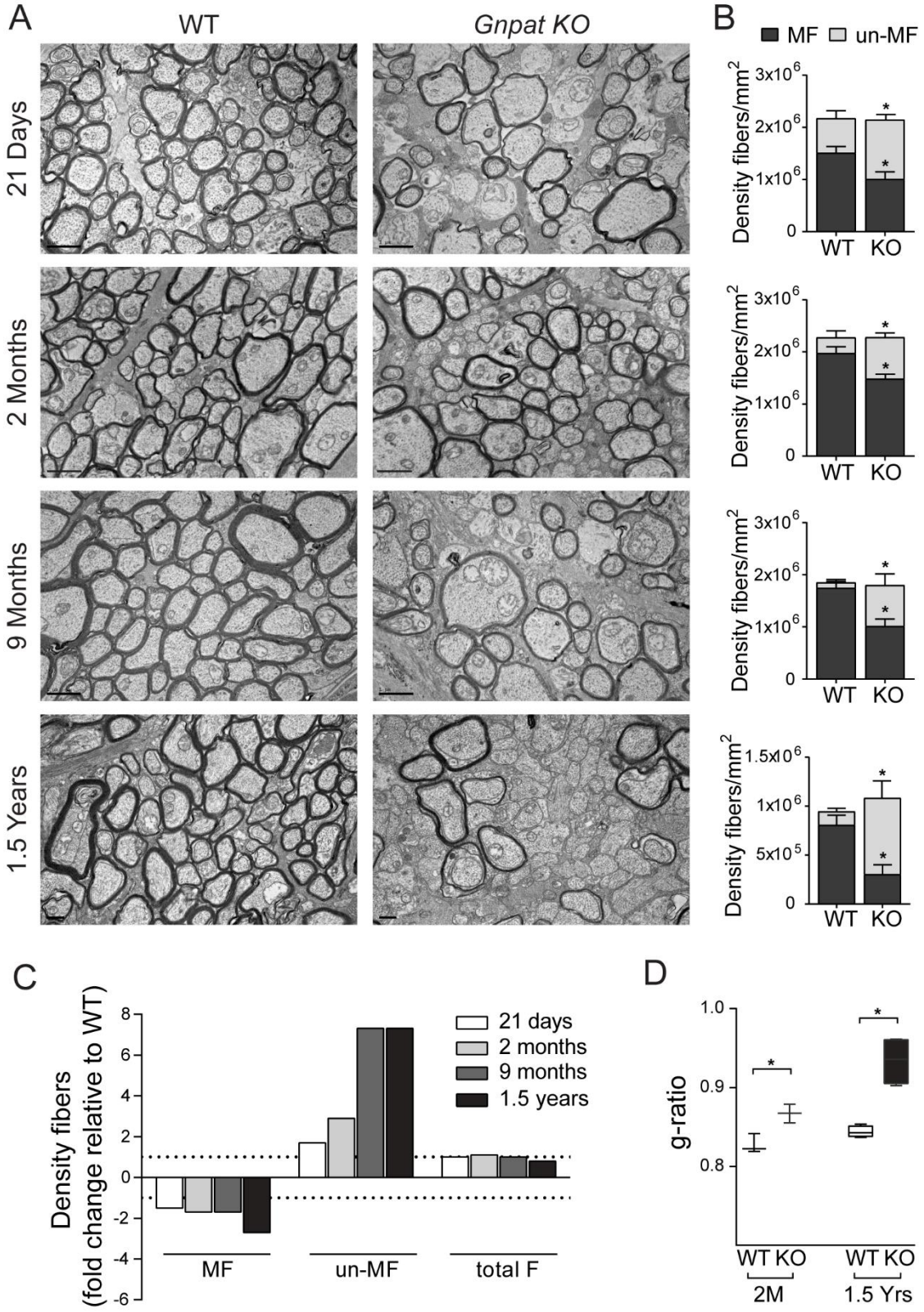

◄Fig. 4. Morphometric analysis of optic nerve from plasmalogen-deficient mice. A Electron micrographs of optic nerves from WT and *Gnpat* KO mice with 21 days (P21); 2 months (2M) 9 months (9M) and 1.5 years (1.5Yrs) old. **B** Quantification of density of myelinated fibers (MF) and non-myelinated fibers (un-MF) in optic nerves from WT and *Gnpat* KO mice at P21; 2M, 9M and 1.5Yrs. **C** Analysis of changes in densities of MF, un-MF and the total fiber count (total F) in optic nerves from WT and *Gnpat* KO mice at P21, 2M, 9M and 1.5 years. **D** g-ratio determination in optic nerves of 2M and 1.5 years old WT and *Gnpat* KO. Student's *T* test in B-D, $n=3-6$ mice per group per time point. *$P<0.05$. Scale bars are 1µm.

Taken together, these results indicate that a plasmalogen deficiency affects the ability of oligodendrocytes to initiate myelination and sustain normal myelin levels in spinal cord and optic nerve.

Targeted and differential composition of plasmalogen-deficient myelin

The deposition of structurally and biochemically normal myelin sheaths around axons is a crucial step for proper myelination. To characterize myelin from plasmalogen-deficient mice, we quantified the levels of seven myelin markers in purified myelin from WT and *Gnpat* KO mice (Fig. 5). During the period of dysmyelination the analysis of myelin isolated from 2M old *Gnpat* KO mice revealed reduced levels of myelin basic protein (MBP) and septin-7 (SEPT7) in spinal cord (Fig. 5A, C) and brain (Fig. 5B, D). However, the abundance of other myelin markers such as 2',3'-cyclic nucleotide 3'-phosphodiesterase (CNPase), myelin-associated glycoprotein (MAG), myelin proteolipid protein (PLP), tubulin polymerization promoting protein (TPPP) and tubulin β-IV were not altered in plasmalogen-deficient myelin (Fig. 5A-D). During the active period of demyelination, myelin isolated from 1.5 years old *Gnpat* KO mice was still characterized by reduced levels of MBP and SEPT7 in both spinal cord (Fig. 5A, C) and brain (Fig. 5B, D). However, levels of MAG were drastically decreased (Fig. 5C, D) whereas the remaining myelin proteins continued to be unaffected.

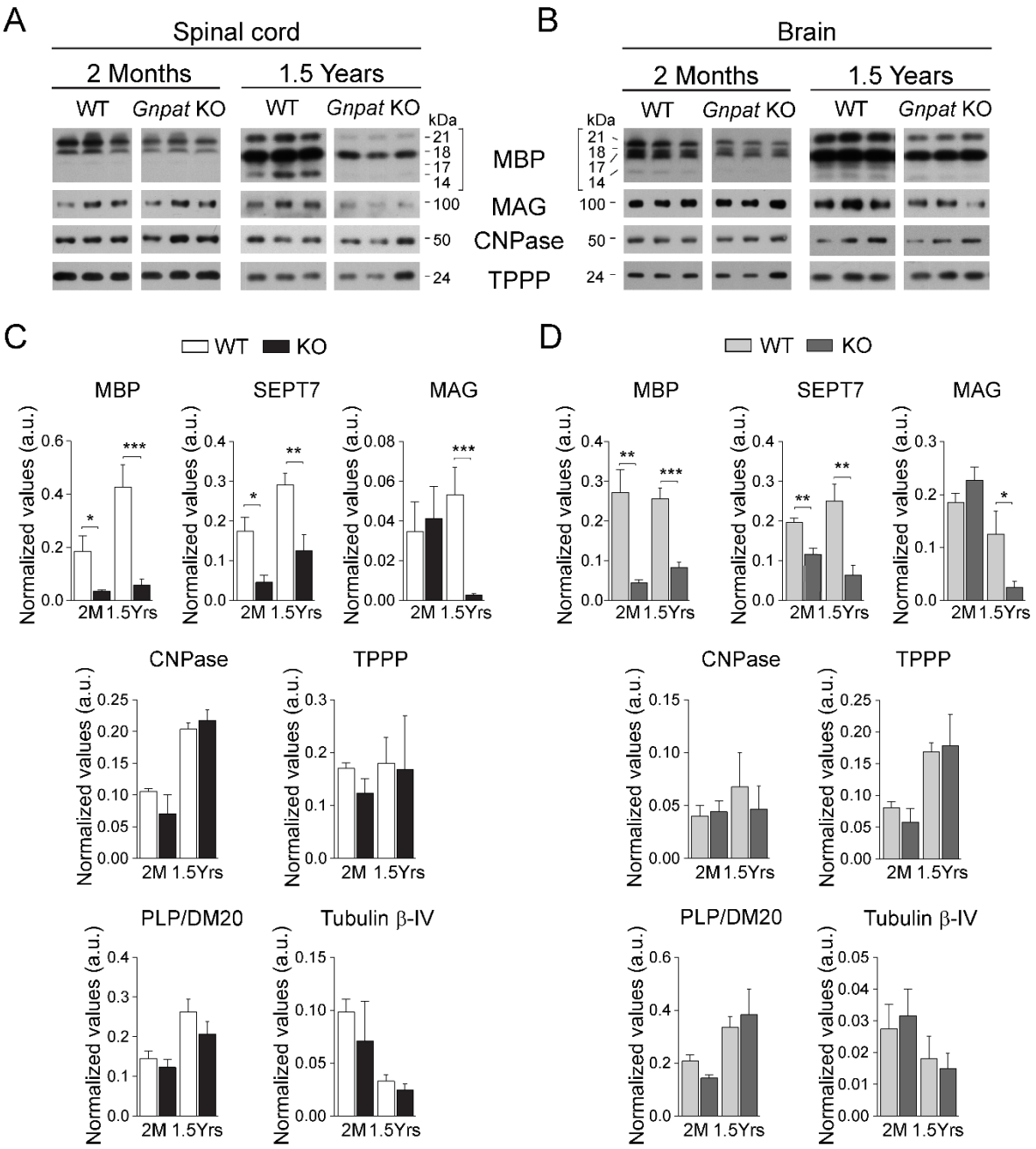

Figure 5. Differential loss of MBP, MAG and SEPT7 in plasmalogen-deficient myelin. A-B Representative western blots of MBP, MAG, CNPase and TPPP in myelin isolated from spinal cord (A) and brain (B) of 2M and 1.5 years old WT and *Gnpat* KO mice. **C** Quantification of MBP, MAG, SEPT7, CNPase, TPPP, PLP/DM20 and tubulin β-IV protein levels normalized to total myelin content in spinal cord-myelin. * P=0.015; ** P=0.005; *** P=0.0005. **D** Quantification of MBP, MAG, SEPT7, CNPase, TPPP, PLP/DM20 and tubulin β-IV protein levels normalized to total myelin content in brain-myelin. * P=0.014; ** P=0.003; *** P=0.0001. Graphs are presented as mean + SEM. n = 4-7 mice per group per time point.

Overall, these results demonstrate that a deficiency in plasmalogens causes a targeted and differential deficiency in myelin protein composition, and suggest that MAG dysregulation in aged myelin may cause or contribute to the progression of demyelination.

Myelination-incompetent oligodendrocytes are maintained in the CNS of *Gnpat* KO mice

The recruitment, proliferation and maturation of oligodendrocyte progenitor cells (OPC) are crucial steps for timely myelination but also remyelination [17]. To determine if the spatiotemporal regulation of OPC was altered in plasmalogen-deficient mice we analyzed the levels of oligodendrocyte transcription factor 2 (Olig-2), and NG2 chondroitin sulphate proteoglycan (NG2) as markers of OPC [18]. Glutathione *S*-transferase pi isoform (GSTπ) and Quaking 7 – clone CC1, were used as markers of differentiated oligodendrocytes [19, 20], in spinal cords of WT and *Gnpat* KO mice. Increased numbers of Olig2- and NG2-positive cells were observed in the white and grey matter of spinal cords from *Gnpat* KO mice from 9 months of age (Fig. 6A-C), suggesting that OPC respond to demyelination and try to compensate the myelin defects. The quantifications of GSTπ- and CC1-positive oligodendrocytes during the course of the disease revealed normal levels at P21 and increased numbers with the onset of demyelination at 9 months of age (Fig. 6D-F). Overall, these results indicate that despite the impaired ability to correctly myelinate the CNS, plasmalogen-deficient oligodendrocytes undergo a normal differentiation process. In addition, the increase numbers of oligodendrocytes during active demyelination suggest failed attempts to rescue myelination. As evidence of this observation, ultrastructural analysis by electron microscopy

revealed the presence of oligodendrocytes in close contact with non-myelinated axons in spinal cord and optic nerves from *Gnpat* KO mice (Fig. 6G).

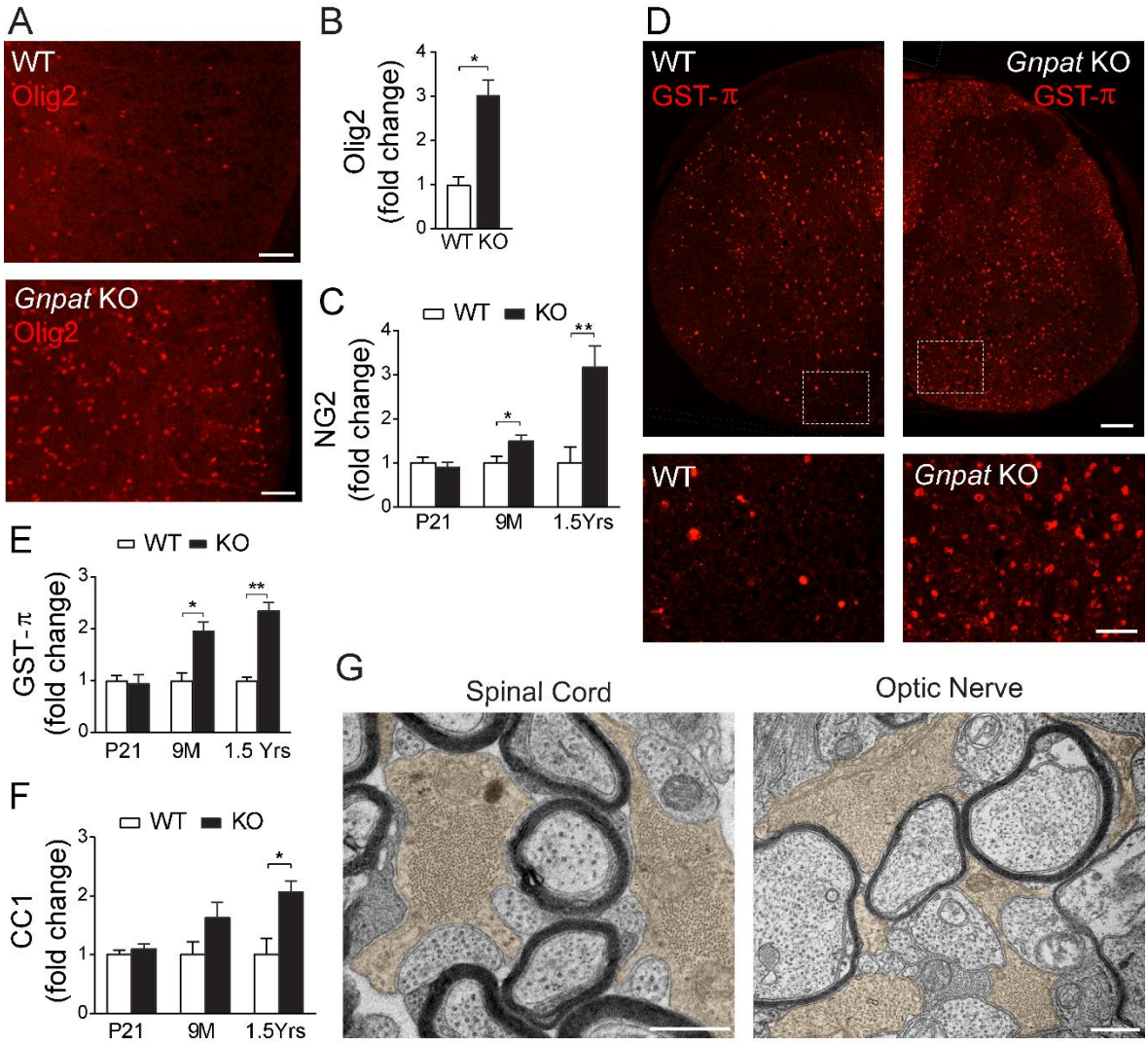

Figure 6. Increased number of OPC and oligodendrocytes during active demyelination in *Gnpat* KO mice. **A** Spinal cord sections from 1.5 years old WT (n=3) and *Gnpat* KO (n=3) mice stained with anti-Olig2 (red). **B** Quantification of Olig2-positive OPC in spinal cords from 1.5 years old WT (n=3) and *Gnpat* KO (n=3) mice. **P*=0.013. **C** Quantification of NG2-positive OPC in spinal cords from WT and *Gnpat* KO mice at P21, 9M and 1.5 years old. * *P*=0.03, ***P*=0.01. **D** Spinal cord sections from 1.5 years old WT and *Gnpat* KO mice stained with GST-π (red) Bottom panels are zoom-in of dotted boxes of upper panels. **E** Quantification of GST-π-positive oligodendrocytes in spinal cords from WT and *Gnpat* KO mice at P21 (n=3 each genotype), 9M (n=6-7 each genotype) and 1.5 years old (n=6-7 each genotype). **P*=0.0017, ***P*=0.0001. **F** Quantification of CC1-positive oligodendrocytes in spinal cords from WT and *Gnpat* KO mice (n=3 each genotype) at P21, 9M and 1.5 years old. **P*=0.02. **G** Ultrastructural analysis by electron microscopy of spinal cord and optic nerve from *Gnpat* KO mice (n=4) revealed the presence of oligodendrocytes (pseudocolored with light brown) associated with non-myelinated axons. Scale bars are 50μm in A, 130μm in large panels and 50μm in small panels in C and 0.5μm in E.

Combined, our results demonstrate that a plasmalogen deficiency does not impair the initial differentiation of oligodendrocytes or their ability to respond to myelin loss and that oligodendrocytes still maintain their role in providing trophic support to axons.

Plasmalogen-deficiency affects the intrinsic capacity of oligodendrocyte to myelinate

To better characterize the process of oligodendrocyte development, we setup an *in vitro* myelination assay using a co-culture system of embryonic cortical neurons and glial cells [21]. In this co-culture system, we were able to identify four types of oligodendrocytes, i.e., highly branched pre-myelinating oligodendrocytes with low MBP expression (Fig. 7A), pre-myelinating oligodendrocytes with high MBP expression (Fig. 7A), myelinating oligodendrocytes with reduced branching and displaying myelin segments (Fig. 7A), and degenerating oligodendrocytes with abnormal morphology and fragmented processes. Quantification of the different populations of oligodendrocytes was performed in WT and *Gnpat* KO co-cultures at 20 days *in vitro* (DIV20) (Fig. 7B). No significant differences were observed in pre-myelinating oligodendrocytes expressing low levels of MBP or in degenerating oligodendrocytes. However, in *Gnpat* KO co-cultures we observed an increase of branched-oligodendrocytes with high levels of MBP and significant decrease of myelinating oligodendrocytes (Fig 7A, B). In addition, we observed that the few myelinating oligodendrocytes in *Gnpat* KO co-cultures displayed shorter myelin segments (Fig. 7A). Measurement of myelin segment length was reduced in *Gnpat* KO co-cultures (Fig. 7C). Corroborating the *in vivo* findings, these results indicate that a plasmalogen deficiency affected oligodendrocyte differentiation during the final stages of maturation with a halted initiation of myelin sheaths.

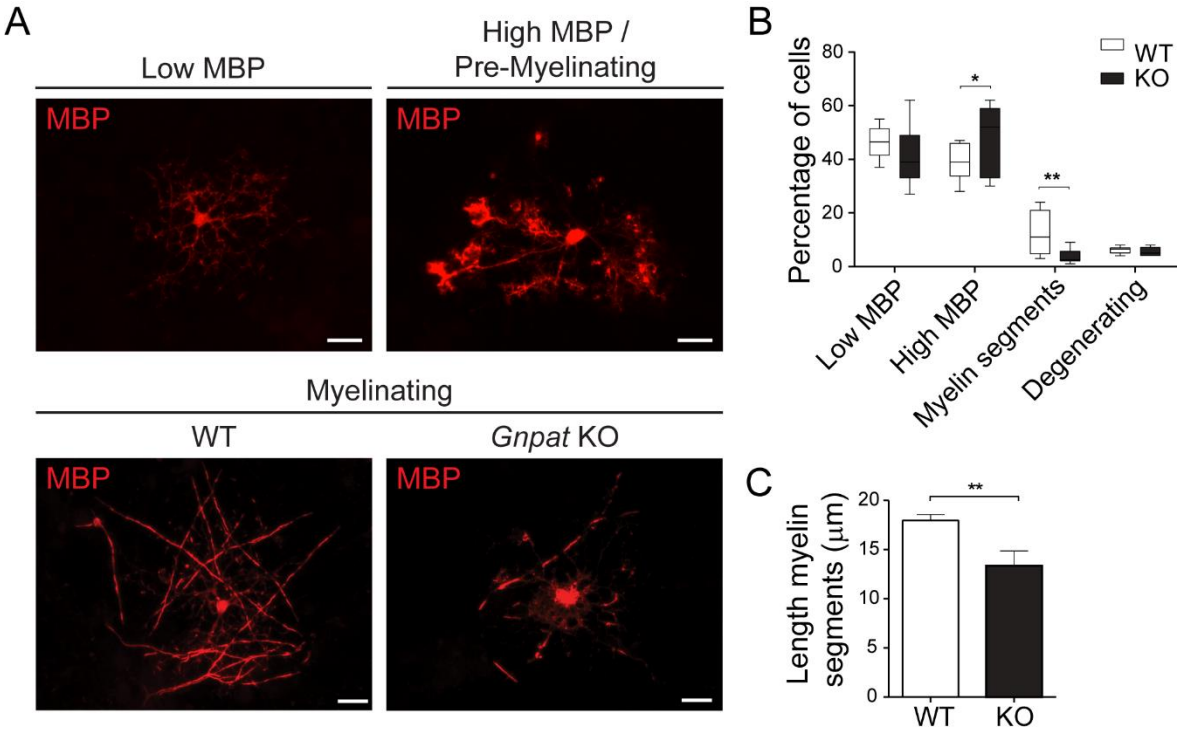
A
Low MBP
High MBP / Pre-Myelinating
MBP
MBP
Myelinating
WT
Gnpat KO
MBP
MBP
B
Percentage of cells
80
60
40
20
0
WT
KO
*
**
Low MBP
High MBP
Myelin segments
Degenerating
C
Length myelin segments (µm)
20
15
10
5
0
**
WT
KO

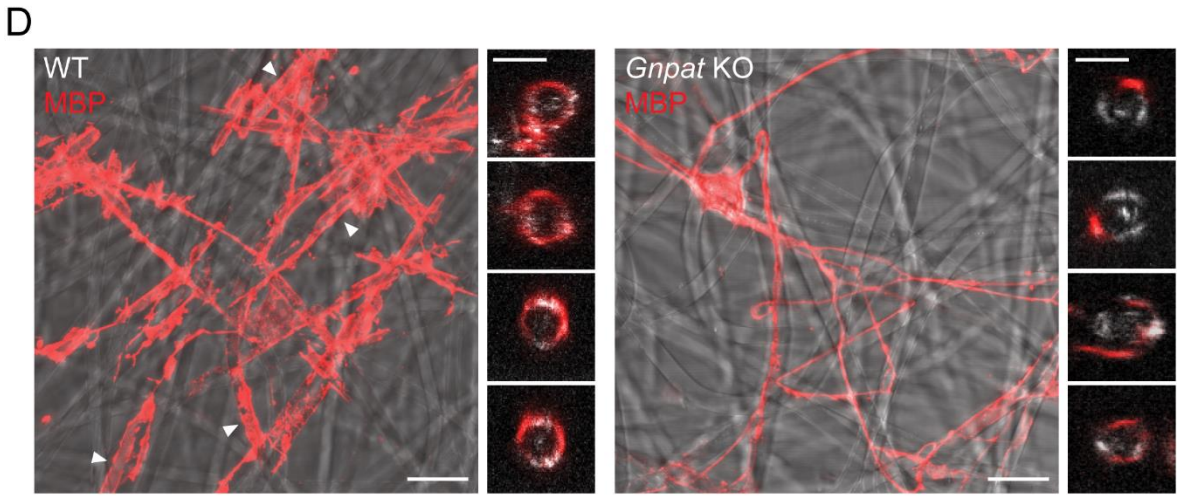
D
WT
MBP
Gnpat KO
MBP

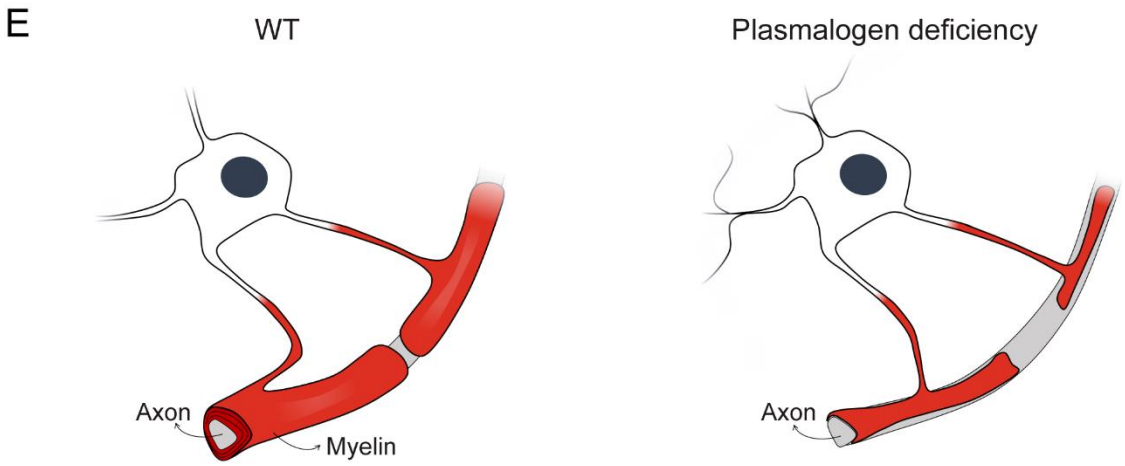
E
WT
Plasmalogen deficiency
Axon
Myelin
Axon

◄**Figure 7. *in vitro* myelination assays reveal oligodendrocyte intrinsic defects. A** *in vitro* myelination of mixed cortical co-cultures from WT and *Gnpat* KO mice at DIV20. Oligodendrocytes were stained with anti-MBP (red). Highly ramified pre-myelinating oligodendrocytes contained low or high levels of MBP (upper panels) whereas myelinating oligodendrocytes displayed reduced branches and myelin segments (bottom panels). Scale bars are 20µm. **B** Quantification of oligodendrocytes during different stages of differentiation in WT and *Gnpat* KO co-cultures (n=4 for each genotype). Data presented as boxes that extend from the 25th to 75th percentiles, with a line at the mean. Whiskers represent the minimal and maximal values. **P*=0.04; ***P*=0.006 using student's T-test. **C** Quantification of the length of myelin segments in myelinating oligodendrocytes from WT and *Gnpat* KO mice (n=4 for each genotype). **P*=0.014. Data presented as mean + SEM and compared using student's T-test. **D** Confocal images of oligodendrocytes from WT and *Gnpat* KO mice (n=3 for each genotype) at DIV12 plated onto electrospun poly-L-lactide microfibers and immunolabeled for MBP (red). Myelin segments produced by WT oligodendrocytes are highlighted with arrowheads. Small panels on the right of WT and *Gnpat* KO images are magnified and cross-section (xz) views of WT oligodendrocytes engulfing microfibers and *Gnpat* KO oligodendrocytes extending single processes that do not engulf the microfiber. Scale bars are 20µm in large panels and 4µm in small panels. **E** Schematic representation of a proposed model depicting the consequences of plasmalogen deficiency in the CNS myelination.

In order to distinguish between oligodendrocyte-driven versus axon-instructed defects, we cultured mouse primary cortical oligodendrocytes on electrospun poly-L-lactide microfibers. In this neuron-free and three-dimensional culture system, the microfibers serve as a scaffold for oligodendrocytes to extend and wrap their processes around them [22]. After DIV12, we analyzed the differentiation of WT and *Gnpat* KO oligodendrocytes and their ability to myelinate the microfibers. We observed that WT oligodendrocytes were able to ensheath and wrap the microfibers, with the formation of thick MBP segments (Fig. 7D). Oligodendrocytes from *Gnpat* KO mice, despite being able to extend processes were not capable of wrapping the microfibers (Fig. 7D). In summary, these results demonstrate that the lack plasmalogens affects the intrinsic capacity of oligodendrocytes to myelinate (Fig. 7E).

Discussion

Here, we unraveled the role of plasmalogens in CNS myelin and during myelination using a mouse model for RCDP. We demonstrate that differentiated oligodendrocytes are the prime target of a deficiency in plasmalogens causing impaired myelination and myelin maintenance. During development, OPC migrate to reach their final destination, and terminate their differentiation into myelin-forming oligodendrocytes [23]. The regulation of these two processes is crucial to ensure adequate numbers of OPC, and consequently appropriate numbers of myelinating oligodendrocytes [24]. Assessment of OPC and oligodendrocyte numbers during the early postnatal period, revealed normal densities in spinal cords and optic nerves from *Gnpat* KO mice, suggesting that the impaired myelination was not caused by defects in OPC migration. The lack of plasmalogens in oligodendrocytes from *Gnpat* KO mice did not affect the initial stages of differentiation. Oligodendrocytes from *Gnpat* KO mice expressed GST-π and CC1, markers of mature oligodendrocytes [18], and *in vitro* assays showed normal oligodendrocyte development up to the final stages of maturation and myelin assembly. The dynamic interplay of intrinsic mechanisms in oligodendrocytes, and axon-derived extrinsic signals, are crucial steps for the suitable balance between differentiation and myelination [25]. Several extrinsic signals derived from axons impact oligodendrocyte's terminal differentiation [26], promote myelination [27], or regulate myelin thickness [28]. Using *in vitro* myelination assays, we identified that only a reduced number of plasmalogen-deficient oligodendrocytes are able to assemble shorter and scarcer myelin sheaths around axons. Using scaffolds of microfibers, we were able to unravel that the defect in assembling myelin sheaths was caused by a compromised intrinsic capacity of plasmalogen-deficient oligodendrocytes to ensheath and assemble myelin segments (Fig. 6E).

In adult mice, the lack of plasmalogens continued to have a negative impact on myelin content throughout the CNS, as evidenced by increased g-ratio and the progressive increase in the density of axons lacking myelin sheaths. These myelin defects correlate with the neurological phenotype of *Gnpat* KO mice. From the age of 9 months, *Gnpat* KO mice start developing a severe and progressive neurological condition that includes tremors and generalized ataxia. This phenotype worsens after 1 year of age with increased tremor frequency and limb paralysis. This led us to hypothesize that altered myelin composition could contribute to the failure in attaining correct myelination and the sustainment of myelin. Differential expression MBP, SEPT7 and MAG was observed in plasmalogen-deficient myelin. Decreased levels of MBP and SEPT7 were observed during the initial hypomyelination. MBP is known to be essential in initiating and driving the axonal wrapping process, myelin compaction and the maintenance of the physical stability of the sheaths [29, 30]. Interestingly, plasmalogens and MBP are two major constituents of myelin at the cytoplasmic apposition [31, 32]. Thus, the complete absence of plasmalogens, together with the decreased levels of MBP could be the major cause of inadequate formation of the myelin sheath, and consequently impaired myelination. The enrichment of septins in mature myelin [33-35], together with the reported importance of septins in myelin disorders, reflects a general association between the abundance of septins and myelin pathology. Recently, it has been described that the presence of myelin outfoldings, a common feature observed in several myelin-related disorders, correlates with a loss of cytoskeletal septins in myelin [36]. Septin filaments are localized to the non-compacted adaxonal myelin compartment, and were judged to be important for scaffolding the axon/myelin-unit at a late stage of myelin maturation [36]. Here we reported that plasmalogen-deficient myelin is characterized by reduced levels of SEPT7. The association of septins with phospholipids was found to be crucial for

the formation and maintenance of membrane domains [37]. Our results underscore a possible role of plasmalogens on correct septin location. Moreover, the intimate relationship between septins and actin cytoskeleton [38, 39], together with the well-known function of actin on myelination [40, 41], may also correlate the decreased levels of SEPT7 and defective myelination. Whereas MBP and SEPT7 levels were consistently reduced in plasmalogen-deficient myelin, the levels of MAG display an additional differential pattern of expression. During the period of hypomyelination, MAG levels were normal in myelin from *Gnpat* KO mice but during the period of demyelination MAG levels decreased in plasmalogen-deficient myelin. MAG is a myelin protein preferentially expressed on the innermost myelin wrap, adjacent to the axon [42]. Analysis of MAG null mutants revealed a surprisingly subtle phenotype, which included mild myelin abnormalities and the lack of a periaxonal cytoplasmic collar [43, 44]. These observations suggest that MAG plays a role in stabilizing oligodendrocyte-axon contacts in mature myelin sheaths, which may be involved in the long-term stability of axons [45]. Therefore, the decreased levels of MAG in plasmalogen-deficient myelin may disturb the myelin-axon stability and lead to the development of the axonal outfoldings observed in *Gnpat* KO axons (for details see Chapter 3). Combined with the reduced levels of SEPT7, we hypothesize that the abnormal myelin composition observed in aged *Gnpat* KO mice, could be the trigger for demyelination and for the engulfment of axonal protrusions that result in the accumulation of the vesicle-like structures.

In summary, our findings substantially increase the understanding of plasmalogens functions in the CNS and highlight that the lack of plasmalogens causes a myelin disorder. The identification of the primary and intrinsic involvement of oligodendrocytes in myelin pathology, combined with the available imaging data of RCDP patients supports the future elucidation of RCDP as a complex leukodystrophy.

Material and Methods

Animal experiments

All procedures made in mice were done according to the European Directive 2010/63/EU established by the European Parliament and of the Council, as well as the National legislation (Decreto-Lei 113/2013). Mice were used only after approval of the Portuguese General Veterinarian Board.

Mouse models

Gnpat KO mice and WT littermates were obtained from mating *Gnpat* heterozygous mice (on a Swiss-Webster background). All animals were maintained with ad libitum access to rodent food and water, and were kept in a 12:12h light and dark cycle facility. Genotyping was performed by the IBMC CCGen facility using previously developed strategies [16].

Histological and morphological analysis

Mice were anesthetized with ketamine/medetomidine mixture (75mg/kg and 1mg/kg body weight, respectively) and lumbar spinal cord, optic nerve and brain were isolated and fixed by immersion. For morphometric analysis, tissues were fixed in 4% glutaraldehyde in 0.1M sodium cacodylate buffer (pH 7.4) for 5 days and processed as previously described [46]. In spinal cords, the region chosen for analysis was the ventral funiculus, immediately adjacent to the ventromedian fissure. Semi-thin sections were cut at 1µm, stained with 1% p-phenylenediamine (PPD), and used to determine density of myelinated fibers. Ultrathin sections were processed for ultrastructural analysis as described [46]. For g-ratio determination, the axonal diameter and the myelin sheath thickness were measured (four measurements per fiber; one hundred fifty fibers per mouse). Pseudocolored electron microscopy images were processed in Photoshop CS3, by selecting the

region of interest and applying color with transparency, in order to highlight the region to be analyzed.

For immunohistochemistry, tissues were fixed by immersion in modified Carnoy's solution (absolute ethanol: methanol: glacial acetic acid – 6:3:1) for 2 hr, processed for paraffin embedding, sectioned at 4µm, cleared and rehydrated. Sections were permeabilized in 100% methanol, treated with 0.1% $NaBH_4$ in 10mM Tris, 1mM EDTA at pH 9.0, and blocked with 5% normal donkey serum (NDS) in PBS. Primary antibodies (Table.1) were diluted in 5% NDS in PBS and incubated over night at 4°C. Secondary antibodies, either biotinylated or conjugated with Alexa Fluor (Jackson ImmunoResearch Europe, Lda.), were diluted in 5% NDS in PBS and incubated at room temperature (RT) for 1 hr. The quantifications were performed using Feature J, a java-based plug-in of the imaging software NIH Image J, using a Hessian-based algorithm [47].

Table 1. List of antibodies used.

Antigen	Company	Catalog	Host	Dilution	Purpose*	Antigen retrival**
Oligodendrocyte transcription factor 2 (Olig-2)	Proteintech	13999-1-AP	rabbit	1:300	IHC	TE solution pH 9.0
Glutatione S-transferase (GST)-pi (GST-π)	MBL Life Science	MBL-311	rabbit	1:1000	IHC	Trypsin 0.05% EDTA
NG2 chondroitin sulphate proteoglycan (NG2)	Proteintech	55027-1-AP	rabbit	1:200	IHC	TE solution pH 9.0
Oligodendrocyte marker clone CC1 (Quaking 7)	Merk	OP80/ clone CC-1	mouse	5µg/ml	IHC	Citrate solution pH 6.0
Myelin basic protein (MBP)	Santa Cruz Biotech.	sc-13914	goat	1:5000	WB	N.A.
	Milipore	MAB386	rat	1:250	IF	N.A.
Tubulin β-III	Synaptic Systems	302302	rabbit	1:500	IF	N.A.
Tubulin β-IV	Sigma-Aldrich	T7941	mouse	1:500	WB	N.A.
Myelin-associated glycoprotein (MAG)	Santa Cruz Biotech.	sc-15324	rabbit	1:1000	WB	N.A.
2',3'-cyclic nucleotide 3'-phosphodiesterase (CNPase)	Thermo Fisher Scientific	MS-349-P1	mouse	2µg/ml	WB	N.A.
Tubulin polymerization promoting protein (TPPP)	Abcam	ab92305	rabbit	1:10000	WB	N.A.
Septin 7 (SEPT7)	Proteintech	13818-1-AP	rabbit	1:2000	WB	N.A.
Proteolipid protein (PLP/DM20)	Abcam	ab105784	rabbit	1µg/ml	WB	N.A.

* IHC: immunohistochemistry; WB: western blot; IF: immunocitofluorescence

** Heat mediated antigen retrieval was performed by boiling slides in the appropriate solutions. TE solution: 10mM Tris, 1mM EDTA pH 9.0; Citrate solution: 10mM sodium citrate buffer pH 6.0; trypsin:0.05%EDTA 1x solution (Invitrogen, cat #25300-062).

N.A. not applicable

Myelin isolation and purification

Myelin was isolated using two rounds of a discontinuous sucrose gradient, adapted from a previous protocol developed by Norton and Poduslo [48]. For these experiments we used ½ cerebrum and the thoracic and cervical portion of the spinal cord from 2 months and 1.5 years old WT and *Gnpat* KO mice. It was important that all solutions and materials were kept on ice. The brains and spinal cords were homogenized separately in ice cold 0.32M sucrose using a mechanical overhead stirrer (Heidolph, Fisher Scientific, North America) followed by a centrifugation to clean the homogenate from tissue debris. In a tube, the supernatant was carefully layered over a layer of 0.85M sucrose, and centrifuged at 75,000g, using a swingout rotor (SW 31 TI, Beckman ultracentrifuge, North America), for 45 min at 4°C. A layer of crude myelin was formed at the interface of the two sucrose solutions. Myelin was removed using a glass pipette, transferred into an ice cold 26.3ml tube and filled with ice cold distilled water to purify the crude myelin by osmotic shock. Afterwards, the tubes were centrifuged at 20,000g in a fixed angle rotor (70.0 TI, Beckman ultracentrifuge, North America) for 15 min at 4°C. Supernatant was discarded, and the pellet was resuspend in 0.32M sucrose, and again layered on a new layer of 0.85M sucrose and centrifuged as described above. A second osmotic shock was performed, after centrifugation, the pellet was resuspend in distilled water and transferred to a 1.5ml tube and centrifuged at 21,000 g at 4°C for 15min. The myelin pellet was kept at -80°C with only a drop or two of water covering the pellet to prevent lyophilization.

Western blots

Isolated myelin from brain and spinal cord was sonicated with PBS containing 1.5% SDS, 0.5% sodium carbonate (Na_2CO_3) and protease inhibitor cocktail (Roche). The samples (2μg of total protein) were separated by SDS-PAGE gels using TGX

Stain-Free™ FastCast™ 12% acrylamide (Bio-Rad) and analyzed using a ChemiDoc imaging system, in order to quantify the total myelin protein. After the proteins were transferred onto nitrocellulose membranes, the membranes were blocked with 5% skim milk (Fluka) in Tris-buffered saline with 1% Tween 20 (TBS-T) for 1h at RT, washed with TBS-T, and probed with different primary antibodies (as shown in Table 1) diluted in 5% BSA + TBS-T (overnight at 4ºC). HRP-labeled secondary antibodies were diluted 1:5000 in 5% skim milk in TBS-T and incubated for 1h at RT. Membranes were developed using ECL (Luminata Crescendo Western HRP Substrate, Milipore). Using Quantity One 4.6.9 software it was possible to scan, using a Molecular Imager GS800, and quantify the blots for further analysis.

Mixed cortical neuron-glial culture

Mixed cortical neuron-glial culture was performed as described [21], with minor alterations. Cortical neurons and glial cells were isolated from mouse embryos, at embryonic day 16-18 (E16-18). Brains were dissected from individually embryos of WT and *Gnpat* KO embryos, and were cleaned from meningeal shreds and superficial blood vessels to allow the cortices to be further dissected and collected in HBSS. The cortices were then washed with DMEM:F12 before incubation with 0.05% Trypsin + 0.2mg/ml EDTA for 8 min at 37ºC. Digestion was stopped by adding DMEM:F12 + 10% FBS, centrifuged at 1700 rpm. The supernatant was removed and the pellet of cortices was resuspend and dissociated in DMEM:F12. The cell suspension was passed through a 70μm strainer and centrifuged at 1700 rpm. The supernatant was removed and replaced with neuron culture medium (Neurobasal medium with 2x B27 supplement, 0.1mM L-glutamine and 1% penicillin-streptomycin). The number of cells present in the suspension was counted using trypan blue-exclusion, and cells were plated at a density of $1.5x10^5$ cells/well onto glass coverslips within 24-well plates, previously

coated with Poly-L-Lysine (20µg/ml in PBS, P2636 Sigma) and laminin (2µg/ml in PBS, L2020-1MG Sigma). Cells were allowed to settle for 30min at 37°C before removing the complete medium and adding a new slightly different plating medium (Neurobasal medium with 1x N21 supplement, 2mM L-glutamine, 1% penicillin-streptomycin). New medium was added every 2 days, and neurons were able to adhere, mature and extend axons for 5 days. At 6 days *in vitro* (DIV), half of the plating medium in each well was removed and the same amount of myelination medium (MyM) was added [49]. The cultures were maintained at 37°C until DIV 20 by adding new myelination medium every 2 days. The cells were fixed at DIV 20 with 4% PFA, and immunolabeled with Tubulin-β -III (for neurons) and myelin basic protein (MBP, for oligodendrocytes, OLs). The fixed and permeabilized cells were incubated for 1 hour at RT with blocking buffer (5% NDS in PBS). Primary antibodies (rabbit anti-βIII-tubulin and rat anti-MBP; see Table 1) were diluted in blocking buffer and incubated for 16 hours at 4°C. After washing with PBS, secondary antibodies were diluted in blocking buffer and incubated for 1 hour at RT. After washing, coverslides were mounted on microscope slides with Fluoroshield with DAPI (F6057, Sigma). Slides were analyzed by epifluorescence on a Zeiss Axio Imager Z1 microscope equipped with an Axiocam MR3.0 camera and Axiovision 4.7 software.

The entire area of the glass coverslip (1,32cm^2) was analyzed and the total number of MBP$^+$ cells (OLs with low levels of MBP, OLs with high levels of MBP, OLs with assembled MBP segments and degenerating OLs) were counted.

Primary OPC cultures

The preparation of mixed glial cell cultures (MGCs, source cultures) was performed as described [50], with some modifications. Neurons and glial cells were isolated from mouse brain hemispheres, at post-natal day 2 (P2). Brains were

dissected from individually WT and *Gnpat* KO embryos, and were cleaned from meningeal shreds and superficial blood vessels to allow the brain hemispheres to be further dissected and collected in HBSS. The brain hemispheres were then washed and digested in 0.05% Trypsin + 0.2mg/ml EDTA, and incubated for 15 min at 37 °C. The enzymatic reaction was terminated with DMEM high glucose containing 10% FBS. The tissue was triturated with a 5ml Pasteur pipette in plating medium (10% fetal bovine serum and 1% penicillin-streptomycin in DMEM high glucose). All cells were seeded onto 25 cm^2 flasks pre-coated with 50µg/ml Poly-D-lysine (PDL; P0899 Sigma), and allowed to grow for 9 days. To obtain pure OPCs, MGCs at DIV 10 were pre-shaken at 70 rpm for 2 hours in a INFORS HT Minitron incubator with a radius of 2.5 cm at 37°C (to remove the majority of microglial cells). Then, each culture flask (with 3 ml of fresh medium) was placed into a culture chamber and allowed to equilibrate with the CO_2-air atmosphere for 2 h. After, the flasks were shaken at 120 rpm during for 15-18 h. Following the shaking period, the suspended cells (oligodendroglia fraction) from all flasks were collected, pooled and resuspended in SATO 1x (SATO 10x with 10ng/ml Human FGF basic (100-18B, PeproTech), 10ng/ml PDGF-AA (100-13A, PeproTech), 5µg/ml insulin (I5500, Sigma) and 1% P/S in DMEM high glucose). SATO 10x is composed by: 600ng/ml progesterone (P8783, Sigma), 400ng/ml sodium selenite (214485, Sigma), 400ng/ml thyroxine (T1775, Sigma), 300ng/ml thiiodo-L-thyronine (T6397, Sigma), 1mg/ml Transferrin (T2036, Sigma), 1mg/ml BSA (A3294, Sigma) and 160ug/ml Putrescine (P5780). Viable cells were seeded onto scaffold discs with a random fiber orientation (The Electrospinning Company Ltd, TECL003-1x). The scaffolds were pre-coated with Poly-L-lysine (100µg/ml; P2636 Sigma) and cells were plated at a density of 15,000 cells/ scaffold. Differentiation was induced at DIV 4 with the removal of PDFG and FGF from medium, and with the addition of 0,5% Fetal Bovine Serum (FBS). In the following days, and every two

days, two-thirds of the medium was replaced with fresh medium. The cells were fixed at DIV 12 with 4% PFA, and immunolabeled with MBP. The fixed and permeabilized cells were incubated for 1 hour at RT with blocking buffer (5% NDS in PBS). Primary antibody (rat anti-MBP; see Table 1) were diluted in blocking buffer and incubated for 16 hours at 4°C. After washing with PBS, secondary antibody was diluted in blocking buffer and incubated for 1 hour at RT. After washing, scaffold discs were mounted on microscope slides with Fluoroshield with DAPI (F6057, Sigma). Cells were viewed on a Laser Scanning confocal microscope Leica TCS SP5 II (Leica Microsystems, Germany) using a 63x magnification objective with a z-step of 0.013µm. For increased z-definition of the poly-L-lactide fibers, we made use of the refraction capability of the confocal microscope using the 405nm laser line at full power, and a detector in the same emission spectrum region. Finally, the cross view of myelinated segments was accomplished by the usage of the orthogonal view function of Fiji.

Statistics analysis

All data were analyzed using GraphPad Prism software, and results are expressed as mean + S.E.M. To compare two different groups, Student's T test (unpaired, two-tailed) was used and $P < 0.05$ was considered a significant difference. For multiple comparisons, one-way ANOVA test was used, followed by Tukey's multiple comparison tests.

Bibliography

1. Vanderver, A., et al., *Case definition and classification of leukodystrophies and leukoencephalopathies.* Mol Genet Metab, 2015. **114**(4): p. 494-500.
2. Nave, K.A. and H.B. Werner, *Myelination of the nervous system: mechanisms and functions.* Annu Rev Cell Dev Biol, 2014. **30**: p. 503-33.
3. Norton, W.T. and S.E. Poduslo, *Myelination in rat brain: changes in myelin composition during brain maturation.* J Neurochem, 1973. **21**(4): p. 759-73.
4. Snyder, F., *The ether lipid trail: a historical perspective.* Biochim Biophys Acta, 1999. **1436**(3): p. 265-78.
5. Wanders, R.J. and H.R. Waterham, *Biochemistry of mammalian peroxisomes revisited.* Annu Rev Biochem, 2006. **75**: p. 295-332.
6. Baroy, T., et al., *A novel type of rhizomelic chondrodysplasia punctata, RCDP5, is caused by loss of the PEX5 long isoform.* Human Molecular Genetics, 2015. **24**(20): p. 5845-5854.
7. Braverman, N.E. and A.B. Moser, *Functions of plasmalogen lipids in health and disease.* Biochim Biophys Acta, 2012. **1822**(9): p. 1442-52.
8. Buchert, R., et al., *A peroxisomal disorder of severe intellectual disability, epilepsy, and cataracts due to fatty acyl-CoA reductase 1 deficiency.* Am J Hum Genet, 2014. **95**(5): p. 602-10.
9. White, A.L., et al., *Natural history of rhizomelic chondrodysplasia punctata.* Am J Med Genet A, 2003. **118A**(4): p. 332-42.
10. Bams-Mengerink, A.M., et al., *MRI of the brain and cervical spinal cord in rhizomelic chondrodysplasia punctata.* Neurology, 2006. **66**(6): p. 798-803; discussion 789.
11. Khanna, A.J., et al., *Cervical stenosis secondary to rhizomelic chondrodysplasia punctata.* Am J Med Genet, 2001. **99**(1): p. 63-6.

12. Alkan, A., et al., *Delayed myelination in a rhizomelic chondrodysplasia punctata case: MR spectroscopy findings.* Magn Reson Imaging, 2003. **21**(1): p. 77-80.
13. Powers, J.M., et al., *Cerebellar atrophy in chronic rhizomelic chondrodysplasia punctata: a potential role for phytanic acid and calcium in the death of its Purkinje cells.* Acta Neuropathol, 1999. **98**(2): p. 129-34.
14. Bams-Mengerink, A.M., et al., *The neurology of rhizomelic chondrodysplasia punctata.* Orphanet J Rare Dis, 2013. **8**: p. 174.
15. da Silva, T.F., et al., *The importance of ether-phospholipids: a view from the perspective of mouse models.* Biochim Biophys Acta, 2012. **1822**(9): p. 1501-8.
16. Rodemer, C., et al., *Inactivation of ether lipid biosynthesis causes male infertility, defects in eye development and optic nerve hypoplasia in mice.* Hum Mol Genet, 2003. **12**(15): p. 1881-95.
17. Bergles, D.E. and W.D. Richardson, *Oligodendrocyte Development and Plasticity.* Cold Spring Harb Perspect Biol, 2015. **8**(2): p. a020453.
18. Billon, N., et al., *Normal timing of oligodendrocyte development from genetically engineered, lineage-selectable mouse ES cells.* Journal of Cell Science, 2002. **115**(18): p. 3657-3665.
19. Miyamoto, N., et al., *Astrocytes Promote Oligodendrogenesis after White Matter Damage via Brain-Derived Neurotrophic Factor.* J Neurosci, 2015. **35**(41): p. 14002-8.
20. Bin, J.M., S.N. Harris, and T.E. Kennedy, *The oligodendrocyte-specific antibody 'CC1' binds Quaking 7.* J Neurochem, 2016. **139**(2): p. 181-186.
21. Lariosa-Willingham, K.D., et al., *Development of a central nervous system axonal myelination assay for high throughput screening.* BMC Neurosci, 2016. **17**: p. 16.

22. Lee, S., et al., *A rapid and reproducible assay for modeling myelination by oligodendrocytes using engineered nanofibers.* Nat Protoc, 2013. **8**(4): p. 771-82.

23. Trapp, B.D., et al., *Differentiation and death of premyelinating oligodendrocytes in developing rodent brain.* J Cell Biol, 1997. **137**(2): p. 459-68.

24. Mitew, S., et al., *Mechanisms regulating the development of oligodendrocytes and central nervous system myelin.* Neuroscience, 2014. **276**: p. 29-47.

25. Emery, B., *Regulation of oligodendrocyte differentiation and myelination.* Science, 2010. **330**(6005): p. 779-82.

26. Ishibashi, T., et al., *Astrocytes promote myelination in response to electrical impulses.* Neuron, 2006. **49**(6): p. 823-32.

27. Bauer, N.G., C. Richter-Landsberg, and C. Ffrench-Constant, *Role of the oligodendroglial cytoskeleton in differentiation and myelination.* Glia, 2009. **57**(16): p. 1691-705.

28. Taveggia, C., et al., *Type III neuregulin-1 promotes oligodendrocyte myelination.* Glia, 2008. **56**(3): p. 284-93.

29. Weil, M.T., et al., *Loss of Myelin Basic Protein Function Triggers Myelin Breakdown in Models of Demyelinating Diseases.* Cell Rep, 2016. **16**(2): p. 314-22.

30. Snaidero, N., et al., *Antagonistic Functions of MBP and CNP Establish Cytosolic Channels in CNS Myelin.* Cell Rep, 2017. **18**(2): p. 314-323.

31. Aggarwal, S., L. Yurlova, and M. Simons, *Central nervous system myelin: structure, synthesis and assembly.* Trends Cell Biol, 2011. **21**(10): p. 585-93.

32. Kirschner, D.A. and A.L. Ganser, *Myelin labeled with mercuric chloride. Asymmetric localization of phosphatidylethanolamine plasmalogen.* J Mol Biol, 1982. **157**(4): p. 635-58.

33. Jahn, O., S. Tenzer, and H.B. Werner, *Myelin proteomics: molecular anatomy of an insulating sheath.* Mol Neurobiol, 2009. **40**(1): p. 55-72.

34. Werner, H.B., et al., *Proteolipid protein is required for transport of sirtuin 2 into CNS myelin.* J Neurosci, 2007. **27**(29): p. 7717-30.

35. Fewou, S.N., et al., *Myelin protein composition is altered in mice lacking either sulfated or both sulfated and non-sulfated galactolipids.* J Neurochem, 2010. **112**(3): p. 599-610.

36. Patzig, J., et al., *Septin/anillin filaments scaffold central nervous system myelin to accelerate nerve conduction.* Elife, 2016. **5**.

37. Barral, Y., et al., *Compartmentalization of the cell cortex by septins is required for maintenance of cell polarity in yeast.* Mol Cell, 2000. **5**(5): p. 841-51.

38. Spiliotis, E.T. and W.J. Nelson, *Here come the septins: novel polymers that coordinate intracellular functions and organization.* J Cell Sci, 2006. **119**(Pt 1): p. 4-10.

39. Gladfelter, A.S., et al., *Septin ring assembly involves cycles of GTP loading and hydrolysis by Cdc42p.* J Cell Biol, 2002. **156**(2): p. 315-26.

40. Zuchero, J.B., et al., *CNS myelin wrapping is driven by actin disassembly.* Dev Cell, 2015. **34**(2): p. 152-67.

41. Nawaz, S., et al., *Actin filament turnover drives leading edge growth during myelin sheath formation in the central nervous system.* Dev Cell, 2015. **34**(2): p. 139-151.

42. Trapp, B.D., et al., *The myelin-associated glycoprotein is enriched in multivesicular bodies and periaxonal membranes of actively myelinating oligodendrocytes.* J Cell Biol, 1989. **109**(5): p. 2417-26.

43. Montag, D., et al., *Mice deficient for the myelin-associated glycoprotein show subtle abnormalities in myelin.* Neuron, 1994. **13**(1): p. 229-46.

44. Bartsch, U., *Myelination and axonal regeneration in the central nervous system of mice deficient in the myelin-associated glycoprotein.* J Neurocytol, 1996. **25**(5): p. 303-13.

45. Schachner, M. and U. Bartsch, *Multiple functions of the myelin-associated glycoprotein MAG (siglec-4a) in formation and maintenance of myelin.* Glia, 2000. **29**(2): p. 154-65.

46. da Silva, T.F., et al., *Peripheral nervous system plasmalogens regulate Schwann cell differentiation and myelination.* J Clin Invest, 2014. **124**(6): p. 2560-70.

47. Grider, M.H., Q. Chen, and H.D. Shine, *Semi-automated quantification of axonal densities in labeled CNS tissue.* J Neurosci Methods, 2006. **155**(2): p. 172-9.

48. Norton, W.T. and S.E. Poduslo, *Myelination in rat brain: method of myelin isolation.* J Neurochem, 1973. **21**(4): p. 749-57.

49. Watkins, T.A., et al., *Distinct stages of myelination regulated by gamma-secretase and astrocytes in a rapidly myelinating CNS coculture system.* Neuron, 2008. **60**(4): p. 555-69.

50. McCarthy, K.D. and J. de Vellis, *Preparation of separate astroglial and oligodendroglial cell cultures from rat cerebral tissue.* J Cell Biol, 1980. **85**(3): p. 890-902.

Chapter 2

Potential therapies to rescue myelination defects in a plasmalogen-deficient mouse model

Potential therapies to rescue myelination defects in a plasmalogen-deficient mouse model

Ana Rita Malheiro[1,2], Barbara Correia[2], Tiago Silva[2], Diogo Neto[2], Paul van Veldoven[3], Pedro Brites[2]

[1]Neurolipid Biology group, Instituto de Biologia Molecular e Celular – IBMC e Instituto de Investigação e Inovação em Saúde – i3S, Universidade do Porto, Rua Alfredo Allen 208 4200-135, Porto, Portugal, [2]ICBAS, Instituto Ciências Biomédicas Abel Salazar, Rua Jorge Viterbo Ferreira 228, 4050-223 Porto, Portugal, [3]Laboratory of Lipid Biochemistry and Protein Interactions (LIPIT), Campus Gasthuisberg-KU Leuven, Herestraat Box 601, B-3000 Leuven, Belgium

Introduction

Plasmalogens are a unique class of membrane glycerophospholipids containing a fatty alcohol with a vinyl-ether bond at the *sn*-1 position, and enriched in polyunsaturated fatty acids at the *sn*-2 position of the glycerol backbone. The vast majority of endogenous mammalian plasmalogens contain at the *sn*-1 position a long chain alcohol composed of either C16:0, C18:0 or C18:1 [1]. The plasmalogen biosynthesis starts in peroxisomes, and defects at these steps cause the Rhizomelic Chondrodysplasia Punctata (RCDP). The several organs affected in RCDP patients, predict developmental roles for plasmalogens in bone, brain, lens, lung, kidney and heart. Additionally, secondary plasmalogen deficiencies are associated with more common disorders, such as Alzheimer's and Parkinson's disease [2].

Treatment options able to rescue the biochemical or pathologic defects caused by a plasmalogen defect are scarce [3, 4]. Ether-linked glycerols (alkyl glycerols (AG)) are known to enter the plasmalogen biosynthetic pathway

downstream of the peroxisomal steps, and can serve as alternative precursors to rescue the biochemical defect, e.g. in Zellweger spectrum and RCDP patients [2, 5, 6]. Although plasmalogens usually contain C16:0, C18:1 and C18:0 moieties at the *sn*-1 position, 1-*O*-heptadecylglycerol (containing a C17:0 alkyl chain) was also shown to be incorporated into plasmalogens [4]. Specifically, rats treated with 1-*O*-heptadecyl-sn-glycerol showed that this uncommon ether lipid was incorporated into the plasmalogens of all tissues except brain [4]. Moreover, Brites et al. [3], using a mouse model for RCDP, showed that early supplementation with 1-*O*-octadecyl-sn-glycerol (batyl alcohol (BA) with a C18 alkyl chain) recovered plasmalogens levels and tissue pathology in peripheral tissues. However, this was not the case for peripheral and central nervous system tissues. Since nervous tissue is highly enriched in plasmalogens, sustained treatment periods may be necessary to overcome the turnover rates and to reach steady-state physiologic levels. In addition, it has been suggested that treatment options providing the naturally occurring alkylglycerols, 1-*O*-hexadecyl-rac-glycerol (chimyl alcohol (CA) with a C16 alkyl chain), batyl alcohol and 1-*O*-octadecenyl-sn-glycerol (selachyl alcohol), in order to recover each plasmalogen class, would be more effective forms of treatment [7]. Even so, there is also a need to determine how to improve the uptake of plasmalogen precursors into the nervous system.

Using mouse models for RCDP, we unraveled that the lack of plasmalogens impairs myelination both in central [8] and peripheral nervous system [9]. Consequently, treatments promoting oligodendrocyte and Schwann cell differentiation are a possible strategy to stimulate remyelination. In the peripheral nervous system (PNS), a deficiency in plasmalogens causes defects in AKT-mediated signaling impairing the GSK3β-mediated differentiation of Schwann cells [9]. Also in central nervous system (CNS), AKT signaling pathway is one of the signaling molecules implicated in controlling CNS myelination [10-13]. Receptor-

mediated signaling, leads to Protein kinase B (AKT) phosphorylation at Ser473 and Thr308 and the activation of a signaling cascade. Active AKT has a myriad of target substrates including glycogen synthase kinase-3β (GSK3β), a constitutively active serine/threonine protein kinase that undergoes an inhibitory phosphorylation at Ser9 by active AKT [14, 15]. The inhibition of GSK3β activity through phosphorylation is necessary to allow the differentiation and maturation of oligodendrocytes [16]. Lithium chloride (LiCl) is a well-established inhibitor of GSK3β activity, and is currently used for the treatment of several disorders [14-20]. Lithium treatment may also induce increased phosphatidylinositol-3-kinase (PI3-K) activity and AKT phosphorylation, leading to increased phosphorylation of GSK3β at Ser9 [14-20]. We previously shown that administration of LiCl is able to rescue Schwann cell differentiation and myelination in the peripheral nervous system of plasmalogen-deficient mice [9].

After observing that the compromised intrinsic ability of *Gnpat* mutant oligodendrocytes causes defects in myelination (see Chapter 1), our goal was to determine whether in the central nervous system, inhibiting GSK3β activity, using LiCl, or activating AKT, using the activator AKT SC79 [21], also has beneficial effects on CNS myelination. Our results demonstrate that treatments promoting AKT activation recovered the myelin pathology in CNS. Additionally, we identified a new alkyl glycerol that can serve as an alternative precursor in the biosynthesis of plasmalogens and can rescue myelination defects of *Gnpat* KO mice.

Results

Impaired CNS myelination in plasmalogen-deficient mice is rescued by treatments promoting AKT activation

To validate the usage of LiCl as potential therapeutic agent, we treated WT and *Gnpat* KO mice with either vehicle (sodium chloride) or LiCl at a dosage of 50mg/Kg, administered via subcutaneous injections according to 2 different setups (Fig. 1A): on setup A, mice were injected daily for 6 days starting at birth; on setup B, mice were injected on alternating days for 8 days starting at the postnatal day 7 (P7).

The histological and morphometric analyses of mouse spinal cords from setup A, showed that at P6, control-treated *Gnpat* KO had a pronounced decrease in the number and density of myelinated fibers (Fig. 1B and C). Interestingly, at this age the LiCl treatment was able to improve the defect in myelination, as we observed an increase in the number of myelinated fibers and a restoration of myelination (Fig. 1B and C). Similar results were obtained with the analyses of mouse spinal cords from setup B. After LiCl administration, we did not observe a difference in the density of myelinated fibers (Fig. 1D). Combined our results seem to indicate that in the central nervous system, treatment with LiCl is able to improve the defective myelination caused by a deficiency in plasmalogens. Surprisingly, the analysis of AKT phosphorylation in P15 *Gnpat* KO mice did not highlight the reductions in the levels of phosphorylated AKT at Ser473 or at Thr308 (Fig. 1E and F). Previously, we showed that plasmalogen defects caused impairment in AKT activation in Schwann cells and peripheral nerves from *Gnpat* KO mice [9]. The observation that at P15 there are mutant oligodendrocytes that accomplished some myelination prompted us to evaluate the levels of phosphorylated AKT in WT and *Gnpat* KO at E17 (Fig. 1 G and H). During this late embryonic period, we observed a reduction in AKT phosphorylation in spinal cords from *Gnpat* KO.

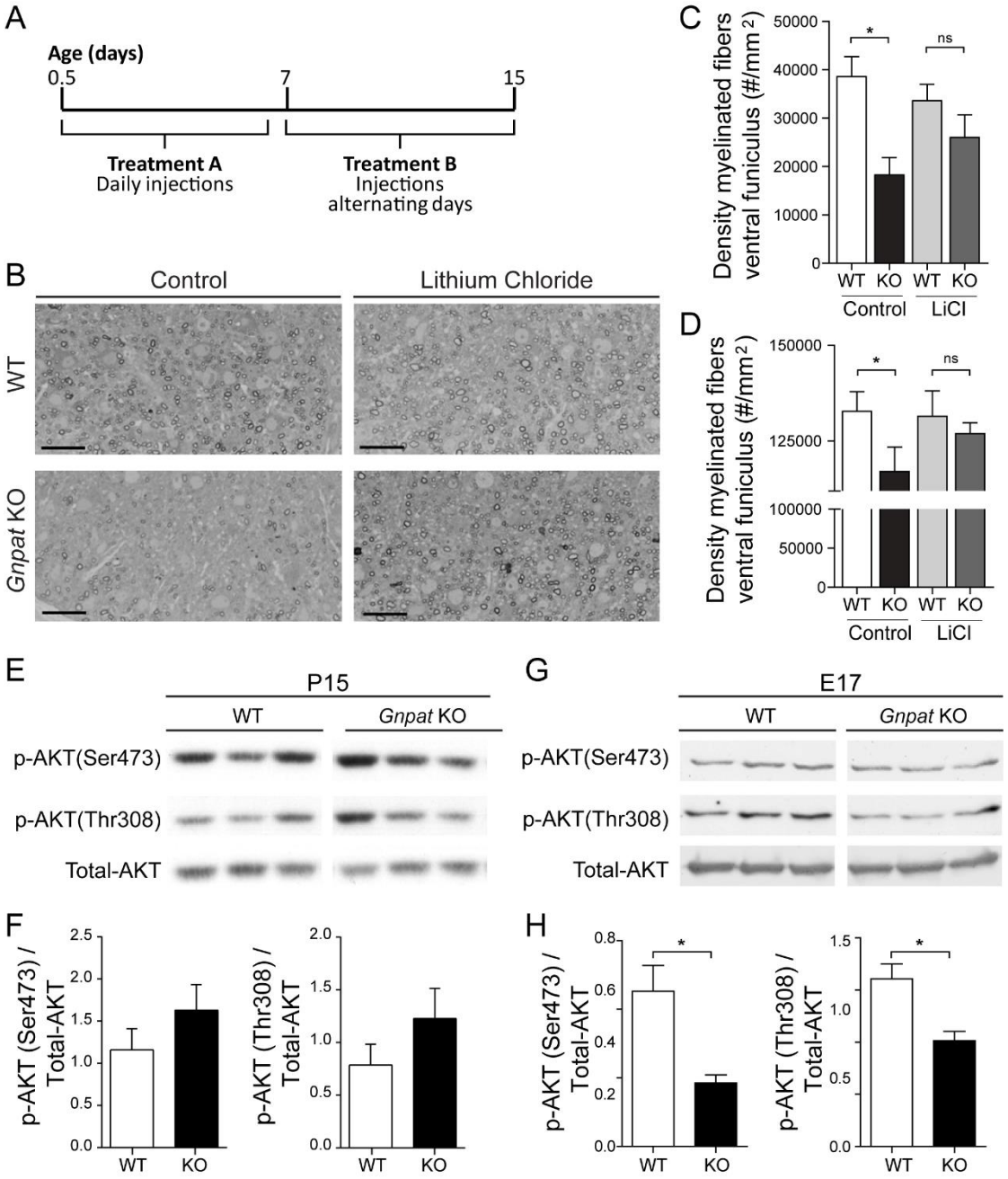

Figure 1. Characterization and morphometric analysis of spinal cord defects in plasmalogen-deficient mice, after the treatment with lithium chloride. A Schematic representation of the treatments with lithium chloride. **B** Light microscopy images of ventral funiculus stained with PPD from control- and LiCl-treated WT and *Gnpat* KO mice at P6. **C** Morphometric analysis of myelinated fibers at P6, after LiCl treatment (daily injections), revealing that LiCl was able to rescue the defect in myelination, as there was no difference in the density of myelinated fibers between WT and *Gnpat* KO mice. **D** Morphometric analysis of myelinated fibers at P15, after LiCl treatment (injections in altering days), showing no differences in the density of myelinated fibers between WT and *Gnpat* KO mice after treatment. **E** Western blot analysis and quantification (F) of AKT phosphorylation (p-AKT) in spinal cord lysates of P15 WT and *Gnpat* KO mice. **G** Western blot analysis and quantification (H) of AKT phosphorylation (p-AKT) in spinal cord lysates of E17 WT and *Gnpat* KO mice. Scale Bars: 20µm. *P<0.05.

As such, we also treated WT and *Gnpat* KO mice with the specific AKT activator SC79 [21]. The small molecule SC79 inhibits the AKT membrane translocation, and paradoxically activates AKT in the cytosol. Specifically, SC79 binds to the PH domain of AKT and, when bound, AKT adopts a favorable conformation for phosphorylation by upstream protein kinases [21]. WT and *Gnpat* KO mice were treated with either vehicle (DMSO) or SC79 at a dosage of 40ug/gr. Mice were injected on alternating days from P5 until P15 and the injections were administered subcutaneously, being the last two injections intraperitoneal.

The morphometric analyses of spinal cords showed that at P15, control-treated *Gnpat* KO mice had a pronounced decrease in the number and density of myelinated fibers (Fig. 2A and B). Nevertheless, SC79 treatment was able to improve the defect in myelination, as we observed an increase in the number of myelinated fibers and a restoration of myelination (Fig. 2A and B). Combined, these results seem to indicate that in the central nervous system, treatments promoting AKT activation are able to improve the defective myelination caused by a deficiency in plasmalogens.

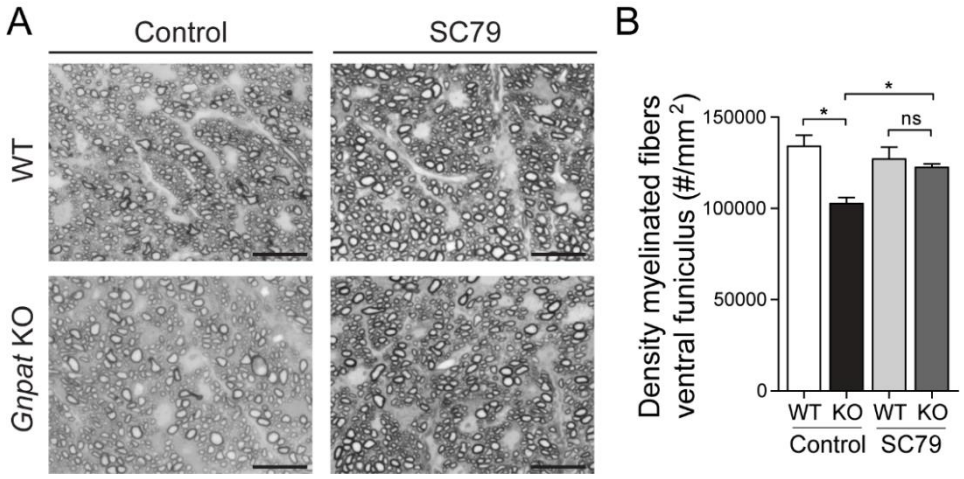

Figure 2. Characterization and morphometric analysis of spinal cord defects in plasmalogen deficient mice, after the treatment with SC79. A Light microscopy images of ventral funiculus stained with PPD from control- and SC79-treated WT and *Gnpat* KO mice at P15. **B** Morphometric analysis of myelinated fibers at P15, after SC79 treatment, showing no differences in the density of myelinated fibers between WT and *Gnpat* KO mice after treatment. Scale bars are 20µm. *P<0.05.

A new alkyl glycerol is able to rescue myelination defects

Alkyl glycerols (AG) can enter the plasmalogen biosynthetic pathway after the peroxisomal steps (Fig. 4A), and serve as alternative precursors to rescue the biochemical defect [4, 5]. Using the *in vitro* myelination system (see chapter 1), we evaluated the ability of batyl and chimyl alcohol (BA and CA), two commonly used alkyl glycerols, to rescue the myelination defect of *Gnpat* KO oligodendrocytes. The treatment with BA and CA was not able to rescue myelination in *Gnpat* KO co-cultures, which continued to present decreased number of myelinating oligodendrocytes, and reduced number of small myelin segments (Fig. 3). Nevertheless, the development of the *in vitro* myelination system allowed us to test the potential of other alkyl glycerols as functional alternative precursors of plasmalogens.

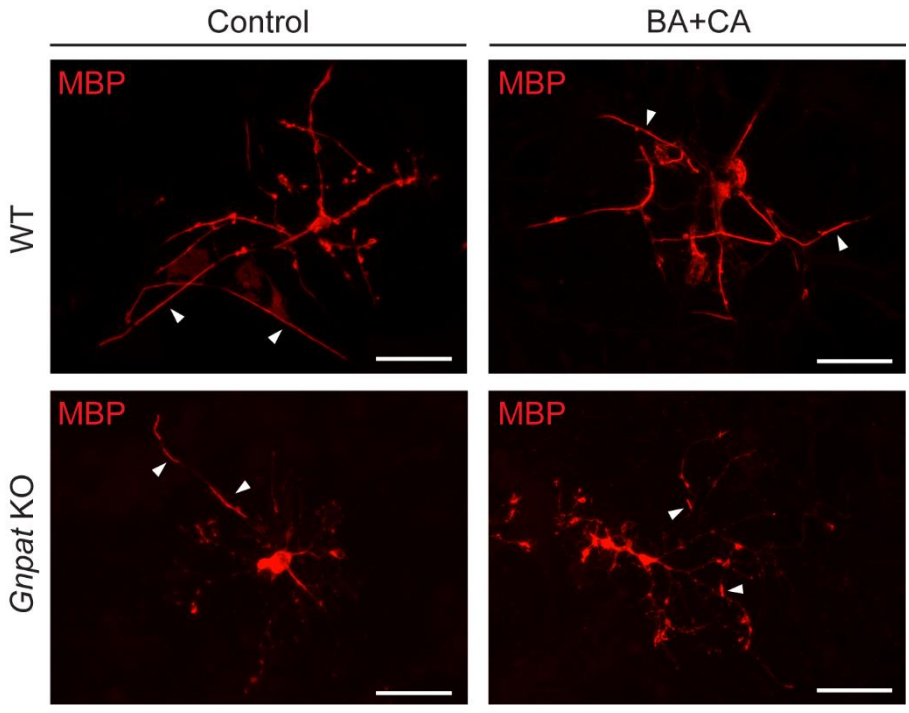

Figure 3. Treatment with batyl and chimyl alcohol does not rescue myelination defects. Myelination of mixed cortical cultures from WT and *Gnpat* KO mice at DIV20 treated with a mixture of BA and CA or control treated, and immunostained for MBP (red). Myelin segments are highlighted with arrowheads. n = 4 mice per group. Scale bars are 50µm.

We assayed the potential of glyceryl 1-myristyl ether (1-*O*-tetradecyl-sn-glycerol; 1-O-TDG), an alkyl glycerol with a shorter C14 alkyl chain. To assay the potential of 1-O-TDG as a plasmalogen precursor we measured plasmalogen levels in WT and *Gnpat* KO fibroblasts. Fibroblasts were chosen because of their generalized usage in assays with alkyl glycerols and to circumvent the inability to obtain sufficient amounts of primary oligodendrocytes necessary for the biochemical assays. As expected, treatment of *Gnpat* KO cells with 1-O-TDG was not able to rescue plasmalogens with C16:0, C18:1 and C18:0 at the *sn*-1 position (Fig. 4B and C). However, 1-O-TDG was successfully converted into plasmalogens with C14:0 at the *sn*-1 position (Fig. 4B and D) and boosted plasmalogen levels in *Gnpat* KO fibroblasts when compared to WT fibroblasts (Fig. 4E).

In addition, using *in vitro* myelination cultures, treatment with 1-O-TDG was able to rescue myelination in *Gnpat* KO co-cultures, as evidenced by the assembly of long myelin segments (Fig 4F, H) and the increased density of myelinating oligodendrocytes (Fig 4G). Combined, these results provide evidence of a differential ability of oligodendrocytes to use different alkyl glycerols as precursors in the biosynthesis of plasmalogens. 1-O-TDG was identified as a new alkyl glycerol that can rescue plasmalogen levels and the intrinsic myelination defect of plasmalogen-deficient oligodendrocytes.

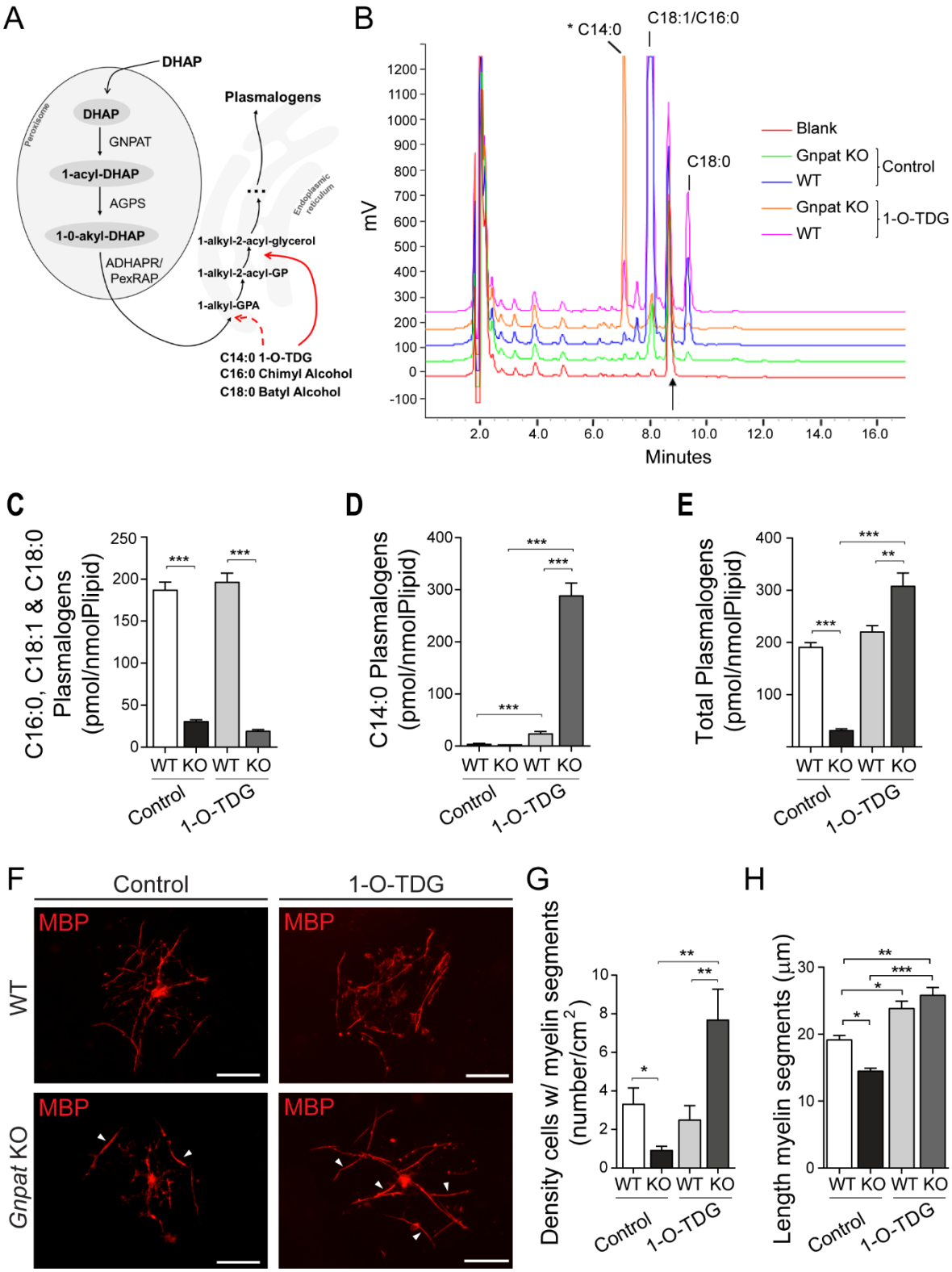
A
DHAP
Plasmalogens
Peroxisome
DHAP
GNPAT
1-acyl-DHAP
AGPS
1-0-akyl-DHAP
ADHAPR/
PexRAP
Endoplasmic reticulum
1-alkyl-2-acyl-glycerol
1-alkyl-2-acyl-GP
1-alkyl-GPA
C14:0 1-O-TDG
C16:0 Chimyl Alcohol
C18:0 Batyl Alcohol
B
* C14:0
C18:1/C16:0
C18:0
mV
Minutes
Blank
Gnpat KO
WT
Control
Gnpat KO
WT
1-O-TDG
C
C16:0, C18:1 & C18:0 Plasmalogens (pmol/nmolPlipid)
WT KO WT KO
Control
1-O-TDG
D
C14:0 Plasmalogens (pmol/nmolPlipid)
E
Total Plasmalogens (pmol/nmolPlipid)
F
Control
1-O-TDG
WT
Gnpat KO
MBP
G
Density cells w/ myelin segments (number/cm2)
H
Length myelin segments (µm)

◄**Figure 4: Identification of 1-*O*-tetradecylglycerol as a new alkyl glycerol capable of rescuing myelination defects**. **A** Schematic representation highlighting the routes at which alkyl glycerols can enter the plasmalogen biosynthesis to rescue defects in the peroxisomal steps. Alkyl glycerols can be phosphorylated (dotted arrow) to generate 1-alkyl-glycero-3-phosphate (GP) or acylated (arrow) to generate 1-alkyl-2-acyl-glycerol. DHAP: dihydroxyacetone phosphate; ADHAPR: acylglycerone-phosphate reductase. **B** Representative chromatograms of lipid extracts from WT and *Gnpat* KO fibroblasts either control or 1-O-TDG treated, subjected to RP-HPLC and detected by fluorimetry. The arrow denotes heptadecanal, used as internal standard. The major peaks in WT fibroblasts correspond to octadecenal (C18:1), eluting ahead of hexadecanal (C16:0) and octadecanal (C18:0). The asterisk indicates the elution of the tetradecanal (C14:0) derivative, only present in samples treated with 1-O-TDG. **C-E** Quantification of plasmalogens in fibroblasts from WT and *Gnpat* KO mice under control conditions (n=3-5 per genotype) and after 1-O-TDG treatment (n=5 per genotype). **C**. Levels of plasmalogens containing C16:0, C18:1 and C18:0; *** $P<0.0001$. **D** Levels of plasmalogens containing C14:0.; *** $P<0.0001$. **E** Total levels of plasmalogens (containing C14:0, C16:0; C18:1 and C18:0; ** $P=0.011$, *** $P<0.001$. **F** *in vitro* myelination of mixed cortical cultures from WT and KO mice (n=3 each genotype) at DIV20 treated with 1-O-TDG or control, and immunostained for MBP (red). Myelin segments are highlighted with arrowheads. Scale bars are 50µm. **G** Quantification of the myelinating oligodendrocytes in control- and 1-O-TDG-treated co-cultures from WT and *Gnpat* KO mice (n=3 each genotype). *$P=0.03$, ** $P=0.01$. **H** Quantification of the length of myelin segments in control- and 1-O-TDG-treated co-cultures from WT and *Gnpat* KO mice (n=3 each genotype). *$P=0.02$, ** $P=0.0024$, ** $P<0.0001$.

Leukodystrophy caused by plasmalogen deficiency rescued by glyceryl 1-myristyl ether treatment

To validate the usage of 1-O-TDG as potential therapeutic agent, we treated WT and *Gnpat* KO mice with either vehicle (1% Tween-80 in saline) or 1-O-TDG in vehicle at a dosage of 5mg/kg. The treatments were administered via subcutaneous injections from P1 to P8 and via intraperitoneal injections from P10 to P18 (Fig. 5A). At the start of the treatment *Gnpat* KO mice displayed reduced body weight (Fig. 8B), a feature of plasmalogen deficiency in mice [3, 22]. However, at the end of treatment 1-O-TDG-treated *Gnpat* KO mice had normal body weight (Fig. 5C) indicative of the improvement on the general well-being, similarly to that observed with batyl alcohol [3]. The histopathological analysis of nervous tissue from *Gnpat* KO mice treated with 1-O-TDG revealed a generalized rescue in

myelination. Histological analysis of myelinated fibers in the dorsal column tract revealed improvements in myelination and axon radial growth (Fig. 8D), and in the ventral funiculus the density of myelinated axons was normalized in *Gnpat* KO mice (Fig. 5E).

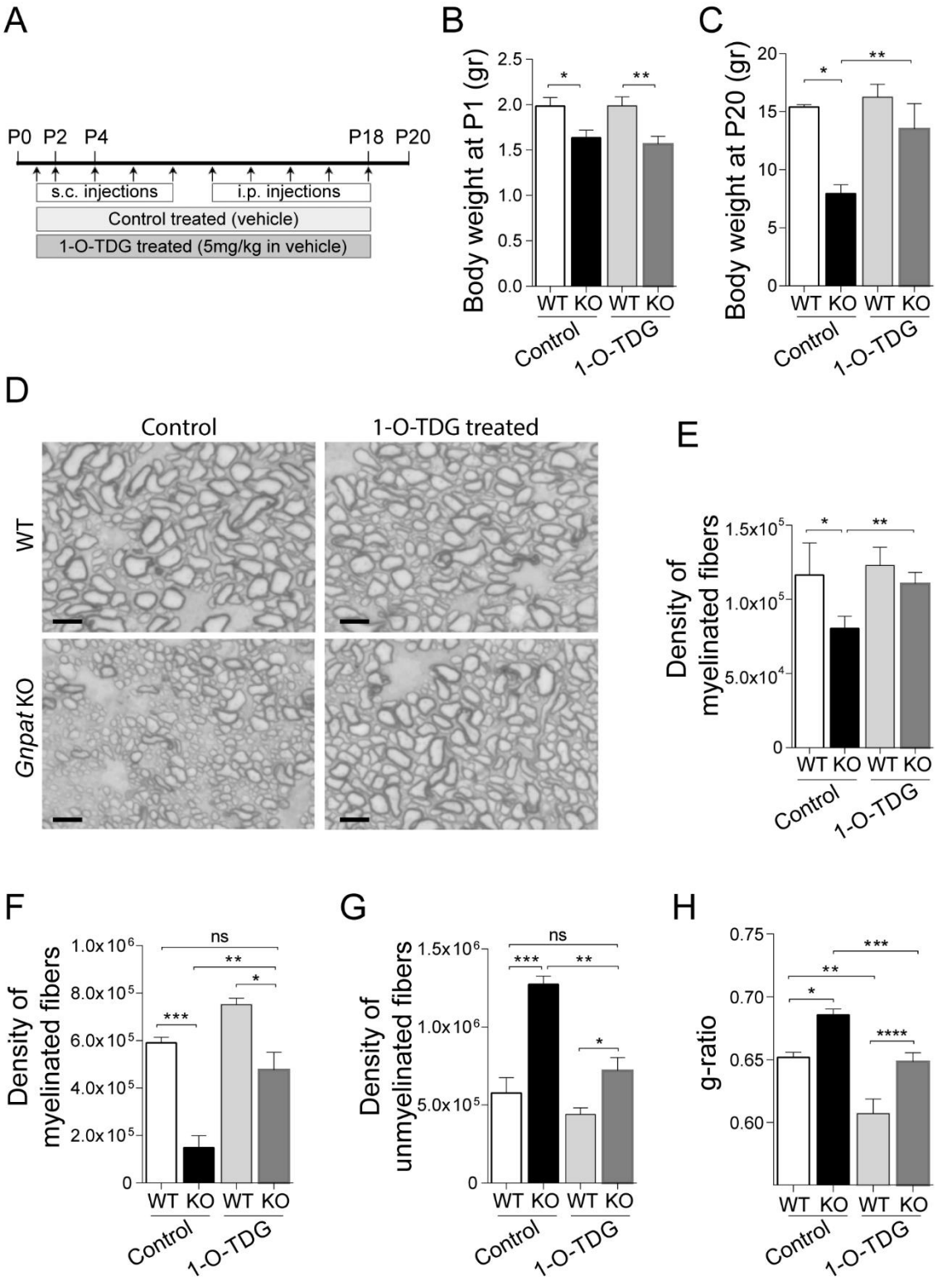

◄Figure 5. Treatment with 1-O-tetradecylglycerol rescues *in vivo* myelination defects. A Schematic representation of *in vivo* treatments. WT and *Gnpat* KO mice were treated from P1 to P18 with 1-O-TDG or control vehicle (n=3 each genotype and treatment). From postnatal day 1 (P1) to P8 treatments were delivered via subcutaneous (s.c.) injections and from P10 to P18 via intraperitoneal (i.p.) injections. Tissues were collected at P20. **B** Body weight at start of treatment. * P= 0.022, *** P= 0.012. **C** Body weight at end of treatment (P20). * P= 0.0004, ** P=0.0037. **D** Light microscopy images of dorsal column track stained with PPD from control- and 1-O-TDG treated WT and *Gnpat* KO mice at P20. Scale bars are 5µm. **E** Quantification of myelinated fibers in the ventral funiculus, of control- and 1-O-TDG-treated, WT and *Gnpat* KO spinal cords at P20. * P= 0.031, ** P=0.014. **F** Quantification of myelinated fibers in optic nerves from of control- and 1-O-TDG-treated WT and *Gnpat* KO mice at P20. * P=0.011, **P=0.0083, *** P=0.0009. **G** Quantification of unmyelinated fibers in optic nerves from of control- and 1-O-TDG-treated WT and *Gnpat* KO mice at P20. * P=0.040, ** P=0.0014, *** P=0.0028. **H** Quantification of myelination by determination of g-ratio in sciatic nerves from of control- and 1-O-TDG-treated WT and *Gnpat* KO mice at P20. *P=0.0049, ** P=0.0017, *** P=0.0066, **** P=0.0073.

In optic nerves, the region most affected by a plasmalogen deficiency, the treatment with 1-O-TDG was able to normalize the densities of myelinated (Fig. 5F) and un-myelinated (Fig. 5G) axons to values observed in control-treated WT mice. During this period of active myelination, WT mice treated with 1-O-TDG also displayed increased numbers of myelinated axons (Fig. 5F). We also addressed if the treatment with 1-O-TDG could rescue the myelination defects observed in the peripheral nervous system [9]. Treatment with 1-O-TDG rescued the impaired myelination observed in sciatic nerves from *Gnpat* KO mice (Fig. 5H). The treatment also induced myelination in sciatic nerves from WT mice with significant decreases in g-ratio (Fig. 5H). Combined, these results demonstrate the ability of 1-O-TDG to rescue the myelination defects observed in the CNS and PNS of plasmalogen-deficient mice.

Discussion

As highlighted by the clinical presentation of RCDP patients, plasmalogen deficiency has major consequences for tissue development and organ function [2]. Therefore, any therapeutic intervention aimed at restoring ether-phospholipid levels or improving pathologic defects associated with the disease should have a beneficial outcome.

In the peripheral nervous system, a deficiency in plasmalogens impairs myelination in an AKT- and GSK3β-dependent manner [9]. In an attempt to rescue the defect in myelination, we tested if administration of lithium chloride (LiCl) or SC79 to plasmalogen-deficient mice would exert its inhibitory action on GSK3β or AKT activation, respectively, and promote oligodendrocyte maturation and therefore induce myelination. Treatments during the first or second week of life, with LiCl or SC79, were able to normalize the densities of myelinated fibers in the spinal cords of *Gnpat* KO mice, indicating that during the active period of myelination, AKT activation and/or GSK3β-inhibition boosts oligodendrocyte maturation and stimulates myelination. GSK3β is emerging as a prominent drug target in the central nervous system, as recent studies described the effect of lithium in the treatment of acute brain injuries, such ischemia and brain trauma, and also in neurodegenerative diseases, including in Parkinson disease, Alzheimer's disease, Multiple Sclerosis, and Huntington disease [20, 23]. Nevertheless, the effect of lithium on myelination of the central nervous system is still poorly investigated. Our results point to a beneficial effect of treating hypomyelinated mice with LiCl, as this inhibitor of GSK3β seems to promote myelination.

In the CNS, AKT is able to enhance survival of oligodendrocytes [24] but its most striking activity was the induction of myelination [10]. We previously showed

that a defect in plasmalogens impairs the ability of Schwann cells and mouse embryonic fibroblasts to mount, following an induction stimuli, an AKT-dependent signaling cascade [9]. The analysis of AKT phosphorylation in spinal cords from *Gnpat* KO mice revealed a differential result. Whereas at P15 AKT phosphorylation levels were similar to WT mice, at E17 *Gnpat* KO mice displayed a defect in AKT phosphorylation. The western blot in spinal cords provides generalized and averaged data on the levels of AKT phosphorylation. Given that the spinal cord is, amongst others, populated by neurons and their axons, astrocytes and microglia, a possible reduction in AKT phosphorylation in mutant oligodendrocytes may not be easily detected due to a dilution effect. In addition, our results may also highlight a precise timeframe in which increased AKT activation induces myelination, and this is followed by a restoration to basal activity to prevent hypermyelination [10]. Nevertheless, our results provide evidence that GSK3β inhibition and AKT activation could be considered as important events to restore myelination defects caused by a plasmalogen deficiency.

Although studies have shown that the alkyl glycerols BA and CA are able to restore plasmalogen levels, a previous study showed that their effectiveness excludes the central and peripheral nervous system [3]. Treatment using BA as a plasmalogen precursor, proved to be effective on peripheral tissues, but inefficient within the nervous system. A possible contribution of the blood-brain barrier (BBB) in the CNS could explain the inability of BA to normalize plasmalogen levels in brain and spinal cord. Using the *in vitro* myelination system, we assayed the potential of BA and CA to rescue myelination defects in *Gnpat* KO oligodendrocytes. Our results demonstrate that these alkyl glycerols are not capable of restoring myelination even in the absence of a functional BBB. The feasibility of the *in vitro* myelination assays allowed us to test and validate the potential of other alkyl glycerols in rescuing CNS defects. We identified 1-O-TDG, as a functional alkyl glycerol capable

of rescuing plasmalogen levels in *Gnpat* KO cells and capable of rescuing the differentiation and myelination potential of *Gnpat* KO oligodendrocytes. Although plasmalogens usually contain C16:0, C18:1 and C18:0 moieties at the *sn*-1 position, 1-*O*-heptadecylglycerol (containing a C17:0 alkyl chain) was also shown to be incorporated into plasmalogens [4]. Our results demonstrate that shorter alkyl chains can also be incorporated into plasmalogens. In addition, our results suggest that the synthesis of plasmalogens with their characteristic vinyl-ether bond is more important than the chain length at the *sn*-1 position [2]. The ability of 1-O-TDG to rescue myelination *in vivo* represents a novel and valid strategy for the development of translatable approaches to rescue plasmalogen levels in the CNS and treatment of the myelination defects observed in RCDP patients [25, 26]

Material and Methods

Animal experiments and mouse models

All procedures made in mice were done according to the European Directive 2010/63/EU established by the European Parliament and of the Council, as well as the National legislation (Decreto-Lei 113/2013). Mice were used only after approval of the Portuguese General Veterinarian Board. *Gnpat* KO mice and WT littermates were obtained from mating *Gnpat* heterozygous mice (on a Swiss-Webster background). All animals were maintained with ad libitum access to rodent food and water, and were kept in a 12:12h light and dark cycle facility. Genotyping was performed by the IBMC CCGen facility using previously developed strategies [27].

To validate the usage of LiCl, we treated WT and *Gnpat* KO mice with sodium chloride or LiCl at a dosage of 50mg/Kg of body weight, administered via subcutaneous (s.c) injections according to 2 different setups (Fig. 1A): on setup A, mice were injected daily for 6 days starting at birth; on setup B, mice were injected on alternating days for 8 days starting at the P7.

For the treatment with the SC79, WT and *Gnpat* KO mice were injected with either vehicle (DMSO) or SC79 at a dosage of 40ug/gr of body weight. Mice were injected on alternating days from P5 until P15 and the injections were administered subcutaneously, being the last two injections intraperitoneal (i.p.).

1-O-TDG was dissolved in 1ml of ethanol and mixed with 1ml of Tween-80 (Sigma-Aldrich). After heating to evaporate the ethanol the mixture was diluted with saline (B. Braun Medical, Portugal) so that Tween-80 was at 1% w/v. 1-O-TDG or vehicle were administered to WT and *Gnpat* KO mice via subcutaneous injections from P1 to P8 and via intraperitoneal injections from P10 to P18. Mice were euthanized at P20 and tissues collected for histological analyses.

Morphological analysis

Electron microscopy

At least 3 knockout and wild type mice from each age were analyzed. Mice were deeply anesthetized with ketamine + medetomidine (75mg/kg + 1mg/kg body weight, respectively); lumbar spinal cord and sciatic nerve were isolated and fixed by immersion. Tissues were fixed by immersion in 4% glutaraldehyde (Sigma) in 0.1M sodium cacodylate buffer (pH 7.4) solution for 5 days. After washing and two hours in post-fixating 1% osmium tetroxide (Sigma-Aldrich) in 0.1M sodium cacodylate buffer (pH 7.4) solution, tissues were washed in buffer, dehydrated through graded series of ethanol, and embedded in Epon (EMS). Semi-thin sections were cut at 1µm, stained with 1% p-phenylenediamine (PPD) in methanol, and used in light microscopy for counting the number of myelinated fibers. In spinal cord, the region chosen for analysis was the ventral funiculus, immediately adjacent to the ventromedian fissure. Ultrathin sections were cut at 50 nm, counterstained with lead citrate and uranyl acetate, and observed in a JEOL JEM-1400 transmission electron microscope (equipped with an Orius Sc1000 Digital Camera).

Western blots

For Western blot analysis, lysates of spinal cord were prepared in lysis buffer (0.3% Triton X-100, 1mM sodium orthovanadate, cOmplete™ Protease Inhibitor Cocktail in PBS), and 5µg protein was run on 12% SDS-PAGE gels. Nitrocellulose membranes blocked with 5% skim milk (Fluka) in Tris-buffered saline with 1% Tween 20 (TBS-T) for 1h at RT, washed with TBS-T, and probed with different primary antibodies (Table 1) diluted in 5% BSA + TBS-T (overnight at 4°C). After incubation with HRP-labeled secondary antibodies, diluted 1:5000 in 5% skim milk in TBS-T and incubated for 1h at RT, the blots were developed with ECL (Pierce)

and exposed to Hyperfilm (Amersham). Films were scanned on a Molecular Imager GS800, and Quantity One (Bio-Rad) was used for quantifications.

Mixed cortical neuron-glial culture

Mixed cortical neuron-glial culture was performed as described [28], with minor alterations. Cortical neurons and glial cells were isolated from individual WT and *Gnpat* KO mouse brains, at embryonic day 17. Cortices were digested in 0.05% Trypsin + 0.2mg/ml EDTA, dissociated, and cells were resuspended in culture medium (Neurobasal medium with 1x N21 supplement, 2mM L-glutamine, 1x P/S). Cells were plated at a density of $1.5x10^5$ cells/well onto glass coverslips coated with poly-L-lysine (20µg/ml, P2636 Sigma) and laminin (2µg/ml, L2020 Sigma). After DIV6 days *in vitro*, cultures were maintained in myelination medium [29]. At DIV20 cells were fixed with 4% PFA, and immunolabeled with anti-tubulin-βIII (to stain neurons) and anti-myelin basic protein (MBP, to stain oligodendrocytes). The fixed cells were processed as described above for immunohistochemistry. The entire area of the glass coverslip ($1.32cm^2$) was analyzed and the total number of MBP-positive cells (i.e., OL with low levels of MBP, OL with high levels of MBP, OL with assembled MBP segments and degenerating OLs) were counted.

For 1-*O*-tetradecylglycerol (1-O-TDG) (Biosynth) treatment, medium was supplemented with 7µM 1-O-TDG in absolute ethanol or 0.1% absolute ethanol (control) starting at DIV 10. For treatment with batyl alcohol (BA; 1-*O*-octadecylglycerol; Sigma-Aldrich) and chimyl alcohol (CA; 1-*O*-hexadecylglycerol; Bachem), medium was supplemented with 7µM BA and 7µM CA in DMSO or with 0.14% DMSO (control) starting at DIV 10. In both treatment schemes, cells were fixed at DIV20 and processed for immunofluorescence as described above.

Table 1. List of antibodies used.

Antigen	Company	Catalog	Host	Dilution	Purpose*
Phospho-Akt (Ser473)	Cell Signaling	#4060	rabbit	1:1000	WB
Phospho-Akt (Thr308)	Cell Signaling	#2965	rabbit	1:500	WB
Akt (pan)	Cell Signaling	#4691	rabbit	1:1000	WB
Myelin basic protein (MBP)	Milipore	MAB386	rat	1:250	IF

* WB: western blot; IF: immunocitofluorescence

Measurement of plasmalogens

Lung-derived mouse embryonic fibroblasts from WT (n=3) and *Gnpat* KO (n=5) at embryonic day 17.5 were cultured in T75 flasks with DMEM supplemented with 10% FBS [30]. The medium was supplemented with 7µM 1-O-TDG or 0.01% absolute ethanol (control) during 12 days. Cells were harvested using trypsin, washed and stored at -80°C until processing. Lipid extracts were prepared as described [31] and analyzed for phospholipid content [32] and plasmalogens. For the latter, lipids were treated with acidic methanol followed by conversion of the liberated aldehydes with 1,3-cyclohexanedione into fluorescent decahydroacridines derivatives, which were separated according the chain length by RP-HPLC (Symmetry C18 column (4.6 × 150 mm; 5 µm; 100 Å; Waters) and monitored by fluorimetry (using a Waters 2475 Multi-Wavelength Fluorescence Detector; Ex 390 nm; Em 460 nm); modified from Mezzar et al. [33] (Van Veldhoven P.P., unpublished data).

Statistical analysis

All data were analyzed using GraphPad Prism software, and results expressed as mean + S.E.M. To compare two different groups, the student's T-test (unpaired, two-tailed) was used and $P<0.05$ was considered a significant difference. For multiple comparisons, one-way ANOVA test was used, followed by Tukey's multiple comparison tests.

Bibliography

1. Brites, P., H.R. Waterham, and R.J. Wanders, *Functions and biosynthesis of plasmalogens in health and disease.* Biochim Biophys Acta, 2004. **1636**(2-3): p. 219-31.
2. Braverman, N.E. and A.B. Moser, *Functions of plasmalogen lipids in health and disease.* Biochim Biophys Acta, 2012. **1822**(9): p. 1442-52.
3. Brites, P., et al., *Alkyl-glycerol rescues plasmalogen levels and pathology of ether-phospholipid deficient mice.* PLoS One, 2011. **6**(12): p. e28539.
4. Das, A.K., et al., *Dietary ether lipid incorporation into tissue plasmalogens of humans and rodents.* Lipids, 1992. **27**(6): p. 401-5.
5. Schrakamp, G., et al., *Plasmalogen biosynthesis in peroxisomal disorders: fatty alcohol versus alkylglycerol precursors.* J Lipid Res, 1988. **29**(3): p. 325-34.
6. Kremser, K. and A. Roscher, *Plasmalogen biosynthesis in the diagnosis of peroxisomal disorders.* J Clin Chem Clin Biochem, 1989. **27**(5): p. 315-7.
7. Iannitti, T. and B. Palmieri, *An update on the therapeutic role of alkylglycerols.* Mar Drugs, 2010. **8**(8): p. 2267-300.
8. Malheiro, A.R., et al., *Leukodystrophy caused by plasmalogen deficiency rescued by glyceryl 1-myristyl ether treatment.* Brain Pathol, 2019.
9. da Silva, T.F., et al., *Peripheral nervous system plasmalogens regulate Schwann cell differentiation and myelination.* J Clin Invest, 2014. **124**(6): p. 2560-70.
10. Flores, A.I., et al., *Constitutively active Akt induces enhanced myelination in the CNS.* J Neurosci, 2008. **28**(28): p. 7174-83.
11. Barros, C.S., et al., *Beta1 integrins are required for normal CNS myelination and promote AKT-dependent myelin outgrowth.* Development, 2009. **136**(16): p. 2717-24.

12. Narayanan, S.P., et al., *Akt signals through the mammalian target of rapamycin pathway to regulate CNS myelination.* J Neurosci, 2009. **29**(21): p. 6860-70.

13. Yu, M., et al., *Visual abnormalities associated with enhanced optic nerve myelination.* Brain Res, 2011. **1374**: p. 36-42.

14. Ogata, T., et al., *Opposing extracellular signal-regulated kinase and Akt pathways control Schwann cell myelination.* J Neurosci, 2004. **24**(30): p. 6724-32.

15. Noel, A., et al., *Lithium chloride and staurosporine potentiate the accumulation of phosphorylated glycogen synthase kinase 3beta/Tyr216, resulting in glycogen synthase kinase 3beta activation in SH-SY5Y human neuroblastoma cell lines.* J Neurosci Res, 2011. **89**(5): p. 755-63.

16. Azim, K. and A.M. Butt, *GSK3beta negatively regulates oligodendrocyte differentiation and myelination in vivo.* Glia, 2011. **59**(4): p. 540-53.

17. Chalecka-Franaszek, E. and D.M. Chuang, *Lithium activates the serine/threonine kinase Akt-1 and suppresses glutamate-induced inhibition of Akt-1 activity in neurons.* Proc Natl Acad Sci U S A, 1999. **96**(15): p. 8745-50.

18. Nemoto, T., et al., *Regulation of Akt mRNA and protein levels by glycogen synthase kinase-3beta in adrenal chromaffin cells: effects of LiCl and SB216763.* Eur J Pharmacol, 2008. **586**(1-3): p. 82-9.

19. Lewitt, M.S., et al., *Lithium chloride inhibits the expression and secretion of insulin-like growth factor-binding protein-1.* J Endocrinol, 2001. **171**(3): p. R11-5.

20. Makoukji, J., et al., *Lithium enhances remyelination of peripheral nerves.* Proc Natl Acad Sci U S A, 2012. **109**(10): p. 3973-8.

21. Jo, H., et al., *Small molecule-induced cytosolic activation of protein kinase Akt rescues ischemia-elicited neuronal death.* Proc Natl Acad Sci U S A, 2012. **109**(26): p. 10581-6.

22. Brites, P., et al., *Plasmalogens participate in very-long-chain fatty acid-induced pathology.* Brain, 2009. **132**(Pt 2): p. 482-92.

23. De Sarno, P., et al., *Lithium prevents and ameliorates experimental autoimmune encephalomyelitis.* J Immunol, 2008. **181**(1): p. 338-45.

24. Flores, A.I., et al., *Akt-mediated survival of oligodendrocytes induced by neuregulins.* J Neurosci, 2000. **20**(20): p. 7622-30.

25. Alkan, A., et al., *Delayed myelination in a rhizomelic chondrodysplasia punctata case: MR spectroscopy findings.* Magn Reson Imaging, 2003. **21**(1): p. 77-80.

26. Bams-Mengerink, A.M., et al., *MRI of the brain and cervical spinal cord in rhizomelic chondrodysplasia punctata.* Neurology, 2006. **66**(6): p. 798-803; discussion 789.

27. Rodemer, C., et al., *Inactivation of ether lipid biosynthesis causes male infertility, defects in eye development and optic nerve hypoplasia in mice.* Hum Mol Genet, 2003. **12**(15): p. 1881-95.

28. Lariosa-Willingham, K.D., et al., *Development of a central nervous system axonal myelination assay for high throughput screening.* BMC Neurosci, 2016. **17**: p. 16.

29. Watkins, T.A., et al., *Distinct stages of myelination regulated by gamma-secretase and astrocytes in a rapidly myelinating CNS coculture system.* Neuron, 2008. **60**(4): p. 555-69.

30. Baglole, C.J., et al., *Isolation and phenotypic characterization of lung fibroblasts.* Methods Mol Med, 2005. **117**: p. 115-27.

31. Van Veldhoven, P.P. and R.M. Bell, *Effect of harvesting methods, growth conditions and growth phase on diacylglycerol levels in cultured human adherent cells.* Biochim Biophys Acta, 1988. **959**(2): p. 185-96.

32. Van Veldhoven, P.P. and G.P. Mannaerts, *Inorganic and organic phosphate measurements in the nanomolar range.* Anal Biochem, 1987. **161**(1): p. 45-8.

33. Mezzar, S., E. de Schryver, and P.P. Van Veldhoven, *RP-HPLC-fluorescence analysis of aliphatic aldehydes: application to aldehyde-generating enzymes HACL1 and SGPL1.* J Lipid Res, 2014. **55**(3): p. 573-82.

Chapter 3

Regional-specific axonal and glial dysfunctions in the demyelinated plasmalogen-deficient CNS

Regional-specific axonal and glial dysfunctions in the demyelinated plasmalogen-deficient CNS

Ana Rita Malheiro[1,2], Pedro Brites[2]

[1]Neurolipid Biology group, Instituto de Biologia Molecular e Celular – IBMC e Instituto de Investigação e Inovação em Saúde – i3S, Universidade do Porto, Rua Alfredo Allen 208 4200-135, Porto, Portugal, [2]ICBAS, Instituto Ciências Biomédicas Abel Salazar, Rua Jorge Viterbo Ferreira 228, 4050-223 Porto, Portugal

Introduction

In the central nervous system (CNS), oligodendrocytes (OLGs) are responsible for the ensheathment and myelination of axons, which not only enables the communication between neurons but also the integrity and functions of axons [1-3]. Abnormal myelination during development or myelin loss (demyelination) in adults is mechanistically related to various central nervous system disorders. In CNS demyelinating diseases, axon-glial cell interactions, axon organization, electrical conduction and connectivity can all be disrupted. In addition, changes in the axonal caliber and axonal transport rates coupled with deficiencies in myelin morphology and composition are also common features [4].

Besides the essential role of oligodendrocytes, signals from other cell types, namely astrocytes and microglia, are also critical participants in every major aspect of CNS development, function, and disease [5]. Astrocytes are known participate in regulating developmental myelination and myelin maintenance in the CNS, playing an active role in OPC survival, oligodendrocyte differentiation, maturation and myelination [6]. However, astrocytes become activated (reactive) in response to many CNS pathologies, such as trauma, hypoxia, and in many neurodegenerative diseases, leading to astrocytosis. Astrocytosis is characterized by cellular hypertrophy, abnormal increase in the number of astrocytes and increased

expression of glial fibrillary acidic protein (GFAP) [7]. The functions of reactive astrocytes are not well understood, and both harmful and beneficial activities have been reported [8]. Microglia, the resident "macrophages" of CNS tissues, also act as sentinels to detect the first signs of invasion, inflammation or injury. Acting as scavengers, these cells are known to remove cell and myelin debris, and may produce inflammatory signaling molecules, contributing for supportive and homeostatic functions within the CNS [9]. In homeostatic conditions, microglia promote oligodendrocyte progenitor cells survival, differentiation and myelination [10, 11]. However, the role of microglia in disease is extremely complex, as these cells may progress from a supportive/sensing role to a reactive status, possibly participating in the further deterioration of neurons and oligodendrocytes [12]. However, like astrocytes, much of their functions and mode of action remain mysterious [5]. Moreover, microgliosis and astrocytosis in some cases occur together, but it is not known whether there is a causal connection and if so in which direction [13].

Axon or neuron degeneration are common features in chronically demyelinated conditions, that can aggravate the pathology, the disease status and its severity. The neuronal cytoskeleton is known to play an essential role during nervous system development, maintenance and also during regenerative processes that follow injury [14, 15]. In this line of thought, there is a new emerging connection, that relates neurodegeneration with abnormal or impaired cytoskeletal processes. The cytoskeletal dysfunctions involved within the neurodegenerative framework include alterations in microtubule stability, altered posttranslational modifications of microtubules (PTMs), alterations in microtubule dynamics, and alterations in microtubule-based organelle transport, which together may have direct implications in the normal functioning of axons and neurons [15, 16].

Here, we unraveled that the progressive demyelination caused by the lack of plasmalogens, is concomitant with generalized astrocytosis and white matter-selective microgliosis. Additionally, the deficiency in plasmalogens modulates a regional-specific axonal damage without causing major axon loss. The observed axonal damage was characterized by axonal swelling, severing and abnormal membrane protrusions that seem to accumulate at the adaxonal membrane of mutant oligodendrocytes. Whilst trying to characterize the basis for the axonal defects we unraveled a major dysregulation in the tubulin cytoskeleton.

Results

Astrocytosis and microgliosis during active demyelination

Following previous descriptions of astrocytosis in cerebellum and brain stem [17, 18], and microgliosis in cerebellar white matter [17] we also analyzed the gliotic status in spinal cord and optic nerve of 1.5 years old *Gnpat* KO mice and age-matched WT mice. GFAP is an intermediate filament protein expressed in astrocytes, whose expression levels increases upon astrocyte activation [7]. Staining with an antibody against GFAP, revealed increased number of astrocytes, with a reactive appearance, in the white and grey matter of spinal cords from *Gnpat* KO mice (Fig. 1A). Ionized calcium binding adaptor molecule 1 (Iba-1) is protein specifically expressed in macrophages and microglia, whose expression is increased upon activation as it is involved in membrane ruffling and phagocytosis [19]. Staining with an antibody against Iba-1, revealed that microgliosis was restricted to the spinal cord whiter matter from *Gnpat* KO mice (Fig. 1C).

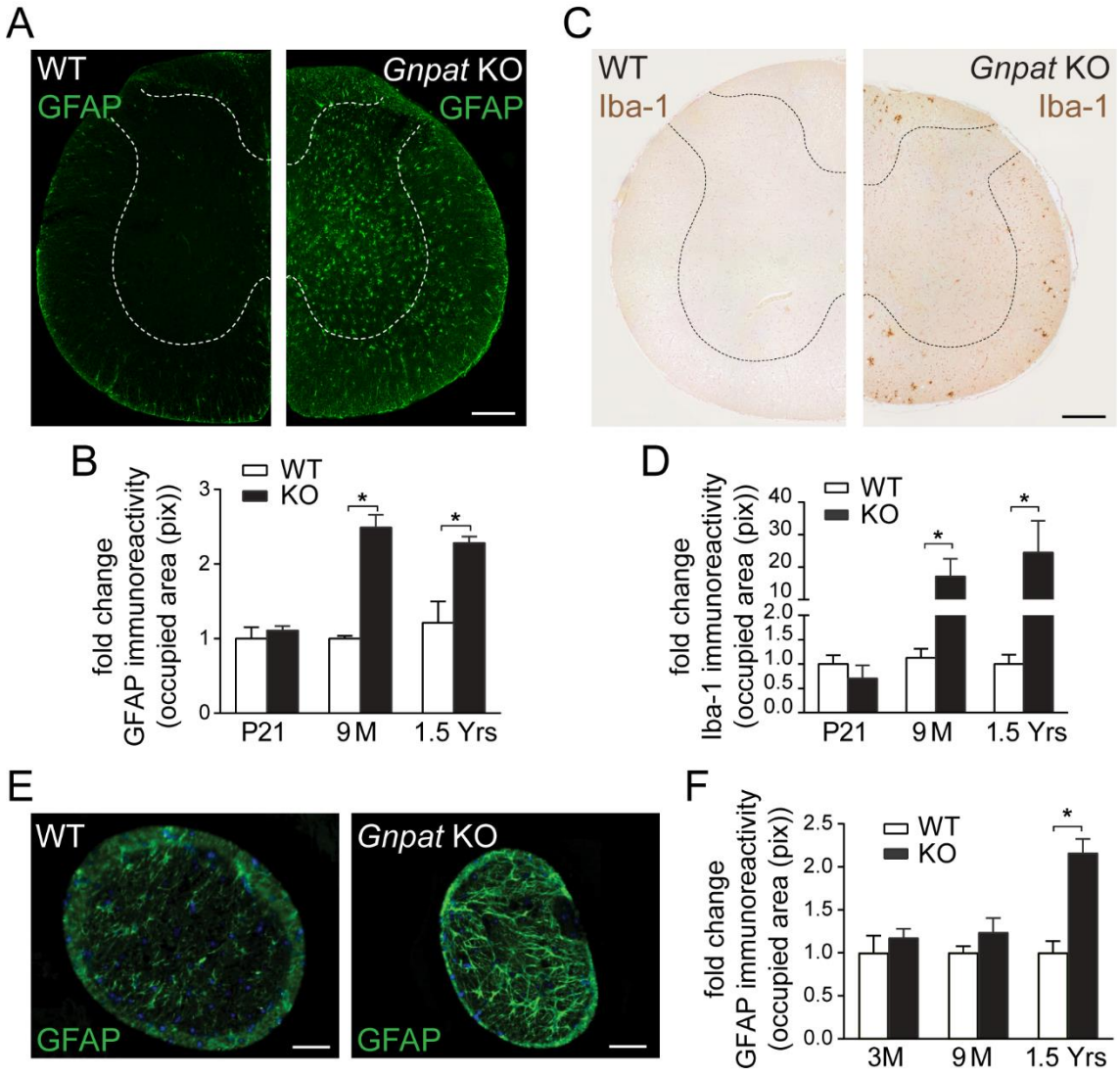

Figure 1. Acquired astrocytosis and microgliosis in demyelinated CNS from plasmalogen-deficient mice. A Representative photomicrographs of staining with GFAP, showing astrocytosis in the spinal cords from 1.5 years old *Gnpat* KO mice. **B** Quantification of GFAP immunoreactivity demonstrating that at 21 days (P21) *Gnpat* KO mice present normal levels of GFAP, but from 9 months (9M) of age, spinal cords from *Gnpat* KO mice showed extensive and progressive astrocytosis, being the reactive astrocytes present both in grey and white matter. **C** Representative photomicrographs of spinal cords stained with Iba-1, revealing extensive microgliosis restricted to the white matter (dotted area) in the spinal cords of *Gnpat* KO mice at 1.5 years old, with very few reactive microglia in the gray matter. **D** Quantification of Iba-1 immunoreactivity showed normal levels of Iba-1 in spinal cords of 21 days old *Gnpat* KO mice, but from 9 months of age spinal cord from *Gnpat* KO mice showed extensive and progressive microgliosis. **E** Representative photomicrographs of staining with GFAP, showing astrocytosis in the optic nerves from *Gnpat* KO mice at 1.5 years. **F** Quantification of GFAP immunoreactivity demonstrating that at 3 and 9 months optic nerves from *Gnpat* KO mice present normal levels of GFAP, but at 1.5 years old showed extensive astrocytosis. Student's T test in B and C, n=4-8 mice per group per time point. * $P<0.05$. Scale bars are 200µm in A and B and 40µm in E.

The assessment of the gliotic status in spinal cord at three different stages of the disease highlighted sustained astrocytosis and microgliosis from 9 months onwards (Fig. 1B, 1D). Surprisingly, analyses in optic nerves revealed the occurrence of astrocytosis only at 1.5 years of age (Fig. 1E and F) and microgliosis was never observed in optic nerves from *Gnpat* KO mice (data not shown). Taken together, these results indicate that during the active demyelination phase, generalized astrocytosis and white matter-selective microgliosis are also observed in a plasmalogen deficient mouse model. Even so, knowing the possible negative consequences of astrocyte and microglial activation, as well as the importance of oligodendrocytes and myelin to maintain axonal health, we investigated whether loss of myelin and activation of glial cells could cause axonal damage.

Regional-specific and demyelination-independent axonal damage in plasmalogen-deficient CNS

Demyelinated and/or damaged axons are known to display a higher proportion of non-phosphorylated neurofilaments [20]. To investigate possible axonal abnormalities, we determined the pattern and expression levels of non-phosphorylated and phosphorylated neurofilaments in spinal cords from WT and plasmalogen-deficient mice from P21 to 1.5 years of age. Staining with SMI-31 antibody, which recognizes phosphorylated neurofilaments did not reveal major abnormalities in spinal cords from *Gnpat* KO mice from P21 to 9 months of age (data not shown). Nevertheless, in spinal cords from 1.5 years old *Gnpat* KO mice, we observed a decrease in immunoreactivity (Fig. 2A and B). Staining with SMI-32 antibody, which recognizes non-phosphorylated neurofilaments, did not reveal any abnormalities in spinal cords from *Gnpat* KO mice from P21 to 9 months of age (data not shown). However, we observed a pronounced increase in non-

phosphorylated neurofilaments in spinal cords from 1.5 years old *Gnpat* KO mice (Fig. 2C and D), which suggest the presence of axonal damage. Optic nerves from *Gnpat* KO mice showed normal levels of phosphorylated and non-phosphorylated neurofilaments (Fig. 3), which combined with the ultrastructural analyses (see chapter 1) suggest absence of axonal damage.

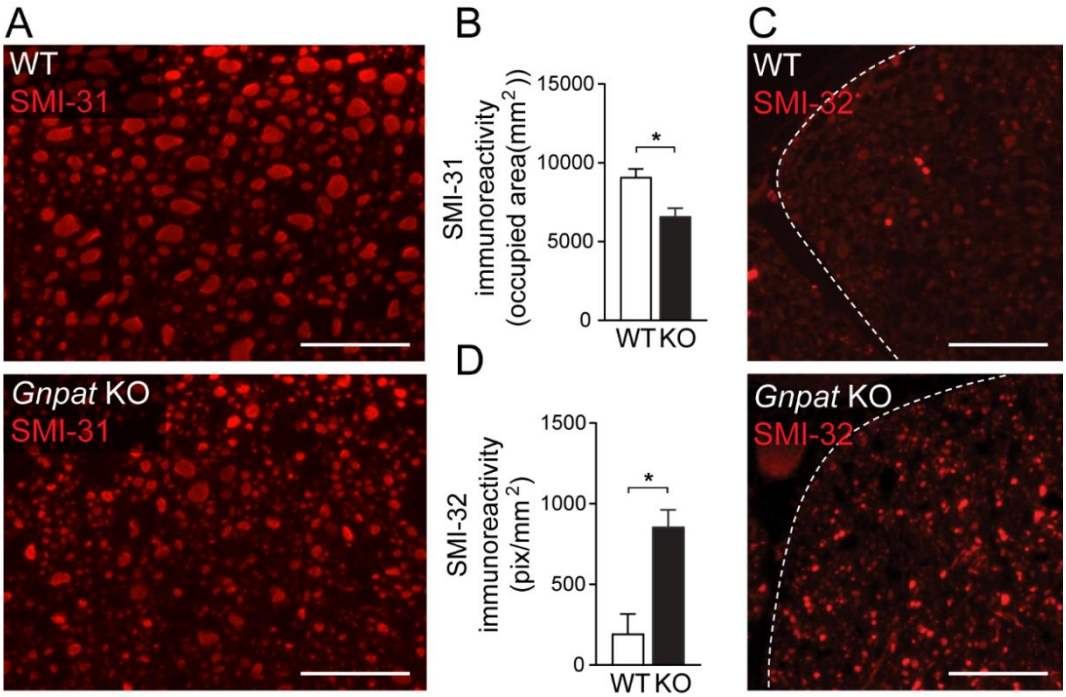

Figure 2. Changes in neurofilament phosphorylation in the spinal cords from plasmalogen-deficient mice. A Representative photomicrographs of spinal cords from 1.5 years old WT and *Gnpat* KO mice labeled with SMI-31 antibody. **B** Quantification of SMI-31 signal revealed a decrease in immunoreactivity in spinal cords of *Gnpat* KO mice, indicating a decrease in phosphorylated neurofilaments. **C** Representative photomicrographs of staining with SMI-32 (a marker of axonal damage) in the ventral funiculus of lumbar spinal cords (delineated by the dotted line) from WT and *Gnpat* KO mice at 1.5 years old. **D** Quantification of SMI-32 signal revealed an increase in immunoreactivity in spinal cords of *Gnpat* KO mice. Scale bars are 50µm.

To evaluate the occurrence of axonal damage in the CNS of plasmalogen-deficient mice we generated a new mouse line. We crossed the *Gnpat* mouse line with mice that express yellow fluorescent protein (YFP) under the neuronal Thy1 promoter (Thy1-YFP; [21]) to generate WT and *Gnpat* KO mice with widespread

neuronal expression of YFP in cell bodies and axons. The analysis of longitudinal sections of spinal cords from 7-month and 1.5-year-old *Gnpat* KO:YFP mice revealed clear signs of axonal damage, including axonal swellings, constrictions and axonal degeneration (Fig. 4A and B). The analysis in non-consecutive sections from spinal cords of *Gnpat* KO mice highlights the extent of the observed axonal abnormalities (Fig. 4C). In accordance with previous analyses, optic nerves from *Gnpat* KO:YFP mice lacked clear signs of axonal damage (Fig. 4D). The ultrastructural analysis of optic nerves from *Gnpat* KO mice highlighted the severe loss of myelin and confirmed the sparing of axons, which lacked any sign of damage (Fig. 4E).

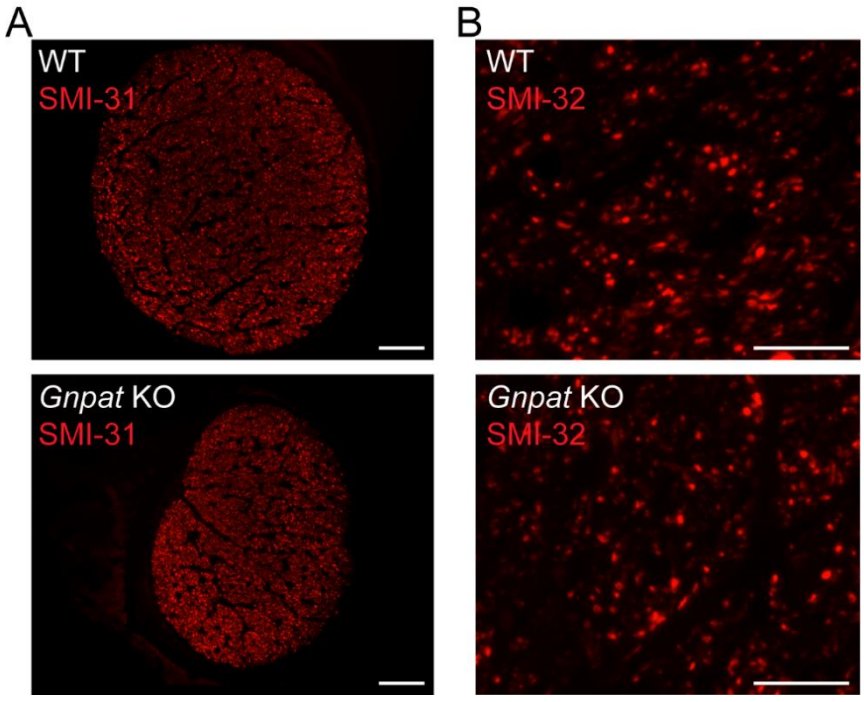

Figure 3. Normal phosphorylation levels of neurofilaments in demyelinated optic nerves from plasmalogen-deficient mice. A Representative photomicrographs of optic nerves from 1.5years old WT and *Gnpat* KO mice labeled with SMI-31 antibody. **B** Representative photomicrographs of staining with SMI-32 (a marker of axonal damage) in optic nerves from WT and *Gnpat* KO mice at 1.5 years old. The histological analysis failed to indicate any changes in the levels of dephosphorylated neurofilaments, suggesting the absence of major sings of axonal damage in the demyelinated fibers of *Gnpat* KO nerves. Scale bars are 50µm in A and 25µm in B.

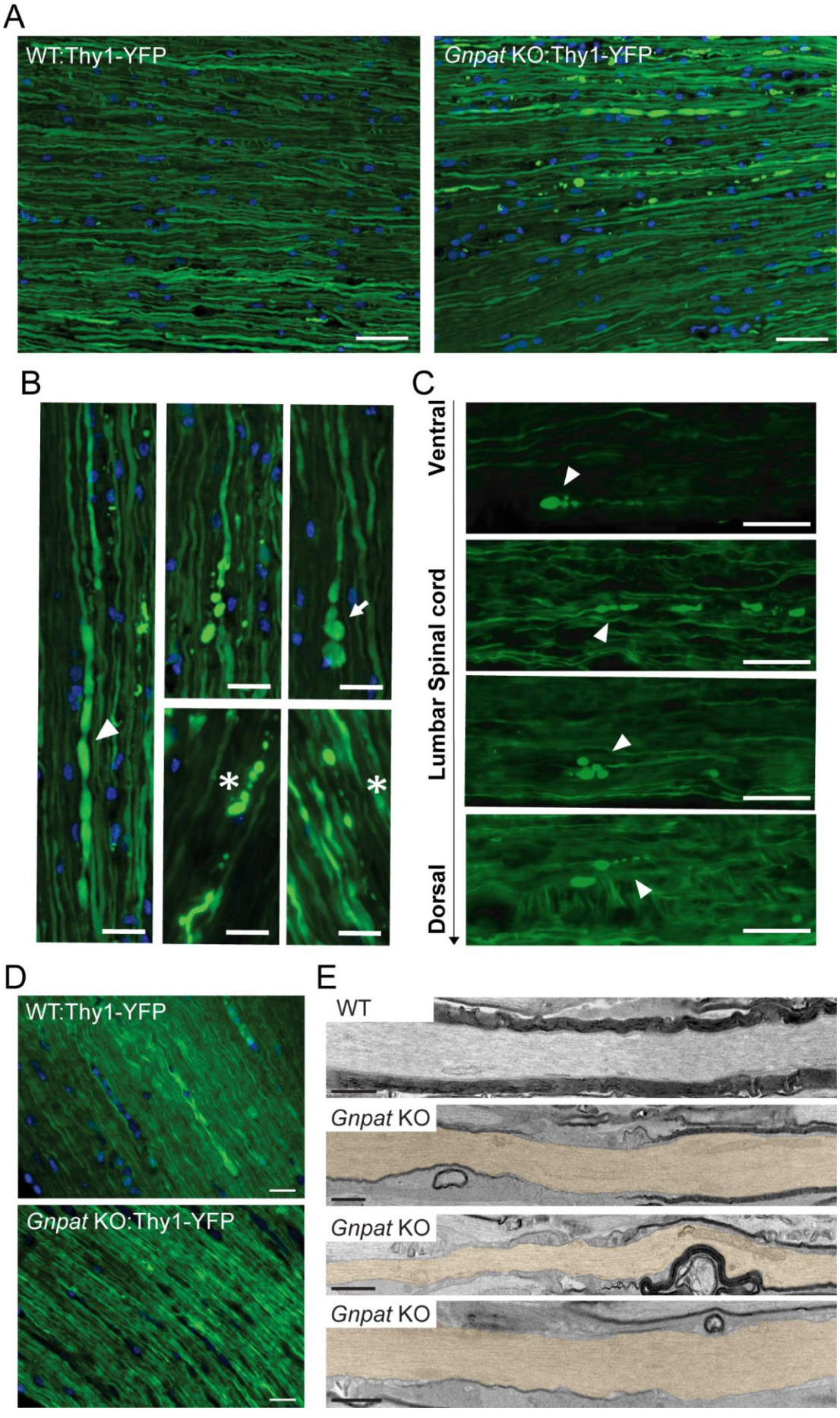
A
WT:Thy1-YFP
Gnpat KO:Thy1-YFP
B
C
Ventral
Lumbar Spinal cord
Dorsal
D
WT:Thy1-YFP
Gnpat KO:Thy1-YFP
E
WT
Gnpat KO
Gnpat KO
Gnpat KO

◄Figure 4. CNS demyelination is accompanied by regional-specific axonal damage. A Fluorescence microscopy analysis of longitudinal spinal cords from 7 months old WT:Thy1-YFP and *Gnpat* KO:Thy1-YFP mice, revealing signs of axonal damage in mutant animals. **B** Fluorescence microscopy analysis of longitudinal sections of spinal cord from 7 months old *Gnpat* KO:Thy1-YFP mice revealing axonal damage. **C** Fluorescence microscopy analysis of longitudinal sections of spinal cord from 1.5 years old *Gnpat* KO:Thy1-YFP mice revealed the extent of axonal damage. Each panel highlights axonal damage events (arrowheads) in non-consecutive sections (spaced by 80µm). **D** Fluorescence microscopy analysis of longitudinal optic nerves from 3 months old WT:Thy1-YFP and *Gnpat* KO:Thy1-YFP mice revealed no signs of axonal damage in mutant animals. **E** Electron micrographs of longitudinal sections of optic nerves from 1.5 years old WT and *Gnpat* KO mice. Axons were pseudocolored in light brown with transparency in order to facilitate visualization. Scale bars are in A 50µm and 25µm in B, 1µm in C, 20µm in D and 1µm in E.

Ultrastructural analysis of longitudinal sections of spinal cords from *Gnpat* KO mice at 1.5 years of age highlighted the extent of axonal damage. The observed defects on spinal cords from *Gnpat* KO mice, included axonal swellings with accumulation of organelles (Fig. 5A) and axonal degeneration (Fig. 5B). In addition, swollen myelinated axons with accumulation of abnormal organelles were observed in the internal capsule and cerebellum (Fig. 6) of *Gnpat* KO mice. Interestingly, the axonal defects were primarily observed in myelinated axons. In addition to the most common defects associated with axonal damage, we also identified outfoldings of the axonal membrane and the presence of vesicle-like structures in spinal cords (Fig. 5C-G) and cerebellum (Fig. 6) of aged *Gnpat* KO mice. Although these vesicle-like structures seemed to reside in the periaxonal space, detailed analysis of the electron microscopy images revealed that the outfoldings of axonal membranes were lined with the oligodendrocyte adaxonal membrane (Fig. 5F, G). The complex nature and the arrangement of the vesicle-like structures seem to derive from the axonal membrane outfoldings. In some cases, the ultrastructural images revealed the continuous adaxonal membrane of the oligodendrocyte and what seems to be an excised vesicle derived from the axonal outfolding (Fig. 5G).

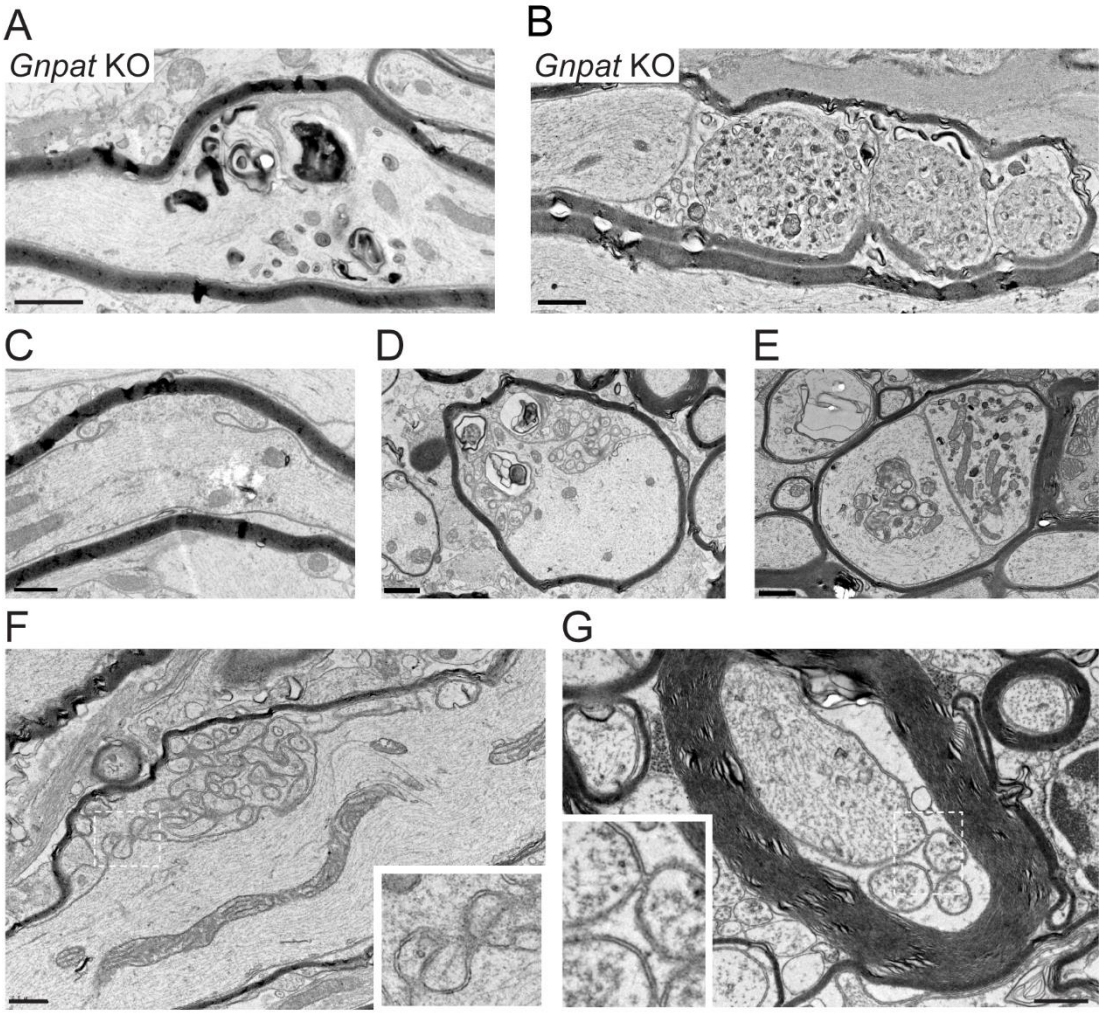

Figure 5. Axonal damage in the demyelinated spinal cords from *Gnpat* KO mice. **A** and **B** Electron micrographs (EM) of spinal cords from *Gnpat* KO mice at 1.5 years old of age revealing axonal swelling with accumulation of organelles (A) and axonal degeneration (B). **C – G** Abnormal axonal outfoldings with multiple large vesicle-like structures in spinal cords from *Gnpat* KO mice at 1.5 years old mice. Scale bars are 1µm.

Combined, these results highlight that a deficiency in plasmalogens modulates regional-specific axonal damage without causing major axon loss. The optic nerve from plasmalogen-deficient mice was spared from axonal damage, although it was characterized by an initial severe dysmyelination and the ensuing demyelination. In other regions of the CNS, including the internal capsule, cerebellum and spinal cord, axonal damage was readily observed and was characterized by axonal swelling, severing and abnormal membrane protrusions that seem to accumulate at the adaxonal membrane of mutant oligodendrocytes.

Although it is widely thought that myelin loss can modulate and contribute to axonal damage, in plasmalogen deficient mice axon damage was observed in myelinated axons, suggesting the existence of an axonal intrinsic, demyelination-independent defect.

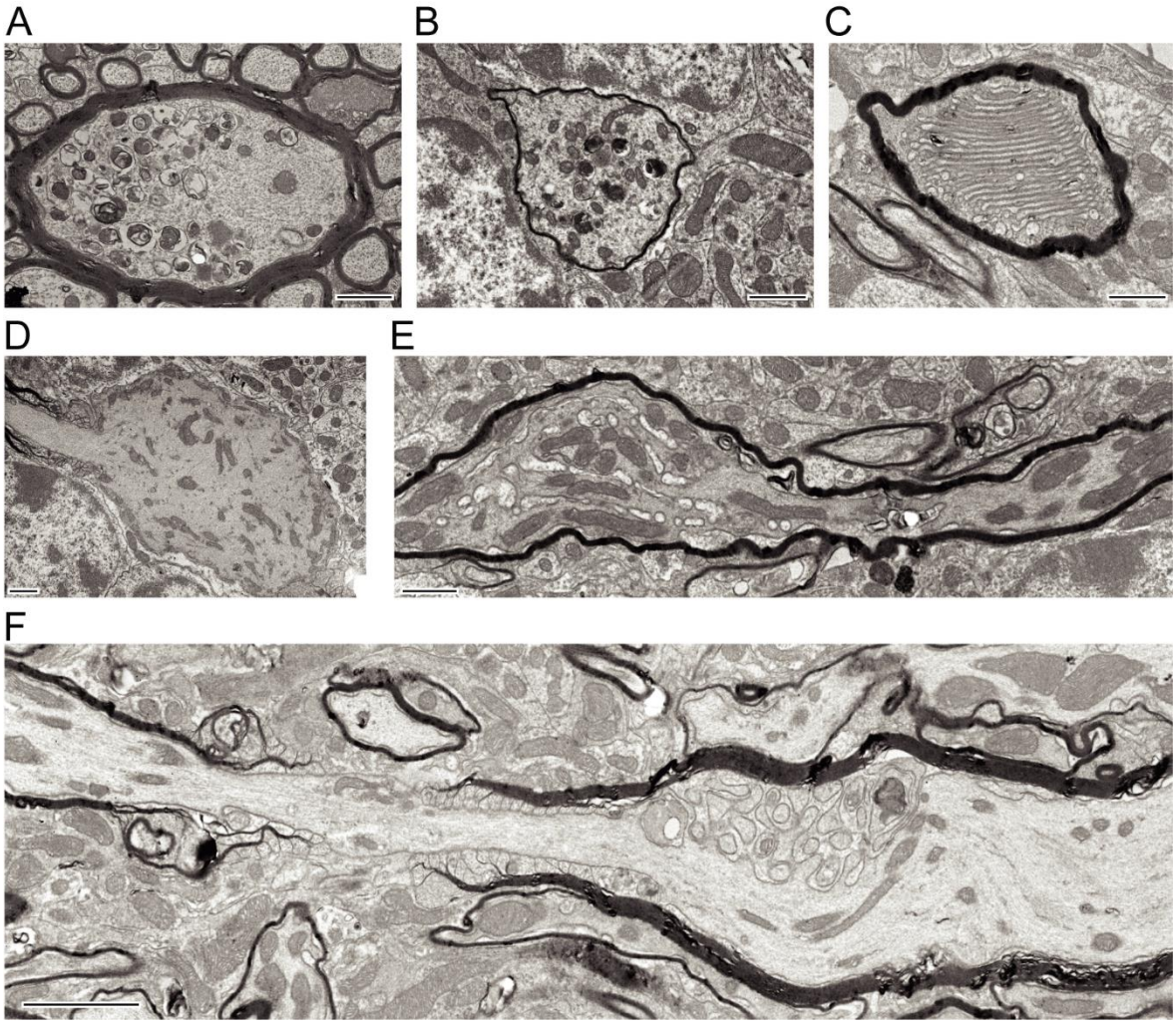

Figure 6. Regional-specific axonal damage in brain from1.5 years old *Gnpat* KO mice. A Electron micrograph of a large swollen myelinated axon with accumulation of abnormal organelles in internal capsule from *Gnpat* KO mice. **B** and **C** Ultrastructure of axonal swellings in cerebellum from *Gnpat* KO mice, containing an accumulation of several organelles, including mitochondria and membranous stacks. **D** Electron micrograph of a giant axonal swelling at the node of Ranvier with accumulation of mitochondria in cerebellum from *Gnpat* KO mice. **E** Electron micrograph of longitudinal section of cerebellum from *Gnpat* KO mice, revealing an axonal swelling with accumulation of mitochondria and organelles. **F** Electron micrograph of longitudinal section of cerebellum from *Gnpat* KO mice, showing multiple large vesicle-like structures. Scale bars are 1µm in A – E, and 2µm in F.

Major dysregulation of tubulin cytoskeleton concomitant with axonal damage in the spinal cords of *Gnpat* KO mice

The axonal damage observed on plasmalogen-deficient axons, together with the emerging connection that relates cytoskeletal impairments with neurodegeneration, prompted us to evaluate the neuronal cytoskeleton. To investigate possible cytoskeletal dysfunctions, we evaluated the levels of tubulins and tubulin post-translational modifications (PTMs) in the spinal cord and optic nerve. The levels of acetylated tubulin, tyrosinated tubulin, de-tyrosinated tubulin, and △2-tubulin, as well as the total expression levels of α-tubulin and βIII-tubulin were determined by western blot (Fig. 7). The levels of total-ERK were used as an internal loading control for the analysis of α- and βIII-tubulin, whereas tubulin PTMs were normalized to the levels of α-tubulin. Quantitative analysis at 1.5 years of age revealed that levels of total α-tubulin and βIII-tubulin were significantly increased in the spinal cords from *Gnpat* KO mice compared to age-matched WT mice (Fig. 7A and B). The analyses of tubulin PTMs showed that the levels of tyrosinated tubulin were increased in *Gnpat* KO mice, whereas the levels of de-tyrosinated tubulin, acetylated tubulin and △2-tubulin were reduced in *Gnpat* KO mice (Fig. 7A and B). The quantitative analysis of tubulin and tubulin PTMs in optic nerves from 1.5 years old WT and *Gnpat* KO mice revealed normal levels of α- and βIII-tubulin (Fig. 7C and D). The levels of acetylated and de-tyrosinated tubulin were normal whereas tyrosinated and △2-tubulin levels were reduced in *Gnpat* KO mice (Fig. 7C and D). We also analyzed the levels of tyrosinated and acetylated tubulin in spinal cords from WT and *Gnpat* KO mice at 7 months of age (data not shown). Our preliminary assessment revealed increased levels of tyrosinated tubulin and decreased acetylated tubulin in spinal cords from *Gnpat* KO mice, and suggest that altered axonal cytoskeleton and possibly impaired axonal function precedes the onset of demyelination and axonal damage.

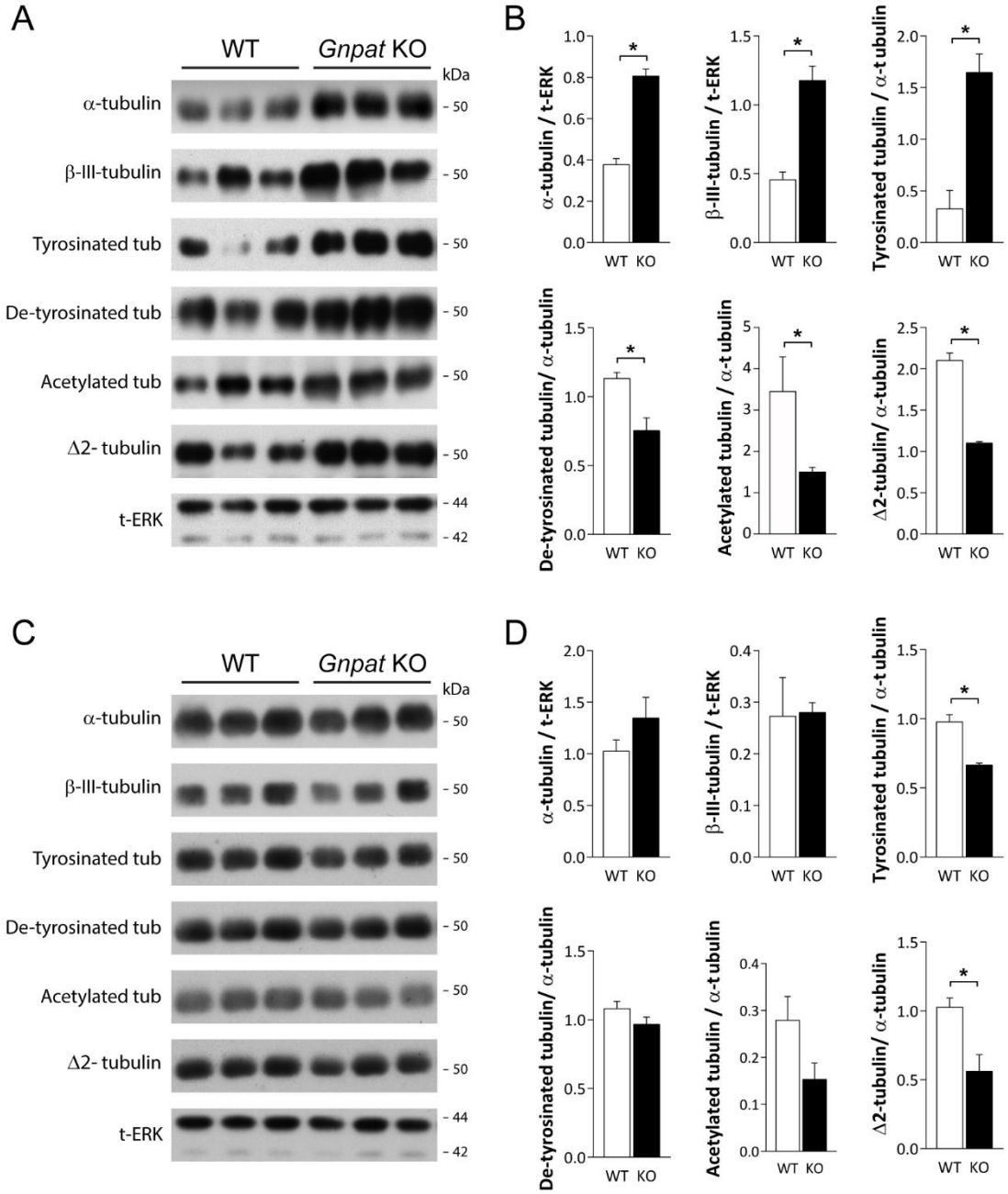

Figure 7. Major dysregulation of tubulin modifications concomitant with axonal damage. A Western blot analysis for α-Tubulin, βIII-Tubulin, tyrosinated tubulin, de-tyrosinated tubulin, acetylated tubulin and Δ-2-Tubulin in spinal cords from 1.5 years old WT and *Gnpat* KO mice. **B** Quantification of the protein levels in spinal cord extracts from WT and *Gnpat* KO mice at 1.5 years old. **C** Western blot analysis for α-Tubulin, βIII-Tubulin, tyrosinated tubulin, de-tyrosinated tubulin, acetylated tubulin and Δ-2-Tubulin in optic nerves from 1.5 years old WT and *Gnpat* KO mice. **D** Quantification of the protein levels in optic nerve extracts from WT and *Gnpat* KO mice at 1.5 years old. Student's T test in B and C, n = 4-6 mice per group per time point. Graphs are presented as mean + SEM. p-value (*) < 0.05.

To determine if the increased levels of α- and βIII-tubulin observed in spinal cords of *Gnpat* KO mice would cause an impact in the tubulin cytoskeleton, we measured the densities of microtubules in spinal cord axons from WT and *Gnpat* KO mice. The results showed a 2-fold increase in the density of microtubules (Fig. 8A and B). This ultrastructural analysis also highlighted a abnormally reduced spacing of neurofilaments in axons of *Gnpat* KO mice (Fig. 9A). These observations fit the known relationship between neurofilament phosphorylation and their spacing [22-24], and our findings that *Gnpat* KO axons had decreased levels of phosphorylated neurofilaments (Fig. 2A).

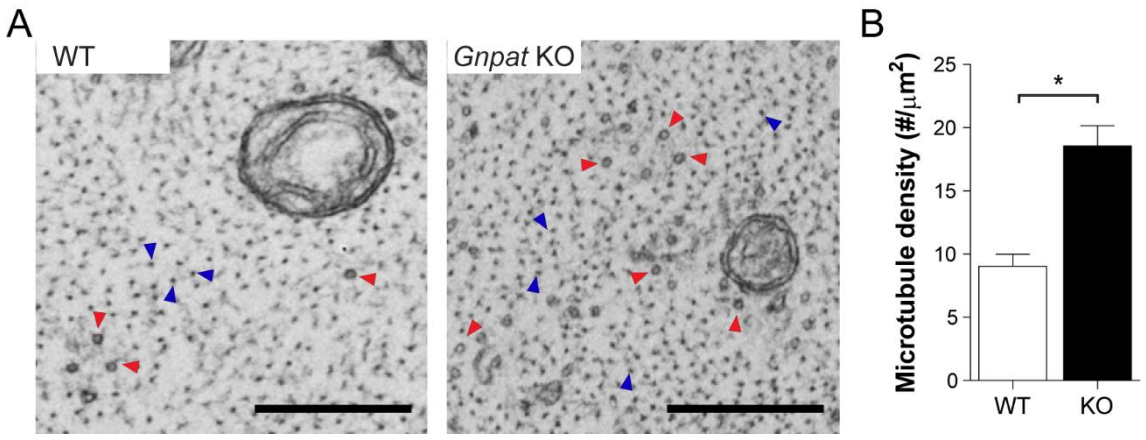

Figure 8. Increased microtubule density in spinal cord axons from older *Gnpat* KO mice. A Electron micrographs of cross sections of spinal cords axons from 1.5 years old WT and *Gnpat* KO mice. The red arrowheads indicate the microtubules and the blue arrowheads the neurofilaments. **B** Quantification of the microtubule density in spinal cord axons from WT and *Gnpat* KO mice. Scale bars are 400 nm.

Together with the histological (Fig. 3) and ultrastructural (Fig. 4E) findings, these results indicate that normal-appearing axons in optic nerves from *Gnpat* KO mice have normal or minimal changes in the tubulin cytoskeleton, whereas spinal cord axons possess multiple signs of degeneration (Fig. 2 and Fig. 5) and abnormal levels of tubulin, its PTMs and microtubules.

Discussion

Previously, we demonstrated that differentiated oligodendrocytes are a prime target of a deficiency in plasmalogens, causing impaired myelination and myelin maintenance. Here, we unraveled the consequences of a plasmalogen deficiency for axon health in a mouse model for RCDP.

Astrocytosis and microgliosis were previously observed in brains of *Gnpat* KO mice [17, 18]. However, the relationship between these anomalies and the precise onset and progression of the pathology in different CNS regions were not elucidated. Here, we unraveled that during the active demyelination phase, a generalized astrocytosis and white matter-selective microgliosis occur in a plasmalogen-deficient mouse model. Astrocytosis and microgliosis can occur in response to different CNS pathologies, including demyelinating diseases. However, the functions of reactive astrocytes and/or microglia are not completely understood, and both harmful and beneficial activities have been observed and/or postulated. In the *Gnpat* KO mice, since the plasmalogen deficiency did not cause neuronal or oligodendrocyte loss, we hypothesized that the presence of activated astrocytes and microglia does not have a major detrimental effect on neurons or oligodendrocytes. However, we cannot exclude a possible contribution of the observed astrocytosis and/or microgliosis in axonal damage. This possibility is raised because in optic nerves from *Gnpat* KO mice the extreme defect in myelin does not cause major axonal changes and we only observed astrocytosis in late stages of the pathology. In clear contrast, major axonal defects were observed in spinal cords from *Gnpat* KO mice, which were also characterized by reactive astrocytosis and microgliosis. However, previous reports revealed that the *Gnpat* KO mice do not display an inflammatory phenotype, as pro-inflammatory cytokines were not induced [18]. In addition, we identified microglia engaged in clearing myelin and myelin debris in spinal cords of *Gnpat* KO mice [25] . As such we favor

the hypothesis that the observed astrocytosis and microgliosis is a consequence of the leukodystrophy and should have a minimal impact in the observed axonal degeneration.

At least two distinct observations warrant the hypothesis that the axon damage observed in *Gnpat* KO mice is not directly caused by the loss of myelin. First, optic nerves from mutant mice are the most severely affected CNS region in terms of myelin loss but we were not able to detect signs of axonal damage, contrary to previous claims [26]. Second, the observed evidences of axonal damage, namely axonal swellings with accumulation of organelles and axon severing, were exclusively found in myelinated axons within several CNS regions (e.g. spinal cord, cerebellar white matter, and internal capsule). In addition to the common signs of axonal damage, we also observed axonal outfoldings in *Gnpat* KO axons. The myelin-associated glycoprotein (MAG) is known to play a role in stabilizing oligodendrocyte-axon contacts in mature myelin sheaths, which may be involved in the long-term stability of axons [27]. Therefore, the decreased levels of MAG observed in plasmalogen-deficient myelin (see chapter 1) may disturb the myelin-axon stability and lead to the development of the axonal outfoldings observed in *Gnpat* KO axons during the late-stages of the disease progression. These scenarios warrant the possibility that a plasmalogen deficiency also causes a neuronal-intrinsic defect.

Specific cellular mechanisms that have been linked to axonal degeneration include deficits in axonal transport, mitochondrial dysfunction, and cytoskeletal breakdown [28]. A major component of the cytoskeleton is formed by microtubules, polarized structures composed of α- and β-tubulin heterodimers. These highly dynamic structures are essential for many cellular functions, including cell polarity, cell division, neuronal differentiation, intracellular trafficking and localization of organelles [29]. In addition, microtubules are subjected to a wide

range of posttranslational modifications, including tyrosination/detyrosination, acetylation and △2-tubulin generation [30]. The carboxy-terminal tyrosine is encoded in most α-tubulins, and most isoforms of α-tubulins undergoes a cycle of detyrosination-tyrosination, by a proteolytic removal of the C-terminal Tyr (Y) residue on α-tubulin [31]. This type of modification is reversible, once the re-addition of Tyr functional group (tyrosination) serves to reverse the modification and to return tubulin to its nascent state [31]. The product of the detyrosination reaction, known as "Glu-tubulin", is prevalent in stable/long-lasting microtubules that display little dynamic, whereas tyrosinated tubulin, "Tyr-tubulin", is found mainly in dynamic microtubules [31]. Interestingly, the detyrosinated α-tubulin can undergo a second proteolysis, in which the penultimate glutamate (E) residue is removed, generating Δ2-tubulin [32]. In its turns, acetylation of Lys40 on α-tubulin, occurs after microtubule assembly [33]. All these PTMs of tubulin subunit diversify the outer and luminal surfaces of microtubules, providing a potential mechanism for their functional specialization. In this way, some of these modifications have been associated with efficient axonal transport, allowing greater binding and movement of motor proteins [34]. Loss or reduction in the levels of one or more tubulin PTMs have been linked with several neurological disorders, including Alzheimer's disease, Huntington's disease, and Charcot-Marie-Tooth [35]. In *Gnpat* KO mice, the observed axonal damage was accompanied by a dysregulation of the tubulin cytoskeleton. Spinal cords from 1.5 years old *Gnpat* KO mice, presented increased density of microtubules, and increased levels of α-tubulin and βIII-tubulin, as well as increased tyrosinated tubulin [30]. In addition to these changes, we also observed abnormal PTMs of tubulin, namely decrease in the levels of de-tyrosinated tubulin, acetylation and △2-tubulin. However, it is difficult to model how a deficiency in plasmalogens would affect at the same time the multiple enzymes [35, 36] necessary for the

different PTMs of tubulin. Based on the observed axon pathology we postulate that: as a consequence of axon dysfunction or damage, neurons undergo a compensatory mechanism that induces overexpression of tubulins in order to assemble more microtubules. The increase in microtubule numbers and/or tubulin polymerization causes an imbalance in the well-regulated process of tubulin PTMs [30]. At least in the case of α-tubulin N-acetyltransferase 1 (α-TAT1), the enzyme that acetylate α-tubulin [37], it is well establish that this enzyme has slow kinetics of microtubule acetylation [38-40]. As such, increased microtubule numbers may be globally less acetylated. The reductions in the microtubule modifications may then cause additional defects and abnormalities. As mentioned, abnormal microtubule-based organelle transport can be caused by abnormal tubulin PTMs and may cause axonal swellings [41, 42]. Abnormal PTMs may also affect microtubule severing though the action of spastin and/or katanin [43]. The severing of microtubules may generate new filaments [44, 45] that will undergo further polymerization and escalate the defects.

Taken together, we unraveled that the deficiency in plasmalogens modulates a regional-specific axonal damage without causing major axon loss. The observed axonal damage was characterized by axonal swellings, severing and abnormal axonal protrusions that seem to accumulate at the adaxonal membrane of oligodendrocytes. We identified a major dysregulation in the tubulin cytoskeleton that may explain the observed pathology and highlights a novel link between membrane phospholipids and the neuron cytoskeleton.

Material and Methods

Animal experiments

All mouse procedures were done according to the European Directive 2010/63/EU established by the European Parliament and of the Council, as well as the National legislation (Decreto-Lei 113/2013). Mice were used only after approval of the Portuguese General Veterinarian Board.

Mouse models

Gnpat KO mice and WT littermates were obtained from mating *Gnpat* heterozygous mice (on a Swiss-Webster background). All animals were maintained with ad libitum access to rodent food and water, and were kept in a 12:12h light and dark cycle facility. Genotyping was performed by the IBMC CCGen facility using previously developed strategies [26]. *Gnpat* KO mice were crossed with Thy1-YFP-16 mice [21]. This line provides a strong and specific marker for axons, from a mid-gestational stage into adulthood.

Histological and morphological analysis

Electron microscopy

At least 3 *Gnpat* KO and WT mice from each age were analyzed. Mice were deeply anesthetized with ketamine + medetomidine (75mg/kg + 1mg/kg body weight, respectively); lumbar spinal cord, optic nerve and brain were isolated and fixed by immersion.

Tissues were fixed by immersion in 4% glutaraldehyde (Sigma) in 0.1M sodium cacodylate buffer (pH 7.4) solution for 5 days. After washing and two hours in post-fixating 1% osmium tetroxide (Sigma-Aldrich) in 0.1M sodium cacodylate buffer (pH 7.4) solution, tissues were washed in buffer, dehydrated through graded

series of ethanol, and embedded in Epon (EMS). Ultrathin sections were cut at 50 nm, counterstained with lead citrate and uranyl acetate, and observed in a JEOL JEM-1400 transmission electron microscope (equipped with an Orius Sc1000 Digital Camera). Pseudocolored electron microscopy images were processed in Photoshop CS3, by selecting the region of interest and giving color with transparency, in order to highlight the region to be analyzed.

Immunohistochemistry

Tissues were fixed by immersion in PGTA (2% paraformaldehyde, 2% glutaraldehyde in PBS) for 48 hours or in Carnoy's solution (alcohol absolute: methanol: glacial acetic acid – 6:3:1) for 2 hours, processed for paraffin embedding and sectioned on a paraffin microtome (Microm HM 335E), according to routine procedures. Paraffin sections, 4 µm thick, were deparaffinized in histoclear and rehydrated using decreasing concentrations of ethanol and used for immunohistochemical analyses. To detect astrocytes, sections were heated in microwave in citrate solution pH 6.0, washed, permeabilized in 100% methanol, endogenous auto-fluorescence blocked with 0.1% sodium borohydride ($NaBH_4$) in TE (10mM Tris, 1mM EDTA buffer pH 9.0), blocked with 5% normal donkey serum (NDS), incubated with primary antibody against GFAP (Dako Z0334) and incubated with secondary fluorescent antibody (donkey anti-rabbit-AF488). Sections were mounted with Vectashield containing DAPI (Vector Laboratories). Samples were viewed on an AxioImager Z1 (Carl Zeiss, Germany). For microglia detection, sections were heated in microwave in citrate solution pH 6.0, washed, blocked with 5% NDS, incubated with primary antibody against Iba-1 (Abcam), incubated with secondary biotinylated antibody and developed with 3,30-diaminobenzidine tetrachloride (DAB; Sigma) as a substrate, using the Vectorstain Elite peroxidase ABC kit (Vector Laboratories). Sections were dehydrated, cleared in histoclear and

mounted in DPX (MERCK). Samples were viewed on Olympus optical microscope (CX31; equipped with an Olympus DP 25 Camera and Cell B Software). For the analysis of non-phosphorylated neurofilaments, sections were heated in microwave in citrate solution pH 6.0, washed, permeabilized in 100% methanol, endogenous auto-fluorescence blocked with 0.1% $NaBH_4$ in TE, endogenous IgG blocked with blocking reagents from MOM kit, incubated with primary antibody against SMI-32 (Covance) and incubated with secondary fluorescent antibody (donkey anti-mouse-AF568). Sections were mounted with Vectashield containing DAPI (Vector Laboratories). Samples were viewed on an AxioImager Z1. The quantification of SMI-32, GFAP and Iba-1 was performed using Feature J, a java-based plug-in to the imaging software NIH Image J, using a Hessian-based algorithm [46].

Western blots

For Western blot analysis, lysates of lumbar spinal cord and optic nerve were prepared in lysis buffer (0.3% Triton X-100, 1mM sodium orthovanadate, cOmplete™ Protease Inhibitor Cocktail in PBS), and 5μg protein was run on 12% SDS-PAGE gels. Nitrocellulose membranes blocked with 5% skim milk (Fluka) in Tris-buffered saline with 1% Tween 20 (TBS-T) for 1h at RT, washed with TBS-T, and probed with different primary antibodies (Table 1) diluted in 5% BSA + TBS-T (overnight at 4°C). After incubation with HRP-labeled secondary antibodies, diluted 1:5000 in 5% skim milk in TBS-T and incubated for 1h at RT, the blots were developed with ECL (Pierce) and exposed to Hyperfilm (Amersham). Films were scanned on a Molecular Imager GS800, and Quantity One (Bio-Rad) was used for quantifications.

Table 1. List of antibodies used.

Antigen	Company	Catalog	Host	Dilution	Purpose*	Antigen retrival**
Non-phosphorylated neurofilament	Covance	SMI-32	mouse	1:500	IHC	none
Phosphorylated neurofilament	Covance	SMI-31	mouse	1:500	IHC	none
Ionized calcium binding adaptor molecule 1 (Iba-1)	Abcam	ab5086	goat	1:200	IHC	Citrate solution pH 6.0
Glial fibrillary acidic protein (GFAP)	DAKO	Z0334	rabbit	1:500	IHC	Citrate solution pH 6.0
Tubulin β-III	Epitomics	1967-1	rabbit	1:10000	WB	N.A.
α-Tubulin	Sigma-Aldrich	T6199	mouse	1:12000	WB	N.A.
Tubulin Alpha antibody | YL1/2 (Tyrosinated tubulin)	Bio-Rad	MCA77G	rat	1:2000	WB	N.A.
Acetylated tubulin	Sigma-Aldrich	T7451	mouse	1:30000	WB	N.A.
Detyrosinated tubulin	Millipore	#AB3201	rabbit	1:15000	WB	N.A.
Δ2-tubulin	Millipore	#AB3203	rabbit	1:12000	WB	N.A.
p44/42 MAPK (Erk1/2) (total ERK)	Cell Signaling	#9102	rabbit	1:2000	WB	N.A.

* IHC: immunohistochemistry; WB: western blot; IF: immunocitofluorescence
** Heat mediated antigen retrieval was performed by boiling slides in the appropriate solutions. TE solution: 10mM Tris, 1mM EDTA pH 9.0; Citrate solution: 10mM sodium citrate buffer pH 6.0; trypsin:0.05%EDTA 1x solution (Invitrogen, cat #25300-062).
N.A. not applicable

Statistics analysis

All data were analyzed using GraphPad Prism software, and results are expressed as mean + S.E.M. To compare two different groups, Student's T test (unpaired, two-tailed) was used and $P < 0.05$ was considered a significant difference. For multiple comparisons, one-way ANOVA test was used, followed by Tukey's multiple comparison tests.

Bibliography

1. Pfeiffer, S.E., A.E. Warrington, and R. Bansal, *The oligodendrocyte and its many cellular processes.* Trends Cell Biol, 1993. **3**(6): p. 191-7.
2. Simons, M. and K.A. Nave, *Oligodendrocytes: Myelination and Axonal Support.* Cold Spring Harb Perspect Biol, 2015. **8**(1): p. a020479.
3. Piaton, G., R.M. Gould, and C. Lubetzki, *Axon-oligodendrocyte interactions during developmental myelination, demyelination and repair.* J Neurochem, 2010. **114**(5): p. 1243-60.
4. Brady, S.T., et al., *Formation of compact myelin is required for maturation of the axonal cytoskeleton.* J Neurosci, 1999. **19**(17): p. 7278-88.
5. Barres, B.A., *The mystery and magic of glia: a perspective on their roles in health and disease.* Neuron, 2008. **60**(3): p. 430-40.
6. Barnett, S.C. and C. Linington, *Myelination: do astrocytes play a role?* Neuroscientist, 2013. **19**(5): p. 442-50.
7. Pekny, M. and M. Nilsson, *Astrocyte activation and reactive gliosis.* Glia, 2005. **50**(4): p. 427-34.
8. Pekny, M., U. Wilhelmsson, and M. Pekna, *The dual role of astrocyte activation and reactive gliosis.* Neurosci Lett, 2014. **565**: p. 30-8.
9. Mosley, R.L., et al., *Neuroinflammation, Oxidative Stress and the Pathogenesis of Parkinson's Disease.* Clin Neurosci Res, 2006. **6**(5): p. 261-281.
10. Nicholas, R.S., M.G. Wing, and A. Compston, *Nonactivated microglia promote oligodendrocyte precursor survival and maturation through the transcription factor NF-kappa B.* Eur J Neurosci, 2001. **13**(5): p. 959-67.
11. Hamilton, S.P. and L.H. Rome, *Stimulation of in vitro myelin synthesis by microglia.* Glia, 1994. **11**(4): p. 326-35.

12. Prinz, M. and A. Mildner, *Microglia in the CNS: immigrants from another world.* Glia, 2011. **59**(2): p. 177-87.

13. Zhang, D., et al., *Astrogliosis in CNS pathologies: is there a role for microglia?* Mol Neurobiol, 2010. **41**(2-3): p. 232-41.

14. Witte, H. and F. Bradke, *The role of the cytoskeleton during neuronal polarization.* Curr Opin Neurobiol, 2008. **18**(5): p. 479-87.

15. Kapitein, L.C. and C.C. Hoogenraad, *Building the Neuronal Microtubule Cytoskeleton.* Neuron, 2015. **87**(3): p. 492-506.

16. Eira, J., et al., *The cytoskeleton as a novel therapeutic target for old neurodegenerative disorders.* Prog Neurobiol, 2016. **141**: p. 61-82.

17. Brites, P., et al., *Plasmalogens participate in very-long-chain fatty acid-induced pathology.* Brain, 2009. **132**(Pt 2): p. 482-92.

18. Bottelbergs, A., et al., *Peroxisome deficiency but not the defect in ether lipid synthesis causes activation of the innate immune system and axonal loss in the central nervous system.* J Neuroinflammation, 2012. **9**: p. 61.

19. Ohsawa, K., et al., *Involvement of Iba1 in membrane ruffling and phagocytosis of macrophages/microglia.* J Cell Sci, 2000. **113 (Pt 17)**: p. 3073-84.

20. Trapp, B.D., et al., *Axonal transection in the lesions of multiple sclerosis.* N Engl J Med, 1998. **338**(5): p. 278-85.

21. Feng, G., et al., *Imaging neuronal subsets in transgenic mice expressing multiple spectral variants of GFP.* Neuron, 2000. **28**(1): p. 41-51.

22. Kriz, J., et al., *Electrophysiological properties of axons in mice lacking neurofilament subunit genes: disparity between conduction velocity and axon diameter in absence of NF-H.* Brain Res, 2000. **885**(1): p. 32-44.

23. Sihag, R.K., et al., *Role of phosphorylation on the structural dynamics and function of types III and IV intermediate filaments.* Exp Cell Res, 2007. **313**(10): p. 2098-109.

24. Barry, D.M., et al., *Expansion of neurofilament medium C terminus increases axonal diameter independent of increases in conduction velocity or myelin thickness.* J Neurosci, 2012. **32**(18): p. 6209-19.

25. Malheiro, A.R., et al., *Leukodystrophy caused by plasmalogen deficiency rescued by glyceryl 1-myristyl ether treatment.* Brain Pathol, 2019.

26. Rodemer, C., et al., *Inactivation of ether lipid biosynthesis causes male infertility, defects in eye development and optic nerve hypoplasia in mice.* Hum Mol Genet, 2003. **12**(15): p. 1881-95.

27. Schachner, M. and U. Bartsch, *Multiple functions of the myelin-associated glycoprotein MAG (siglec-4a) in formation and maintenance of myelin.* Glia, 2000. **29**(2): p. 154-65.

28. Coleman, M., *Axon degeneration mechanisms: commonality amid diversity.* Nat Rev Neurosci, 2005. **6**(11): p. 889-98.

29. Westermann, S. and K. Weber, *Post-translational modifications regulate microtubule function.* Nat Rev Mol Cell Biol, 2003. **4**(12): p. 938-47.

30. Janke, C. and J.C. Bulinski, *Post-translational regulation of the microtubule cytoskeleton: mechanisms and functions.* Nat Rev Mol Cell Biol, 2011. **12**(12): p. 773-86.

31. Webster, D.R., et al., *Differential turnover of tyrosinated and detyrosinated microtubules.* Proc Natl Acad Sci U S A, 1987. **84**(24): p. 9040-4.

32. Paturle-Lafanechere, L., et al., *Characterization of a major brain tubulin variant which cannot be tyrosinated.* Biochemistry, 1991. **30**(43): p. 10523-10528.

33. L'Hernault, S.W. and J.L. Rosenbaum, *Chlamydomonas .alpha.-tubulin is posttranslationally modified by acetylation on the .epsilon.-amino group of a lysine.* Biochemistry, 1985. **24**(2): p. 473-478.

34. Hammond, J.W., et al., *Posttranslational modifications of tubulin and the polarized transport of kinesin-1 in neurons.* Mol Biol Cell, 2010. **21**(4): p. 572-83.

35. Janke, C. and M. Kneussel, *Tubulin post-translational modifications: encoding functions on the neuronal microtubule cytoskeleton.* Trends Neurosci, 2010. **33**(8): p. 362-72.

36. Garnham, C.P. and A. Roll-Mecak, *The chemical complexity of cellular microtubules: tubulin post-translational modification enzymes and their roles in tuning microtubule functions.* Cytoskeleton (Hoboken), 2012. **69**(7): p. 442-63.

37. Kalebic, N., et al., *alphaTAT1 is the major alpha-tubulin acetyltransferase in mice.* Nat Commun, 2013. **4**: p. 1962.

38. Kalebic, N., et al., *Tubulin acetyltransferase alphaTAT1 destabilizes microtubules independently of its acetylation activity.* Mol Cell Biol, 2013. **33**(6): p. 1114-23.

39. Coombes, C., et al., *Mechanism of microtubule lumen entry for the alpha-tubulin acetyltransferase enzyme alphaTAT1.* Proc Natl Acad Sci U S A, 2016. **113**(46): p. E7176-E7184.

40. Szyk, A., et al., *Molecular basis for age-dependent microtubule acetylation by tubulin acetyltransferase.* Cell, 2014. **157**(6): p. 1405-15.

41. Magiera, M.M., et al., *Excessive tubulin polyglutamylation causes neurodegeneration and perturbs neuronal transport.* EMBO J, 2018. **37**(23).

42. Franker, M.A. and C.C. Hoogenraad, *Microtubule-based transport – basic mechanisms, traffic rules and role in neurological pathogenesis.* J Cell Sci, 2013. **126**(Pt 11): p. 2319-29.

43. Lacroix, B., et al., *Tubulin polyglutamylation stimulates spastin-mediated microtubule severing.* J Cell Biol, 2010. **189**(6): p. 945-54.

44. Waclawek, E. and D. Wloga, *[Role of microtubule severing proteins in cytoskeleton reorganization].* Postepy Biochem, 2016. **62**(1): p. 52-59.

45. Roll-Mecak, A. and R.D. Vale, *Making more microtubules by severing: a common theme of noncentrosomal microtubule arrays?* J Cell Biol, 2006. **175**(6): p. 849-51.

46. Grider, M.H., Q. Chen, and H.D. Shine, *Semi-automated quantification of axonal densities in labeled CNS tissue.* J Neurosci Methods, 2006. **155**(2): p. 172-9.

General conclusions and future perspectives

General conclusions and future perspectives

Highlighted by the severe clinical presentation of RCDP patients, it is fully accepted that plasmalogens play a crucial role in the processes governing the development of eye, heart and bone development [1]. In addition, the neurological involvement in RCDP, combined with the observation of plasmalogen deficiencies in several neurodegenerative disorders underscores the role and function of these phospholipids in neurons and myelinating glia [1]. It is thus crucial to understand the neuropathogenesis behind defects in the biosynthesis of plasmalogens. As main purpose, this work provided a deeper understanding of plasmalogen's role in CNS myelin and during myelination. To accomplish our objectives, we made use of the *Gnpat* KO mouse, a mouse model that fully mimics RCDP, in terms of the biochemical defect as well as the phenotypic presentation [2].

Here, we demonstrated that differentiated oligodendrocytes are a prime target of a deficiency in plasmalogens, causing impaired myelination and myelin maintenance. Assessment of OPC and oligodendrocyte numbers during the early postnatal period revealed normal densities in spinal cords and optic nerves from *Gnpat* KO mice, suggesting that impaired myelination was not caused by defects in OPC migration. The lack of plasmalogens in oligodendrocytes from *Gnpat* KO mice did not affect the initial stages of differentiation. In addition, using *in vitro* assays, oligodendrocytes from *Gnpat* KO mice showed normal development up to the final stages of maturation and myelin assembly. Specifically, only a reduced number of plasmalogen-deficient oligodendrocytes were able to assemble shorter and scarcer myelin sheaths around axons. Using scaffolds of microfibers, we were able to unravel that the defect in assembling myelin sheaths was caused by a compromised intrinsic capacity of plasmalogen-deficient oligodendrocytes to ensheath and assemble myelin segments. It would be interesting to determine in more detail how the cross talk between neurons and glia is affected by the deficiency and causes

the observed pathology of *Gnpat* KO mice. The generation of a floxed allele of the murine *Gnpat* gene to obtain conditional mutants, could lead to important advances and unravel how the pathology is orchestrated. For example, the use of the neuron-specific (DCX-cre) and oligodendrocyte-specific (CNPase-cre) mutants, would be good mouse models to determine how the cross talk between neurons and glia is affected by the deficiency and causes the observed pathology of generalized *Gnpat* KO mice. The neuropathological assessment of these two mouse lines would allow the discovery of whether the neuronal pathology is due to intrinsic or extrinsic defects, leading to a deep understanding of the disease and therefore having a strong impact on how candidate therapies are assayed for efficacy. In addition, these mice will allow to dissect and identify the mechanisms and cellular processes behind the pathology. Moreover, to a deeper comprehension on how plasmalogen deficiency impacts oligodendrocyte terminal differentiation and establishment of axonal contact, *in vitro* studies could be performed. One of the questions that can be addressed is the relevance of plasmalogens for the protrusions extension by the oligodendrocytes to interact and engulf axons. Using primary OPC cultures, the morphological differentiation of oligodendrocytes could be followed using phalloidin staining. As previously shown phalloidin labels the actin cytoskeleton of the entire oligodendrocyte and allows to follow fine changes in cell shape to assess morphological changes in oligodendrocytes [3, 4]. Moreover, to characterize the dynamics of oligodendrocyte-axon contact it would be interesting to perform live-imaging of mixed cortical neuron-glial cultures in real time, allowing the analysis of the oligodendrocytes ability to establish axonal contact, as well as their capacity to extend and retract processes.

During adulthood, the lack of plasmalogens continued to have a negative impact on myelin content throughout the CNS, as evidenced by reduced g-ratio and the progressive increase in the density of axons lacking myelin sheaths. These

myelin defects correlate with the neurological phenotype of *Gnpat* KO mice. From the age of 9 months, *Gnpat* KO mice start developing a severe and progressive neurological condition that includes tremors and generalized ataxia, worsening after 1 year of age with increased tremor frequency and hindlimb paralysis. Demyelination was observed throughout the CNS, although different degrees of severity were noted. In addition, we observed that severe demyelination did not cause major axonal loss, suggesting an unaltered trophic support capacity by mutant oligodendrocytes. Notably, whereas the optic nerve was the most severely affected CNS region with regard to myelin content, it completely lacked signs of axonal loss or damage. However, axonal damage occurred with an apparent regional specificity since was more prominent in other CNS areas (e.g., spinal cord, cerebellar white matter and internal capsule). The presence of hallmark signs of axonal damage (e.g., axonal swellings with accumulation of organelles) in myelinated axons and in regions with moderate myelin defects (e.g., cerebellar white matter) suggests a demyelination-independent contribution to the sustainment of healthy axons. Therefore, we hypothesize that a plasmalogen deficiency may differentially affect different subsets of neurons or that subtle alterations in myelin content or composition may affect these subsets of neurons leading to axonal dysfunction.

Concomitant with the aggravated phenotype of the *Gnpat* KO mice, differential expression MBP, SEPT7 and MAG was observed in plasmalogen-deficient myelin. Decreased levels of MBP and SEPT7 were observed during the initial hypomyelination and during late-stages of demyelination, being consistently reduced in plasmalogen-deficient myelin. During the period of hypomyelination, MAG levels were normal in myelin from *Gnpat* KO mice but during the period of demyelination MAG levels decreased in plasmalogen-deficient myelin. MBP resides at the cytoplasmic apposition of the myelin sheath, as well as plasmalogens [5, 6].

This topographical coincidence of plasmalogens and MBP brings several issues to be addressed. Namely, whether an altered lipid composition due to the lack of plasmalogens may affect the correct localization of MBP and/or other myelin proteins. To address this question and analyze if in the *Gnpat* KO mice the decreased levels of MBP are the major cause of inadequate formation of the myelin sheath, and consequently impaired myelination, a generation of double mutant for *GNPAT* and MBP could have great study interest. S*hiverer* is an autosomal recessive mouse mutation characterized by the lack of MBP [7, 8]. However, the primary defect in *shiverer* mice is a complete hypomyelination of the CNS, which would preclude its usage to understand if abnormal levels of MBP and plasmalogens mediate the observed myelin defects. A possible way to overcome this caveat could be the usage of a MBP conditional allele and the usage of an inducible cre recombinase to drive MBP deletion in adult mice. Similar strategies could be envisioned for the role of SEPT7 and MAG. The single mutants of SEPT7 [9] and MAG [10] do not impair myelination and the MAG-null mutants present a subtle phenotype which may be exacerbated by a plasmalogen deficiency.

Treatment options able to rescue the biochemical or pathologic defects caused by a plasmalogen defect are scarce. Here we tested and validated the potential of a new alkyl glycerol in rescuing CNS defects. We identified 1-O-TDG as a functional alkyl glycerol capable of rescuing plasmalogen levels in *Gnpat* KO cells and capable of rescuing the differentiation and myelination potential of *Gnpat* KO oligodendrocytes. Although plasmalogens usually contain C16:0, C18:1 and C18:0 moieties at the *sn*-1 position, 1-*O*-heptadecylglycerol (containing a C17:0 alkyl chain) was also shown to be incorporated into plasmalogens [11]. Our results demonstrate that shorter alkyl chains can also be incorporated into plasmalogens. In addition, our results suggest that the synthesis of plasmalogens with their characteristic vinyl-ether bond is more important than the chain length at the *sn*-

1 position [1]. The ability of 1-O-TDG to rescue myelination *in vivo* represents a novel and valid strategy for the development of translatable approaches to rescue plasmalogen levels in the CNS and treatment of the myelination defects observed in RCDP patients. Following these promising results, it would be extremely interesting to analyze the effectiveness of the treatment in *Gnpat* KO mice, looking concretely for the myelination of CNS and PNS in adulthood and during aging.

In summary, our results demonstrate the importance of plasmalogens for oligodendrocyte function and myelin assembly, and identified a novel strategy to promote myelination in nervous tissue.

Bibliography

1. Braverman, N.E. and A.B. Moser, *Functions of plasmalogen lipids in health and disease.* Biochim Biophys Acta, 2012. **1822**(9): p. 1442-52.
2. Rodemer, C., et al., *Inactivation of ether lipid biosynthesis causes male infertility, defects in eye development and optic nerve hypoplasia in mice.* Hum Mol Genet, 2003. **12**(15): p. 1881-95.
3. Dancker, P., et al., *Interaction of actin with phalloidin: polymerization and stabilization of F-actin.* Biochim Biophys Acta, 1975. **400**(2): p. 407-14.
4. D'Este, E., et al., *Subcortical cytoskeleton periodicity throughout the nervous system.* Sci Rep, 2016. **6**: p. 22741.
5. Aggarwal, S., L. Yurlova, and M. Simons, *Central nervous system myelin: structure, synthesis and assembly.* Trends Cell Biol, 2011. **21**(10): p. 585-93.
6. Kirschner, D.A. and A.L. Ganser, *Myelin labeled with mercuric chloride. Asymmetric localization of phosphatidylethanolamine plasmalogen.* J Mol Biol, 1982. **157**(4): p. 635-58.
7. Chernoff, G.F., *Shiverer: an autosomal recessive mutant mouse with myelin deficiency.* J Hered, 1981. **72**(2): p. 128.
8. Readhead, C. and L. Hood, *The dysmyelinating mouse mutations shiverer (shi) and myelin deficient (shiml d).* Behav Genet, 1990. **20**(2): p. 213-34.
9. Patzig, J., et al., *Septin/anillin filaments scaffold central nervous system myelin to accelerate nerve conduction.* Elife, 2016. **5**.
10. Montag, D., et al., *Mice deficient for the myelin-associated glycoprotein show subtle abnormalities in myelin.* Neuron, 1994. **13**(1): p. 229-46.
11. Das, A.K., et al., *Dietary ether lipid incorporation into tissue plasmalogens of humans and rodents.* Lipids, 1992. **27**(6): p. 401-5.

Appendix

Brain Pathology ISSN 1015-6305

RESEARCH ARTICLE

Leukodystrophy caused by plasmalogen deficiency rescued by glyceryl 1-myristyl ether treatment

Ana R. Malheiro[1,2]; Barbara Correia[1]; Tiago Ferreira da Silva[1]; Diogo Bessa-Neto [1]; Paul P. Van Veldhoven[3]; Pedro Brites [1]

[1] Neurolipid Biology, Instituto de Investigação e Inovação em Saúde - i3S, Instituto de Biologia Molecular e Celular – IBMC e Universidade do Porto, Porto, Portugal.
[2] ICBAS, Instituto Ciências Biomédicas Abel Salazar, Porto, Portugal.
[3] Laboratory of Lipid Biochemistry and Protein Interactions (LIPIT), KU Leuven, Leuven, Belgium.

Keywords
leukodystrophy, myelin, oligodendrocytes, peroxisomal disorders.

Corresponding author:
Pedro Brites, PhD, Neurolipid Biology, i3S - Instituto de Investigação e Inovação em Saúde, Rua Alfredo Allen 208, 4200-135 Porto, Portugal (E-mail: *pedro.brites@ibmc.up.pt*)

Received 22 October 2018
Accepted 16 January 2019
Published Online Article Accepted 22 January 2019

doi:10.1111/bpa.12710

Abstract

Plasmalogens are the most abundant form of ether phospholipids in myelin and their deficiency causes Rhizomelic Chondrodysplasia Punctata (RCDP), a severe developmental disorder. Using the *Gnpat*-knockout (KO) mouse as a model of RCDP, we determined the consequences of a plasmalogen deficiency during myelination and myelin homeostasis in the central nervous system (CNS). We unraveled that the lack of plasmalogens causes a generalized hypomyelination in several CNS regions including the optic nerve, corpus callosum and spinal cord. The defect in myelin content evolved to a progressive demyelination concomitant with generalized astrocytosis and white matter-selective microgliosis. Oligodendrocyte precursor cells (OPC) and mature oligodendrocytes were abundant in the CNS of Gnpat KO mice during the active period of demyelination. Axonal loss was minimal in plasmalogen-deficient mice, although axonal damage was observed in spinal cords from aged Gnpat KO mice. Characterization of the plasmalogen-deficient myelin identified myelin basic protein and septin 7 as early markers of dysmyelination, whereas myelin-associated glycoprotein was associated with the active demyelination phase. Using *in vitro* myelination assays, we unraveled that the intrinsic capacity of oligodendrocytes to ensheath and initiate membrane wrapping requires plasmalogens. The defect in plasmalogens was rescued with glyceryl 1-myristyl ether [1-O-tetradecyl glycerol (1-O-TDG)], a novel alternative precursor in the plasmalogen biosynthesis pathway. 1-O-TDG treatment rescued myelination in plasmalogen-deficient oligodendrocytes and in mutant mice. Our results demonstrate the importance of plasmalogens for oligodendrocyte function and myelin assembly, and identified a novel strategy to promote myelination in nervous tissue.

INTRODUCTION

Leukodystrophies are a complex group of genetically distinct disorders characterized by the pathological involvement of central nervous system (CNS) white matter because of abnormalities in myelination or in myelin homeostasis (54). Heterogeneous and diverse cellular deficiencies mediate complex mechanisms that ultimately cause myelin defects. The myelin sheath is the extended and modified plasma membrane of oligodendrocytes in the CNS, wrapped in multilayered stacks around axons (36). In addition to its unique architecture, the distinctive lipid-rich composition of myelin sets it apart from other membranes. Myelin contains high amounts of plasmalogens, a membrane phospholipid that can account for up to 70% of the pool of ethanolamine glycerophospholipids in myelin (38). Plasmalogens are a class of ether phospholipids characterized by a vinyl-ether bond at the *sn*-1 position of the glycerol backbone (46). The biosynthesis of plasmalogens initiates in peroxisomes through the activity of two peroxisomal enzymes, namely glyceronephosphate O-acyltransferase (GNPAT) and alkylglycerophosphate synthase (AGPS), and the subsequent steps take place in the endoplasmic reticulum (55). Impairments in the biosynthesis of plasmalogens are the hallmark of Rhizomelic Chondrodysplasia Punctata (RCDP). RCDP is a genetically heterogeneous autosomal recessive disorder, with an estimated incidence of 1:100 000 newborns. Mutations in five different genes (ie, *PEX7*, *GNPAT*, *AGPS*, *FAR1* and *PEX5L*), involved in the biosynthesis of ether phospholipids, characterize the five types of RCDP (RCDP types 1 to 5, respectively) (6, 13, 16). The impaired biosynthesis of plasmalogens leads to multiple developmental malformations, including congenital cataracts, shortening of proximal

limbs, profound growth deficiency and intellectual disability (59). Abnormal signal intensities on magnetic resonance imaging (MRI) are suggestive of dys- and/or hypomyelination (2, 5, 27) but the generalized lack of histopathological analysis has hindered the characterization of myelin defects (41). The occurrence of seizures in RCDP patients, the development of epilepsy and the increased latencies of evoked potentials have also been proposed to correlate with impaired CNS myelination (4). The neurological involvement in RCDP patients combined with the observation of plasmalogen deficiencies in several neurodegenerative disorders underscores the role and function of these phospholipids in myelinating glia (13). The understanding of the pathology and disease mechanisms caused by the deficiency in plasmalogens has been powered by the characterization of mouse models for RCDP (18). Using the *Gnpat* KO mice (42) as a model of RCDP type 2, we analyzed the consequences of a plasmalogen deficiency in the CNS.

Here we unravel how a plasmalogen deficiency compromises myelination and myelin content throughout the CNS. The disease progression in a murine model of RCDP is complex with an initial generalized hypomyelination that evolves into active demyelination. Our results demonstrate that a plasmalogen defect affects the intrinsic ability of oligodendrocytes to myelinate and we identified a new alkyl glycerol that can serve as an alternative precursor in the biosynthesis of plasmalogens and can rescue myelination defects in *Gnpat* KO mice.

MATERIALS AND METHODS

Mouse strains

All mouse procedures were performed according to the European Directive 2010/63/EU established by the European Parliament and of the Council, as well as the National legislation (Decreto-Lei 113/2013). Animal studies were reviewed and approved by the Portuguese General Veterinarian Board (DGAV, #011852).

Gnpat knockout (KO) mice and wild-type (WT) littermates were obtained from mating *Gnpat* heterozygous mice on a Swiss-Webster background. All animals were maintained with ad libitum access to rodent food and water, and were kept in a 12:12 h light and dark cycle facility. Genotyping was performed as previously described (42). *Gnpat* heterozygous mice were crossed with Thy1-YFP 16Jrs/J mice (JAX mice) that express yellow fluorescent protein (YFP) from the neuronal Thy1-promoter (21).

Histological and morphological analysis

Mice were anesthetized with ketamine/medetomidine mixture (75 and 1 mg/kg body weight, respectively) and lumbar spinal cord, optic nerve and brain were isolated and fixed by immersion. For morphometric analysis, tissues were fixed in 4% glutaraldehyde in 0.1M sodium cacodylate buffer (pH 7.4) for 5 days and processed as previously described (17). In spinal cords, the region chosen for analysis was the ventral funiculus, immediately adjacent to the ventromedian fissure. Semi-thin sections were cut at 1μm, stained with 1% p-phenylenediamine (PPD) and used to determine the density of myelinated fibers. Ultrathin sections were processed for ultrastructural analysis as described (17). For g-ratio determination, the axonal diameter and the myelin sheath thickness were measured (four measurements per fiber; one hundred and fifty fibers per mouse). Pseudocolored electron microscopy images were processed in Photoshop CS3, by selecting the region of interest and applying color with transparency in order to highlight the region to be analyzed.

For immunohistochemistry, tissues were fixed by immersion in modified Carnoy's solution (absolute ethanol: methanol: glacial acetic acid – 6:3:1) for 2 h, processed for paraffin embedding, sectioned at 4μm, cleared and rehydrated. Sections were permeabilized in 100% methanol, treated with 0.1% $NaBH_4$ in 10 mM Tris, 1mM EDTA at pH 9.0 and blocked with 5% normal donkey serum (NDS) in PBS. Primary antibodies (Supplemental Figure 1) were diluted in 5% NDS in PBS and incubated over night at 4°C. Secondary antibodies, either biotinylated or conjugated with Alexa Fluor (Jackson ImmunoResearch Europe, Lda, Ely, UK), were diluted in 5% NDS in PBS and incubated at room temperature (RT) for 1 h. The quantifications were performed using Feature J, a java-based plug-in of the imaging software NIH Image J, using a Hessian-based algorithm (24).

Myelin isolation and western blot analysis

Myelin was isolated after two rounds of osmotic shock and discontinuous sucrose gradients, as previously described (39). Cerebrum and spinal cord from 2-month (WT n = 4 and *Gnpat* KO n = 4) to 1.5-year-old (WT n = 7 and *Gnpat* KO n = 6) mice were used to isolate and purify myelin. Isolated myelin was sonicated in PBS containing 1.5% SDS, 0.5% Na_2CO_3 and protease inhibitor cocktail (Roche), and total protein levels were measured using DC™ Protein Assay (Bio-Rad). The samples (2 μg of total myelin protein) were separated by SDS-PAGE gels using TGX Stain-Free™ FastCast™ 12% acrylamide (Bio-Rad) and analyzed using a ChemiDoc imaging system to measure the amount of myelin proteins in the gel. Nitrocellulose membranes were blocked with 5% skim milk (Fluka) in Tris-buffered saline with 1% Tween 20 (TBS-T) for 1 h at RT, washed and incubated overnight at 4°C with different primary antibodies (section above) diluted in 5% BSA in TBS-T. HRP-labeled secondary antibodies were diluted 1:5000 in 5% skim milk in TBS-T and incubated for 1 h at RT. Membranes were developed using ECL (Luminata Crescendo Western HRP Substrate, Milipore, Algés, Portugal). Blots were scanned in a Molecular Imager GS800, and quantified using Quantity One 4.6.9 software.

Mixed cortical neuron-glial culture

Mixed cortical neuron-glial culture was performed as described (29), with minor alterations. Cortical neurons and glial cells were isolated from individual WT and *Gnpat* KO mouse brains, at embryonic day 17. Cortices were digested in 0.05% Trypsin + 0.2 mg/mL EDTA, dissociated and cells were resuspended in culture medium (Neurobasal medium with 1x N21 supplement, 2 mM L-glutamine, 1× P/S). Cells were plated at a density of 1.5×10^5 cells/well onto glass coverslips coated with poly-L-lysine (20 µg/mL, P2636 Sigma) and laminin (2 µg/mL, L2020 Sigma). After 6 days *in vitro*, cultures were maintained in myelination medium (56). At DIV20, cells were fixed with 4% PFA, and immunolabeled with anti-tubulin-βIII (to stain neurons) and anti-myelin basic protein (MBP to stain oligodendrocytes). The fixed cells were processed as described above for immunohistochemistry. The entire area of the glass coverslip (1.32 cm^2) was analyzed and the total number of MBP-positive cells (ie, OL with low levels of MBP, OL with high levels of MBP, OL with assembled MBP segments and degenerating OLs) was counted.

For 1-O-tetradecylglycerol (1-O-TDG) (Biosynth) treatment, medium was supplemented with 7 µM 1-O-TDG in absolute ethanol or 0.1% absolute ethanol (control) starting at DIV 10. For treatment with batyl alcohol (BA; 1-*O*-octadecylglycerol; Sigma-Aldrich) and chimyl alcohol (CA; 1-*O*-hexadecylglycerol; Bachem), medium was supplemented with 7 µM BA and 7 µM CA in DMSO or with 0.14% DMSO (control) starting at DIV 10. In both treatment schemes, cells were fixed at DIV20 and processed for immunofluorescence as described above.

Primary OPC cultures

The preparation of mixed glial cell cultures was performed as described (31). Neurons and glial cells were isolated from WT and *Gnpat* KO brain hemispheres at postnatal day 2. Brain hemispheres were digested in 0.05% Trypsin + 0.2 mg/mL EDTA, dissociated, cells were resuspended in plating medium (DMEM high glucose with 10% FBS and 1× P/S) and seeded onto 25 cm^2 flasks pre-coated with 50 µg/mL poly-D-lysine (P0899 Sigma). After 9 days in culture, oligodendrocyte precursor cells (OPC) were obtained by differential shaking and resuspended in 1× SATO (31). Cells were seeded at a density of 15 000 cells/well onto scaffold discs of randomly oriented poly-L-lactide microfibers (The Electrospinning Company Ltd.), pre-coated with poly-L-lysine (100 µg/mL; P2636 Sigma). Differentiation was induced at DIV four with the removal of PDGF and FGF from the medium, and with the addition of 0.5% FBS. The cells were fixed at DIV12 with 4% PFA, and immunolabeled with anti-MBP as described above. The scaffolds were mounted on microscope slides and imaged on Leica TCS SP5 II confocal (Leica Microsystems, Germany) using a 63× magnification objective with a *z*-step of 0.013 µm. For increased *z*-definition of the poly-L-lactide fibers, we made use of the refraction capability of the confocal microscope using the 405 nm laser line at full power, and a detector in the same emission spectrum region. Finally, the cross-sectional view of myelinated segments was accomplished by the usage of the orthogonal view function of Fiji.

Measurement of plasmalogens

Lung-derived mouse embryonic fibroblasts from WT (n = 3) and *Gnpat* KO (n = 5) at embryonic day 17.5 were cultured in T75 flasks with DMEM supplemented with 10% FBS (3). The medium was supplemented with 7 µM 1-O-TDG or 0.01% absolute ethanol (control) during 12 days. Cells were harvested using trypsin, washed and stored at −80°C until processing. Lipid extracts were prepared as described (52) and analyzed for phospholipid content (53) and plasmalogens. For the latter, lipids were treated with acidic methanol followed by conversion of the liberated aldehydes with 1,3-cyclohexanedione into fluorescent decahydroacridines derivatives, which were separated according to the chain length by RP-HPLC (Symmetry C18 column (4.6 × 150 mm; 5 µm; 100 Å; Waters) and monitored by fluorimetry (using a Waters 2475 Multi-Wavelength Fluorescence Detector; Ex 390 nm; Em 460 nm); modified from Mezzar *et al* (32) (Van Veldhoven P.P., unpublished data).

In vivo treatment

1-O-TDG was dissolved in 1 mL of ethanol and mixed with 1 mL of Tween-80 (Sigma-Aldrich). After heating to evaporate the ethanol, the mixture was diluted with saline (B. Braun Medical, Portugal) so that Tween-80 was at 1% w/v. 1-O-TDG or vehicle was administered to WT and *Gnpat* KO mice via subcutaneous (s.c.) injections from P1 to P8 and via intraperitoneal (i.p) injections from P10 to P18. Mice were euthanized at P20 and tissues collected for histological analyses.

Statistical analysis

All data were analyzed using GraphPad Prism software, and results are expressed as mean + S.E.M. To compare two different groups, Student's *T* test (unpaired, two-tailed) was used and $P < 0.05$ was considered a significant difference. For multiple comparisons, one-way ANOVA test was used, followed by Tukey's multiple comparison tests.

RESULTS

Lack of plasmalogens causes generalized myelin deficits

To determine if plasmalogens play a role in myelination and myelin maintenance, different regions within the CNS were analyzed during the end stages of the disorder. Ultrastructural analysis using electron microscopy revealed

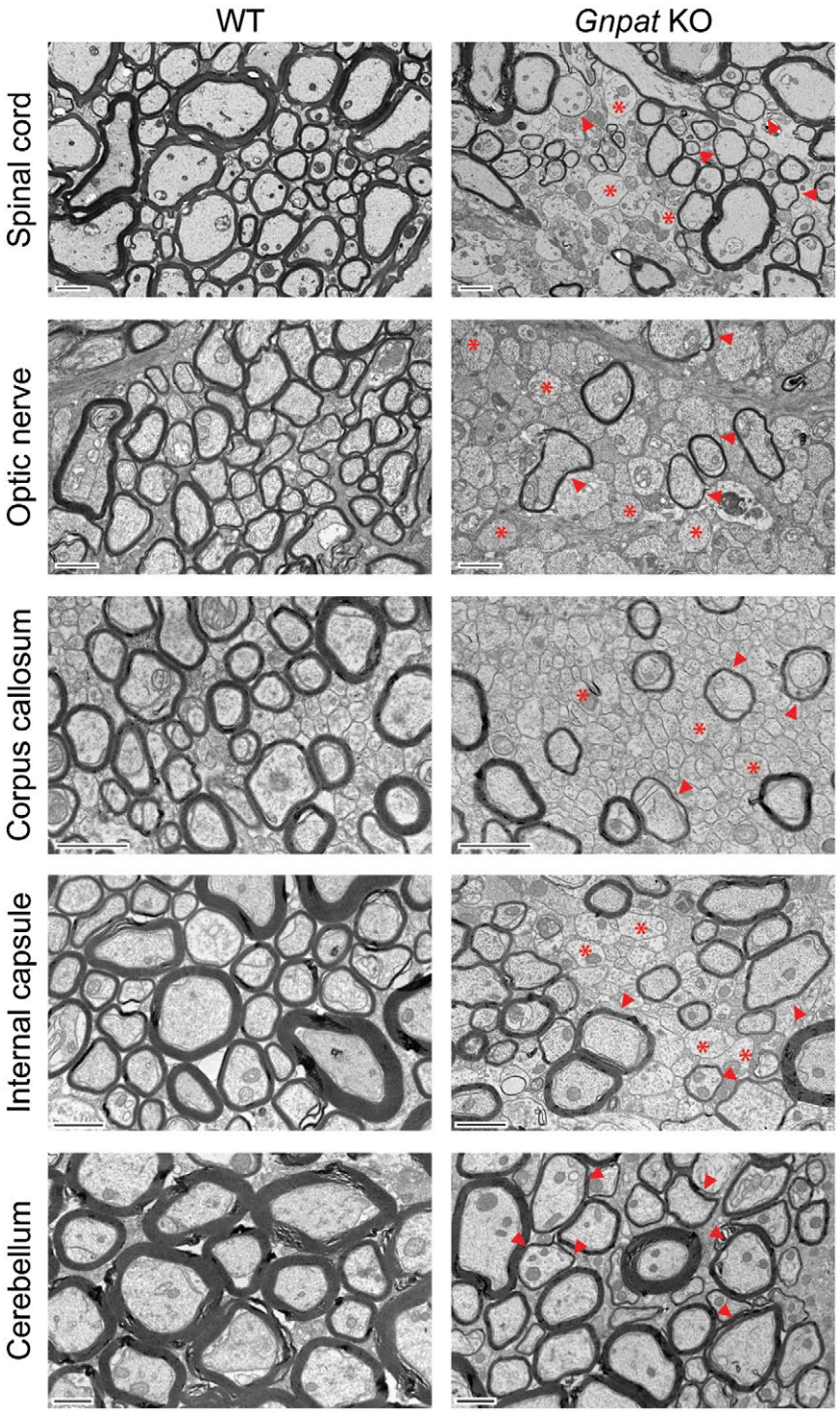

Figure 1. *Plasmalogen deficiency causes generalized myelin deficits throughout the CNS.* Electron microscopy images of the spinal cord (n = 6 per genotype), optic nerve (n = 7 per genotype), corpus callosum (n = 3 per genotype), internal capsule (n = 3 per genotype) and cerebellum (n = 3 per genotype) from 1.5-year-old WT and *Gnpat* KO mice. Examples of axons devoid of myelin are highlighted with asterisks and axons with thinner myelin sheaths are highlighted with arrowheads. *Scale bars* are 2 μm in spinal cord and 1μm in the remaining CNS regions.

that a plasmalogen deficiency caused generalized reduction in myelin in several CNS regions (Figure 1). The optic nerve, corpus callosum and spinal cord were the most affected regions in the *Gnpat* KO mice. In these regions, we observed an extreme loss of myelin as many axons were devoid of myelin (Figure 1) and the vast majority

of myelinated axons contained thinner myelin sheaths (Figure 1). In spinal cords from *Gnpat* KO mice, the generalized deficiency in myelin was detected in all white mater tracts, including the ventral and lateral funiculus, and the corticospinal and dorsal column tracts (Supplemental Figure 2). The cerebellar white matter tract was the least affected region as axons devoid of myelin were not frequent, despite the generalized occurrence of thinner myelin sheaths. The internal capsule of *Gnpat* KO mice displayed an intermediate pathology, with severe features when compared to cerebellar white matter (ie, presence of axons devoid of myelin) and milder features when compared to the corpus callosum and optic nerves (ie, increased number of axons that still contain a myelin sheath). These results highlight that a deficiency in plasmalogens causes a complex myelin disorder. To understand the role of plasmalogens in oligodendrocytes and myelin pathology, we set out to perform a detailed characterization of the optic nerve and spinal cord in *Gnpat* KO mice.

Complex defects in myelinogenesis are aggravated by active demyelination

The previous results prompted us to evaluate the process of myelination from the early postnatal period until the end stages of the disease at 1.5 years of age. We characterized in detail the myelination defects present in spinal cords and optic nerves of WT and *Gnpat* KO mice. The qualitative analysis of myelination in spinal cords from 2- to 1.5–year-old *Gnpat* KO mice highlighted the progressive worsening of myelin defects (Supplemental Figure 2). Spinal cords from aged *Gnpat* KO mice displayed a notable hypoplasia with a decrease in white matter area (Supplemental Figure 2).

The morphometric analysis of spinal cords from WT and *Gnpat* KO mice was performed in the ventral funiculus. A decreased density of myelinated fibers was observed in the spinal cord from *Gnpat* KO mice at 21 days (P21), 9 months and 1.5 years of age (Figure 2A). Surprisingly, at 2 months of age, the density of myelinated fibers was normal suggesting that at younger ages there was a delay in the process of myelination. However, the determination of the g-ratio revealed that at 2 months of age, spinal cords from *Gnpat* KO mice contained less myelin when compared to WT mice (Figure 2B). Thus, despite reaching a normal density of myelinated axons, the extent of myelination was defective. The analysis also revealed a progressive loss of myelin with higher g-ratio in 1.5-year-old *Gnpat* KO mice (Figure 2B). To distinguish if the demyelination observed in spinal cords from aged *Gnpat* KO mice was because of the loss of myelinated axons and/or loss of myelin, we performed a detailed ultrastructural analysis. The morphometric analysis (Figure 2C) revealed decreased density of myelinated fibers and a significant increase in axons that completely lacked myelin and in axons with visible reductions in myelin thickness. Given that the total number of axons did not differ between WT and *Gnpat* KO spinal cords, these results indicate that a deficiency in plasmalogens causes a severe loss of myelin, without causing major axonal loss (Figure 2C–D). The ultrastructural analysis was crucial for the validation of an active period of myelin loss. In spinal cords from *Gnpat* KO mice, we observed myelin debris (Figure 2E), as well as the presence of myelin-laden cells (Figure 2F–G). These cells, presumably macrophages, were frequently found close to naked axons and contained lipid accumulations and whorls of myelin. We analyzed the gliotic status in the spinal cord of 1.5-year-old *Gnpat* KO mice and age-matched WT mice. Increased number of astrocytes with a reactive appearance were observed in the white and grey matter of spinal cords from *Gnpat* KO mice (Supplemental Figure 3). However, microgliosis was restricted to the spinal cord white matter (Supplemental Figure 3). Combined, these results demonstrate that a deficiency in plasmalogens causes an initial hypomyelination that progress to a late onset demyelination.

The ultrastructural analysis of optic nerves from WT and *Gnpat* KO mice also revealed the severe consequences of a plasmalogen deficiency. Optic nerves from mutant mice at 21 days of age contained axons devoid of myelin and axons with reduced amounts of myelin (Figure 2H). Similarly, to what was observed in spinal cords, the morphometric analysis revealed a progressive loss of myelinated fibers with a concomitant increase in axons lacking myelin sheaths (Figure 2I). Measurements of g-ratio confirmed hypomyelination in 2-month-old *Gnpat* KO nerves and progressive loss of myelin in aged mice (Figure 2J). When compared to the spinal cord, the optic nerve from *Gnpat* KO mice was more severely affected in terms of myelin loss (Figures 1 and 2I). However, the general appearance of axons was better in optic nerves when compared to spinal cords. Completely demyelinated optic nerve axons lacked evident signs of axonal damage, whereas in the spinal cord some axonal damage could be detected (Figure 2D, asterisks).

Combined, these results indicate that a plasmalogen deficiency affects the ability of oligodendrocytes to initiate myelination and sustain normal myelin levels in the spinal cord and optic nerve. Given the importance of oligodendrocytes and myelin to maintain axonal health, we investigated if the loss of myelin could cause axonal damage.

Regional-specific and demyelination-independent axonal damage in plasmalogen-deficient CNS

Demyelinated and damaged axons are known to display a higher proportion of non-phosphorylated neurofilaments (51). To investigate possible axonal abnormalities, we evaluated the expression levels of non-phosphorylated neurofilaments in spinal cords from WT and *Gnpat* KO mice from P21 to 1.5 years of age. We observed a pronounced increase in non-phosphorylated neurofilaments in spinal cords from 1.5-year-old *Gnpat* KO mice (Supplemental Figure 4). To further evaluate the occurrence of axonal damage in the CNS of plasmalogen-deficient mice, we generated a new mouse line. We crossed

Gnpat mice with mice expressing yellow fluorescent protein (YFP) under the neuronal Thy1 promoter (Thy1-YFP) to generate WT and *Gnpat* KO mice with widespread neuronal expression of YFP. The analysis of longitudinal sections of spinal cords from 7-month and 1.5-year-old *Gnpat* KO:YFP mice revealed clear signs of axonal damage, including axonal swellings, constrictions and axonal degeneration (Figure 3A). The analysis in non-consecutive sections from spinal cords of *Gnpat* KO mice highlights the extent of the observed axonal abnormalities (Supplemental Figure 4). In accordance with previous analyses, optic nerves from *Gnpat* KO:YFP mice lacked clear signs of axonal damage (Supplemental Figure 4). The ultrastructural analysis of optic nerves from *Gnpat* KO mice highlighted the severe loss of myelin and confirmed the sparing of axons, which lacked any sign of

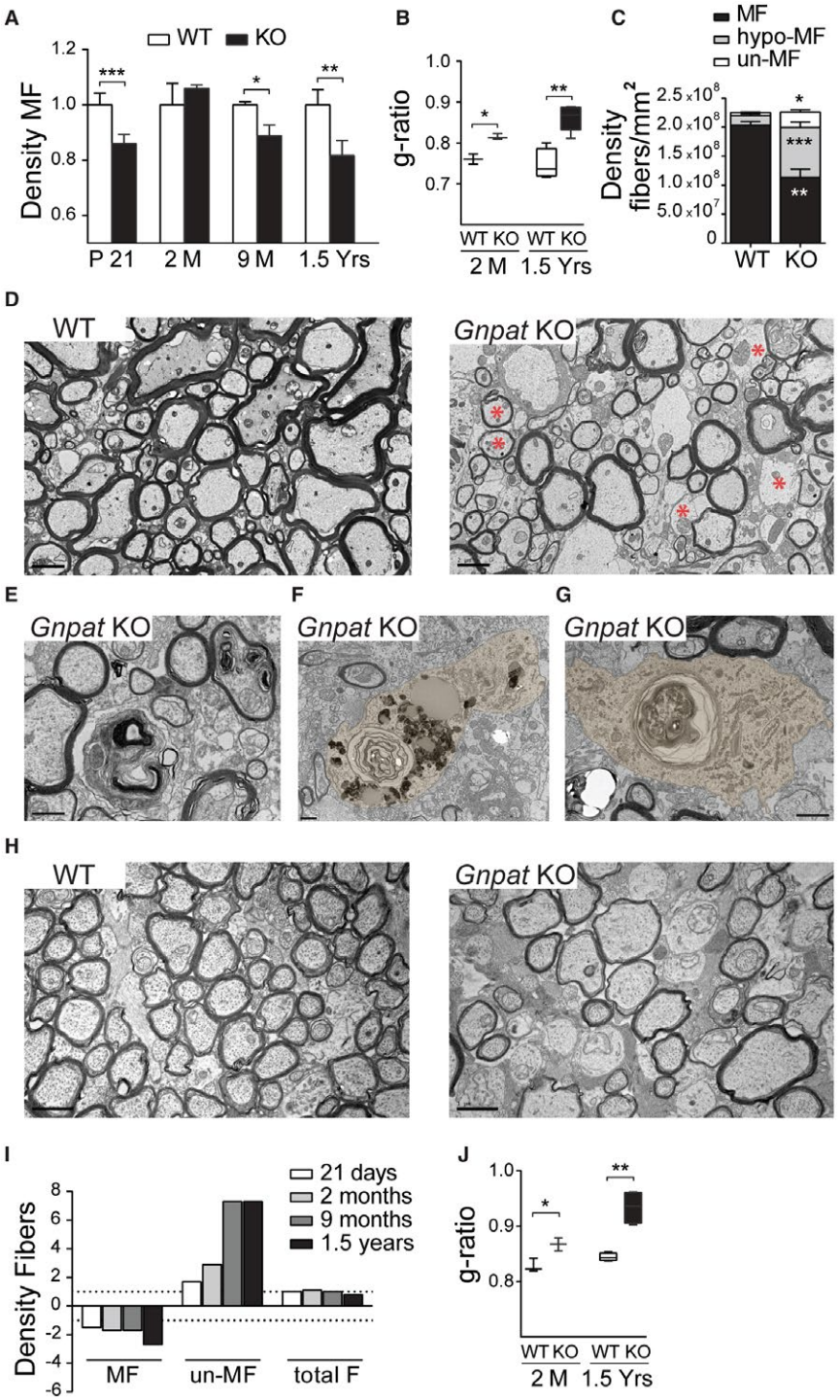

Figure 2. *Plasmalogen deficiency impairs myelination and myelin maintenance.* **A.** Quantification of myelinated fibers (MF) in the ventral funiculus of WT and *Gnpat* KO spinal cords at different ages. [n = 5 per genotype at 21 days (P21); n = 3 per genotype at 2 and 9 months (M); and n = 6 per genotype at 1.5 years (Yrs)]. ***P = 0.014; *P = 0.037; **P = 0.021. **B.** Quantification of myelin by determination of g-ratio in spinal cords of 2-month (n = 3 each genotype) and 1.5-year-old (n = 6 each genotype) WT and *Gnpat* KO mice. *P = 0.0014; **P = 0.0007. **C.** Quantification of myelinated fibers (MF), hypo-myelinated (hypo-MF) and un-myelinated fibers (un-MF) in spinal cords of 1.5-year-old WT and *Gnpat* KO mice (n = 6 per genotype). *P = 0.0012, **P = 0.00036; ***P = 0.0001. **D.** Ultrastructural analysis by electron microscopy of spinal cords from 1.5-year-old WT and *Gnpat* KO mice (n = 3 per genotype) highlighting severe demyelination and signs of axonal damage (asterisks). **E-G.** Ultrastructural analysis of spinal cords from *Gnpat* KO mice (n = 6) revealing the presence of myelin debris (**E**) and myelin-laden cells (pseudocolored in **F,G**). **H.** Ultrastructural analysis of optic nerves from P21 WT and *Gnpat* KO mice (n = 3 per genotype) revealed a defect in myelination with increased number of axons devoid of myelin (asterisks) and thinner myelin sheaths (arrowheads). **I.** Fiber density analysis of myelinated fibers (MF), un-myelinated fibers (un-MF) and the total fiber count (total F) at different ages in optic nerves from WT and *Gnpat* KO mice (n = 3–7 per genotype). **J.** The quantification of myelination by determining g-ratio in optic nerves from WT and *Gnpat* KO mice at 2 months (n = 3 per genotype) and 1.5 years of age (n = 7 per genotype). *P = 0.027, **P = 0.008. Scale bars are 1 μm in **D-H**, and 200 μm in **G**.

damage (Figure 3D). Ultrastructural analysis of longitudinal sections of spinal cords from *Gnpat* KO mice at 1.5 years of age highlighted the extent of axonal damage. The observed defects included axonal swellings with accumulation of organelles (Figure 3B) and axonal degeneration (Figure 3C). In addition, swollen myelinated axons with accumulation of abnormal organelles were observed in the internal capsule and cerebellum (Supplemental Figure 4) of *Gnpat* KO mice. Interestingly, the axonal defects were primarily observed in myelinated axons. In addition to the most common defects associated with axonal damage, we also identified outfoldings of the axonal membrane and the presence of vesicle-like structures in spinal cords (Figure 3E–I) and cerebellum (Supplemental Figure 4) of aged *Gnpat* KO mice. Although these vesicle-like structures seemed to reside in the periaxonal space, detailed analysis of the electron microscopy images revealed that the outfoldings of axonal membranes were lined with the oligodendrocyte adaxonal membrane (Figure 3H). The complex nature and the arrangement of the vesicle-like structures seem to derive from the axonal membrane outfoldings. In some cases, the ultrastructural images revealed the continuous adaxonal membrane of the oligodendrocyte and what seems to be an excised vesicle derived from the axonal outfolding (Figure 3I).

Combined, these results highlight that a deficiency in plasmalogens modulates regional-specific axonal damage without causing major axon loss. The optic nerve from plasmalogen-deficient mice was spared from axonal damage, although it was characterized by an initial severe dysmyelination and the ensuing demyelination. In other regions of the CNS, including the internal capsule, cerebellum and spinal cord, axonal damage was readily observed and was characterized by axonal swelling, severing and abnormal membrane protrusions that seem to accumulate at the adaxonal membrane of mutant oligodendrocytes. Although it is widely thought that myelin loss can modulate and contribute to axonal damage, in plasmalogen-deficient mice axon damage was observed in myelinated axons, suggesting the existence of an axonal intrinsic, demyelination-independent defect.

Targeted and differential composition of plasmalogen-deficient myelin

The deposition of structurally and biochemically normal myelin sheaths around axons is a crucial step for proper myelination. To characterize myelin from plasmalogen-deficient mice, we quantified the levels of seven myelin markers in purified myelin from WT and *Gnpat* KO mice (Figure 4). During the period of dysmyelination, the analysis of myelin isolated from 2-month-old *Gnpat* KO mice revealed reduced levels of myelin basic protein (MBP) and septin-7 (SEPT7) in the spinal cord (Figure 4A,C) and brain (Figure 4B,D). However, the abundance of other myelin markers such as 2′,3′-cyclic nucleotide 3′-phosphodiesterase (CNPase), myelin-associated glycoprotein (MAG), myelin proteolipid protein (PLP), tubulin polymerization promoting protein (TPPP) and tubulin β-IV were not altered in plasmalogen-deficient myelin (Figure 4A–D). During the active period of demyelination, myelin isolated from 1.5-year-old *Gnpat* KO mice was still characterized by reduced levels of MBP and SEPT7 in both spinal cord (Figure 4A,C) and brain (Figure 4B,D). However, levels of MAG were drastically decreased (Figure 4C,D), whereas the remaining myelin proteins continued to be unaffected. Overall, these results demonstrate that a deficiency in plasmalogens causes a targeted and differential deficiency in myelin protein composition, and suggest that MAG dysregulation in aged myelin may cause or contribute to the progression of demyelination.

Myelination-incompetent oligodendrocytes are maintained in the CNS of *Gnpat* KO mice

The recruitment, proliferation and maturation of oligodendrocyte progenitor cells (OPC) are crucial steps for timely myelination but also remyelination (10). To determine if the spatiotemporal regulation of OPC was altered in plasmalogen-deficient mice, we analyzed the levels of oligodendrocyte transcription factor 2 (Olig-2) and NG2 chondroitin sulphate proteoglycan (NG2) as markers of OPC (11). Glutathione *S*-transferase pi isoform (GSTπ)

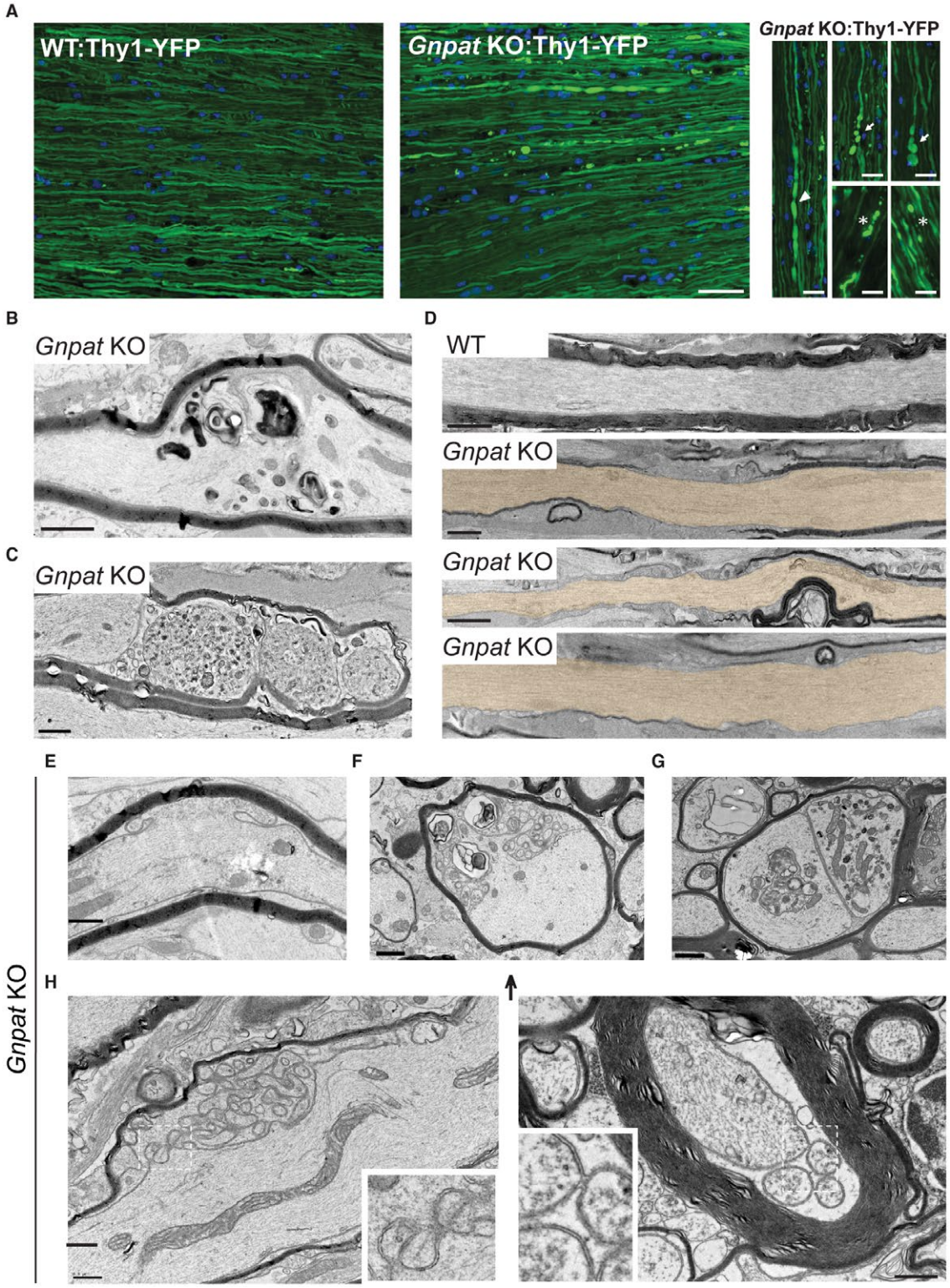

Figure 3. Plasmalogen deficiency causes axonal damage in myelinated axons. **A.** Fluorescence microscopy analysis of longitudinal sections of spinal cords from 7-month-old WT:Thy1-YFP (n = 3) and *Gnpat* KO:Thy1-YFP mice (n = 4). Asterisks and arrowheads highlight signs of axonal damage, including axonal swellings, constrictions axonal degeneration. **B-C.** Ultrastructural analysis of spinal cords from *Gnpat* KO mice at 1.5 years of age (n = 3) revealed axonal swellings with accumulation of organelles (**B**) and axonal degeneration with severing (**C**). **D.** Ultrastructural analysis of longitudinal sections of optic nerves from 1.5-year-old WT (n = 3) and *Gnpat* KO (n = 4) mice highlighted the severe loss of myelin and the sparing of axons (pseudocolored with light brown), which lacked any signs of damage. **E-I.** Several abnormal axonal outfoldings with multiple large vesicle-like structures in spinal cords from *Gnpat* KO mice (n = 6) at 1.5 years. Scale bars are: A 25 µm in small panels and 50 µm in large panels; **B-I** 1 µm.

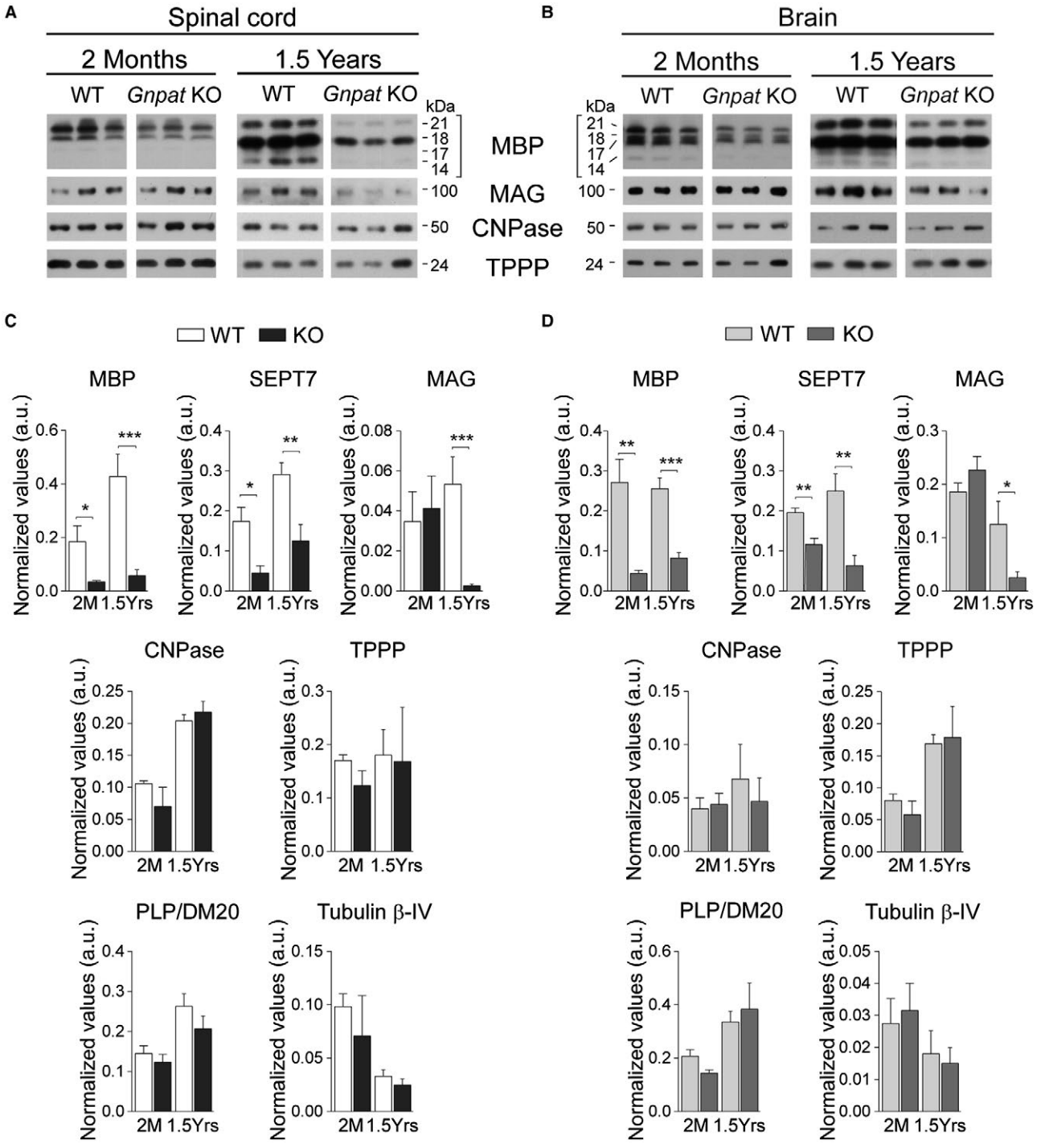

Figure 4. *Differential loss of MBP, MAG and SEPT7 in plasmalogen-deficient myelin.* **A-B.** Representative western blots of MBP, MAG, CNPase and TPPP in myelin isolated from the spinal cord (**A**) and brain (**B**) of 2-month (n = 5–6 per genotype) and 1.5-year-old (n = 5–7 per genotype) WT and *Gnpat* KO mice. **C.** Quantification of MBP, MAG, SEPT7, CNPase, TPPP, PLP/DM20 and tubulin β-IV protein levels normalized to total myelin content in spinal cord myelin. **P* = 0.015; ***P* = 0.005; ****P* = 0.0005. **D.** Quantification of MBP, MAG, SEPT7, CNPase, TPPP, PLP/DM20 and tubulin β-IV protein levels normalized to total myelin content in brain myelin. **P* = 0.014; ***P* = 0.003; ****P* = 0.0001.

and Quaking 7 – clone CC1 were used as markers of differentiated oligodendrocytes (12, 34) in spinal cords of WT and *Gnpat* KO mice. Increased number of Olig2- and NG2-positive cells was observed in the white and grey matter of spinal cords from *Gnpat* KO mice at 9 months of age (Figure 5A–C), suggesting that OPC

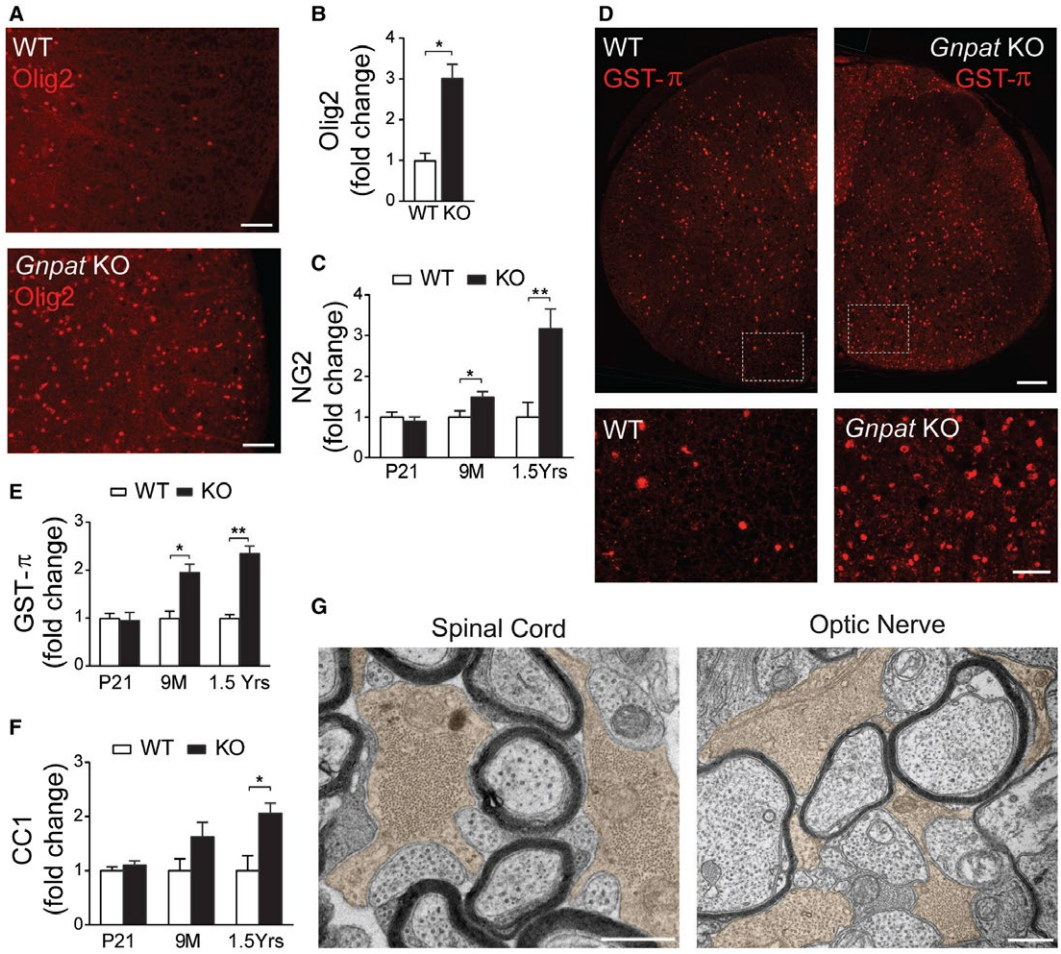

Figure 5. *Increased number of OPC and oligodendrocytes during active demyelination in* Gnpat *KO mice.* **A.** Spinal cord sections from 1.5-year-old WT (n = 3) and Gnpat KO (n = 3) mice stained with anti-Olig2 (red). **B.** Quantification of Olig2-positive OPC in spinal cords from 1.5-year-old WT (n = 3) and *Gnpat* KO (n = 3) mice. **P* = 0.013. **C.** Quantification of NG2-positive OPC in spinal cords from WT and *Gnpat* KO mice at P21, 9M and 1.5 years old. **P* = 0.03, ***P* = 0.01. **D.** Spinal cord sections from 1.5-year-old WT and Gnpat KO mice stained with GST-π (red). Bottom panels are zoom-in of dotted boxes of upper panels. **E.** Quantification of GST-π-positive oligodendrocytes in spinal cords from WT and *Gnpat* KO mice at P21 (n = 3 each genotype), 9M (n = 6–7 each genotype) and 1.5 years old (n = 6–7 each genotype). **P* = 0.0017, ***P* = 0.0001. **F.** Quantification of CC1-positive oligodendrocytes in spinal cords from WT and *Gnpat* KO mice (n = 3 each genotype) at P21, 9M and 1.5 years old. **P* = 0.02. **G.** Ultrastructural analysis by electron microscopy of the spinal cord and optic nerve from *Gnpat* KO mice (n = 4) revealed the presence of oligodendrocytes (pseudocolored with light brown) associated with non-myelinated axons. Scale bars are 50 μm in A; 130 μm in large panels and 50 μm in small panels in C; 0.5 μm in E.

respond to demyelination and try to compensate the myelin defects. The quantifications of GSTπ- and CC1-positive oligodendrocytes during the course of the disease revealed normal levels at P21 and increased numbers with the onset of demyelination at 9 months of age, both in the spinal cord and brain (Figure 5D–F). Overall, these results indicate that despite the impaired ability to correctly myelinate the CNS, plasmalogen-deficient oligodendrocytes undergo a normal differentiation process. In addition, the increased numbers of oligodendrocytes during active demyelination suggest failed attempts to rescue myelination. As evidence of this observation, ultrastructural analysis by electron microscopy revealed the presence of oligodendrocytes in close contact with non-myelinated axons in the spinal cord and optic nerves from *Gnpat* KO mice (Figure 5G). Combined, our results demonstrate that a plasmalogen deficiency does not impair the initial differentiation of oligodendrocytes or their ability to respond to myelin loss and that oligodendrocytes still maintain their role in providing trophic support to axons.

Plasmalogen deficiency affects the intrinsic capacity of oligodendrocytes to myelinate

To better characterize the process of oligodendrocyte development, we setup an *in vitro* myelination assay using a co-culture system of embryonic cortical neurons and

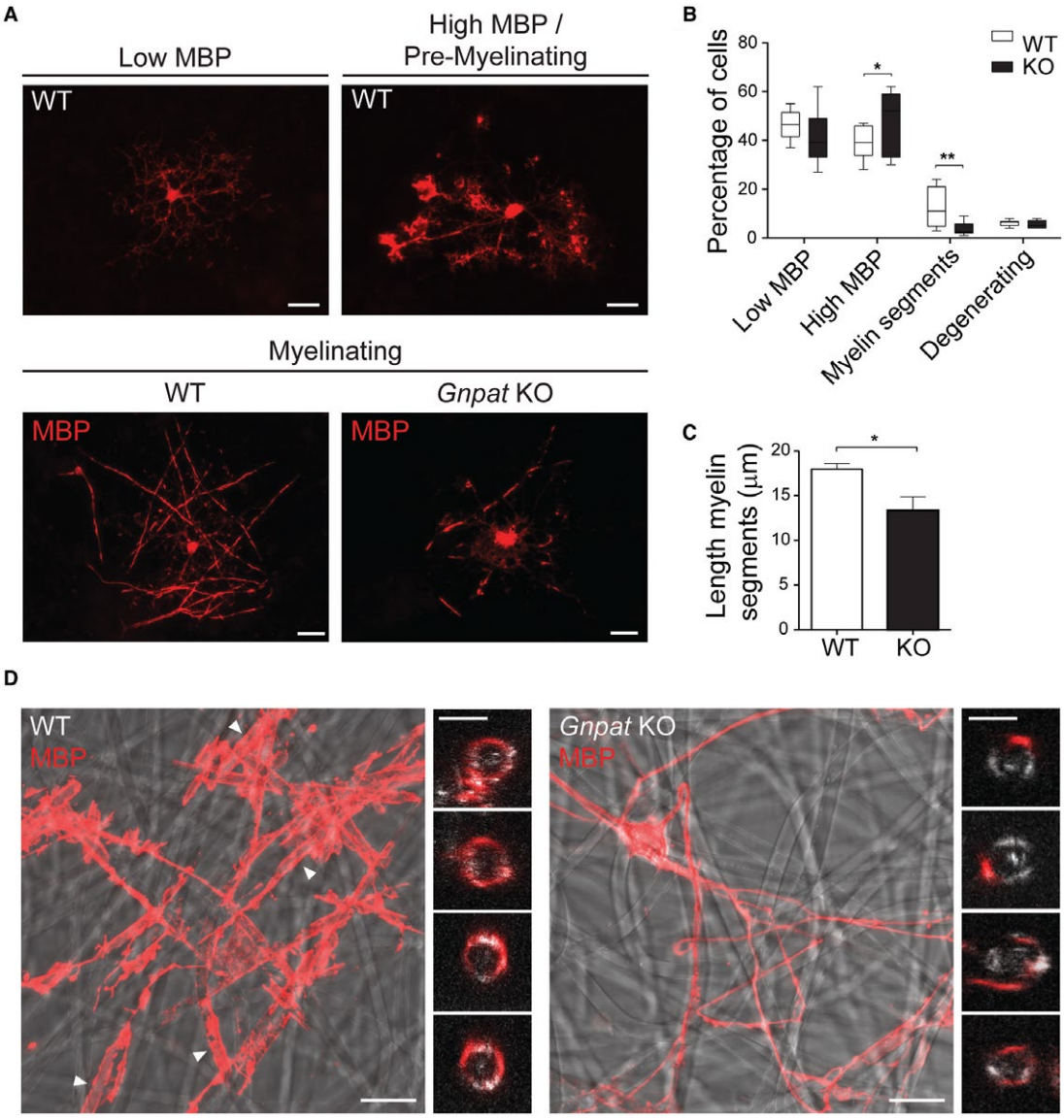

Figure 6. In vitro *myelination assays reveal oligodendrocyte intrinsic defects*. **A.** *In vitro* myelination of mixed cortical co-cultures from WT and KO mice at DIV20. Oligodendrocytes were stained with anti-MBP (red). Highly ramified pre-myelinating oligodendrocytes contained low or high levels of MBP (upper panels), whereas myelinating oligodendrocytes displayed reduced branches and myelin segments (bottom panels). Scale bars are 20 µm. **B.** Quantification of oligodendrocytes during different stages of differentiation in WT and Gnpat KO co-cultures (n = 4 for each genotype). Data presented as boxes that extend from the 25th to 75th percentiles, with a line at the mean. Whiskers represent the minimal and maximal values. $*P = 0.04$; $**P = 0.006$ using Student's *T* test. **C.** Quantification of the length of myelin segments in myelinating oligodendrocytes from WT and *Gnpat* KO mice (n = 4 for each genotype). $*P = 0.014$. Data presented as mean + SEM and compared using Student's *T* test. **D.** Confocal images of oligodendrocytes from WT and *Gnpat* KO mice (n = 3 for each genotype) at DIV12 plated onto electrospun poly-L-lactide microfibers and immunolabeled for MBP (red). Myelin segments produced by WT oligodendrocytes are highlighted with arrowheads. Small panels on the right of WT and *Gnpat* KO images are magnified and cross-sectional (xz) views of WT oligodendrocytes engulfing microfibers and *Gnpat* KO oligodendrocytes extending single processes that do not engulf the microfiber. Scale bars are 20 µm in large panels and 4 µm in small panels.

glial cells (29). In this co-culture system, we were able to identify four types of oligodendrocytes: highly branched pre-myelinating oligodendrocytes with low MBP expression (Figure 6A), pre-myelinating oligodendrocytes with high MBP expression (Figure 6A), myelinating oligodendrocytes with reduced branching and displaying myelin segments (Figure 6A) and degenerating oligodendrocytes with abnormal morphology and fragmented processes. Quantification of the different populations of oligodendrocytes was performed in WT and *Gnpat* KO co-cultures at 20 days *in vitro* (DIV20) (Figure 6B). No significant differences were observed in pre-myelinating

oligodendrocytes expressing low levels of MBP or in degenerating oligodendrocytes. However, in *Gnpat* KO co-cultures, we observed an increase in branched oligodendrocytes with high levels of MBP and significant decrease in myelinating oligodendrocytes (Figure 6A,B). In addition, we observed that the few myelinating oligodendrocytes in *Gnpat* KO co-cultures displayed shorter myelin segments (Figure 6A). Measurement of the myelin segment length was reduced in *Gnpat* KO co-cultures (Figure 6C). Corroborating the *in vivo* findings, these results indicate that a plasmalogen deficiency affected oligodendrocyte differentiation during the final stages of maturation with a halted initiation of myelin sheaths.

In order to distinguish between oligodendrocyte-driven vs. axon-instructed defects, we cultured mouse primary cortical oligodendrocytes on electrospun poly-L-lactide microfibers. In this neuron-free and three-dimensional culture system, the microfibers serve as a scaffold for oligodendrocytes to extend and wrap their processes around them (30). After DIV12, we analyzed the differentiation of WT and *Gnpat* KO oligodendrocytes and their ability to myelinate the microfibers. We observed that WT oligodendrocytes were able to ensheath and wrap the microfibers, with the formation of thick MBP segments (Figure 6D). Oligodendrocytes from *Gnpat* KO mice, despite being able to extend processes, were not capable of wrapping the microfibers (Figure 6D). In summary, these results demonstrate that the lack plasmalogens affects the intrinsic capacity of oligodendrocytes to myelinate.

A new alkyl glycerol is able to rescue myelination defects

Ether-linked glycerols (alkyl glycerols) are known to enter the plasmalogen biosynthetic pathway after the peroxisomal steps (Figure 7A), and can serve as alternative precursors to rescue the biochemical defect (19, 44). Using the *in vitro* myelination system, we evaluated the ability of two commonly used alkyl glycerols to rescue the myelination defect of *Gnpat* KO oligodendrocytes. WT and *Gnpat* KO co-cultures were treated with a mixture of batyl and chimyl alcohol (BA and CA). The treatment with BA and CA was not able to rescue myelination in *Gnpat* KO co-cultures, which continued to present decreased number of myelinating oligodendrocytes and reduced number of small myelin segments (Supplemental Figure 5). The development of the *in vitro* myelination system allowed us to test the potential of other alkyl glycerols as functional alternative precursors of plasmalogens. We assayed the potential of glyceryl 1-myristyl ether (1-*O*-tetradecyl-sn-glycerol; 1-O-TDG), an alkyl glycerol with a shorter C14 alkyl chain. To assay the potential of 1-O-TDG as a plasmalogen precursor, we measured plasmalogen levels in WT and *Gnpat* KO fibroblasts. Fibroblasts were chosen because of their generalized usage in assays with alkyl glycerols and to circumvent the inability to obtain sufficient amounts of primary oligodendrocytes necessary for the biochemical assays. As expected, treatment of *Gnpat* KO cells with 1-O-TDG was not able to rescue plasmalogens with C16:0, C18:1 and C18:0 at the *sn*-1 position (Figure 7B and C). However, 1-O-TDG was successfully converted into plasmalogens with C14:0 at the *sn*-1 position (Figure 7B and D) and boosted the plasmalogen levels in *Gnpat* KO fibroblasts when compared to WT fibroblasts (Figure 7E).

In addition, using *in vitro* myelination cultures, treatment with 1-O-TDG was able to rescue myelination in *Gnpat* KO co-cultures, as evidenced by the assembly of long myelin segments (Figure 7F, H) and the increased density of myelinating oligodendrocytes (Figure 7G). Combined, these results provide evidence of a differential ability of oligodendrocytes to use different alkyl glycerols as precursors in the biosynthesis of plasmalogens. 1-O-TDG was identified as a new alkyl glycerol that can rescue plasmalogen levels and the intrinsic myelination defect of plasmalogen-deficient oligodendrocytes.

To validate the usage of 1-O-TDG as a potential therapeutic agent, we treated WT and *Gnpat* KO mice with either vehicle (1% Tween-80 in saline) or 1-O-TDG in vehicle at a dosage of 5 mg/kg. The treatments were administered via subcutaneous injections from P1 to P8 and via intraperitoneal injections from P10 to P18 (Figure 8A). At the start of the treatment, *Gnpat* KO mice displayed reduced body weight (Figure 8B), a feature of plasmalogen deficiency in mice (14, 15). However, at the end of the treatment, 1-O-TDG-treated *Gnpat* KO mice had normal body weight (Figure 8C) indicative of the improvement on the general well-being, similar to that observed with batyl alcohol (14). The histopathological analysis of nervous tissues from *Gnpat* KO mice treated with 1-O-TDG revealed a generalized rescue in myelination. Histological analysis of myelinated fibers in the dorsal column tract revealed improvements in myelination and axon radial growth (Figure 8D), and in the ventral funiculus the density of myelinated axons was normalized in *Gnpat* KO mice (Figure 8E). In optic nerves, the region most affected by a plasmalogen deficiency (Figure 1A, Figure 2H), the treatment with 1-O-TDG was able to normalize the densities of myelinated axons (Figure 8F) and un-myelinated axons (Figure 8G) to values observed in control-treated WT mice. During this period of active myelination, WT mice treated with 1-O-TDG also displayed increased number of myelinated axons (Figure 8F). We also addressed if the treatment with 1-O-TDG could rescue the myelination defects observed in the peripheral nervous system (PNS) (17). Treatment with 1-O-TDG rescued the impaired myelination observed in sciatic nerves from *Gnpat* KO mice (Figure 8H). The treatment also induced myelination in sciatic nerves from WT mice with significant decreases in g-ratio (Figure 8H). Combined, these results demonstrate the ability of 1-O-TDG to rescue the myelination defects observed in the CNS and PNS of plasmalogen-deficient mice.

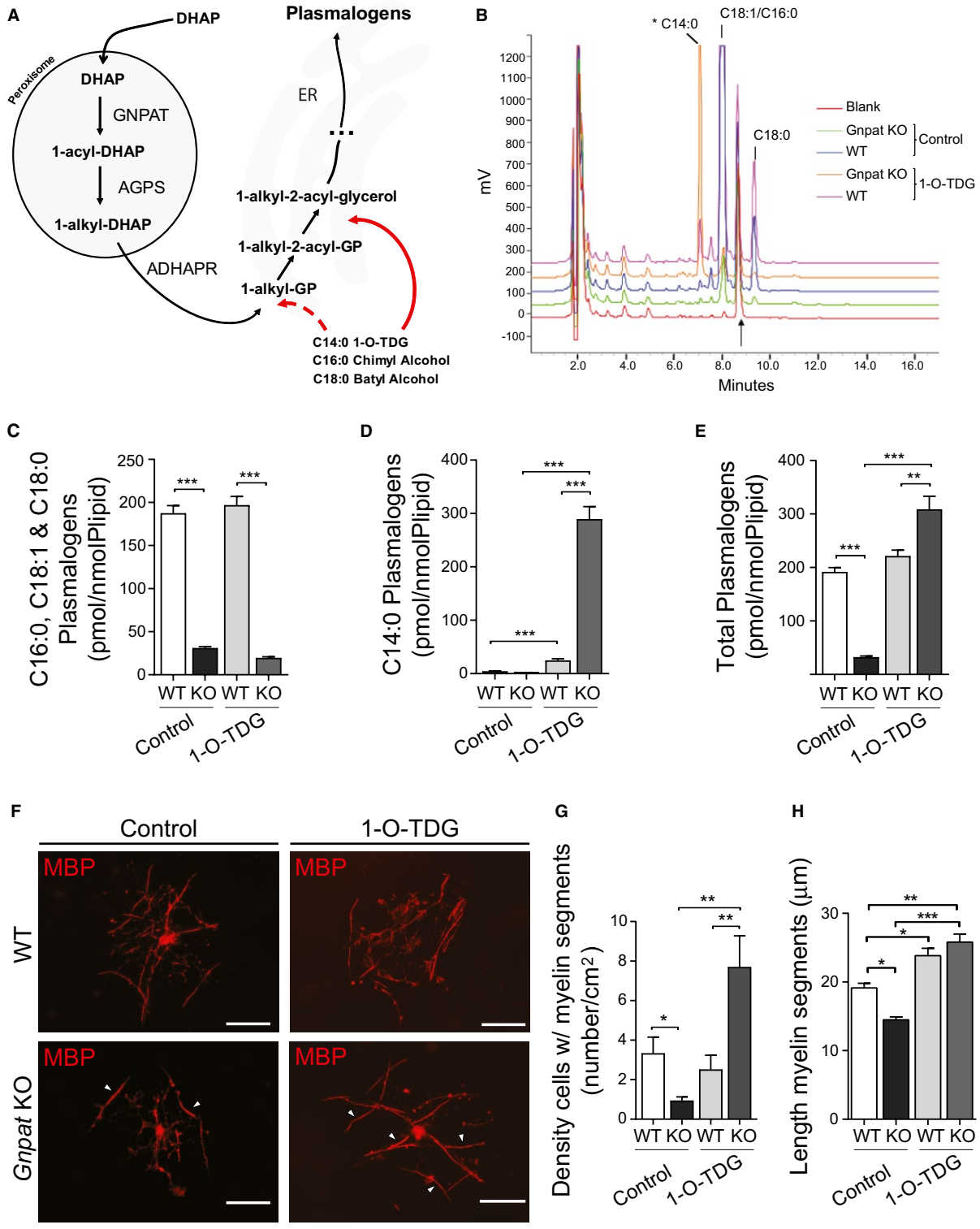

Figure 7. *Identification of 1-O-tetradecylglycerol as a new alkyl glycerol capable of rescuing myelination defects.* **A.** Schematic representation highlighting the routes at which alkyl glycerols can enter the plasmalogen biosynthesis to rescue defects in the peroxisomal steps. Alkyl glycerols can be phosphorylated (dotted arrow) to generate 1-alkyl-glycero-3-phosphate (GP) or acylated (arrow) to generate 1-alkyl-2-acyl-glycerol. DHAP: dihydroxyacetone phosphate; ADHAPR: acylglycerone-phosphate reductase. **B.** Representative chromatograms of lipid extracts from WT and *Gnpat* KO fibroblasts either control or 1-O-TDG treated, subjected to RP-HPLC and detected by fluorimetry. The arrow denotes heptadecanal, used as internal standard. The major peaks in WT fibroblasts correspond to octadecenal (C18:1), eluting ahead of hexadecanal (C16:0) and octadecanal (C18:0). The asterisk indicates the elution of the tetradecanal (C14:0) derivative, only present in samples treated with 1-O-TDG. **C-E.** Quantification of plasmalogens in fibroblasts from WT and *Gnpat* KO mice under control conditions (n = 3–5 per genotype) and after 1-O-TDG treatment (n = 5 per genotype). **C.** Levels of plasmalogens containing C16:0, C18:1 and C18:0; $***P < 0.0001$. **D.** Levels of plasmalogens containing C14:0.; $***P < 0.0001$. **E.** Total levels of plasmalogens (containing C14:0, C16:0; C18:1 and C18:0; $**P = 0.011$, $***P < 0.001$. **F.** *in vitro* myelination of mixed cortical cultures from WT and KO mice (n = 3 each genotype) at DIV20 treated with 1-O-TDG or control, and immunostained for MBP (red). Myelin segments are highlighted with arrowheads. Scale bars are 50 μm. **G.** Quantification of the myelinating oligodendrocytes in control- and 1-O-TDG-treated co-cultures from WT and *Gnpat* KO mice (n = 3 each genotype). $*P = 0.03$, $**P = 0.01$. **H.** Quantification of the length of myelin segments in control- and 1-O-TDG-treated co-cultures from WT and *Gnpat* KO mice (n = 3 each genotype). $*P = 0.02$, $**P = 0.0024$, $***P < 0.0001$.

DISCUSSION

Here, we unraveled the role of plasmalogens in CNS myelin and during myelination using a mouse model for RCDP. We demonstrate that differentiated oligodendrocytes are the prime target of a deficiency in plasmalogens causing impaired myelination and myelin maintenance. During development, OPC migrate to reach their final destination and terminate their differentiation into myelin-forming oligodendrocytes (50). The regulation of these two processes is crucial to ensure adequate numbers of OPC, and consequently appropriate numbers of myelinating oligodendrocytes (33). Assessment of OPC and oligodendrocyte numbers during the early postnatal period revealed normal densities in spinal cords and optic nerves from *Gnpat* KO mice, suggesting that impaired myelination was not caused by defects in OPC migration. The lack of plasmalogens in oligodendrocytes from *Gnpat* KO mice did not affect the initial stages of differentiation. Oligodendrocytes from *Gnpat* KO mice expressed GST-π and CC1, markers of mature oligodendrocytes (11), and *in vitro* assays showed normal oligodendrocyte development up to the final stages of maturation and myelin assembly. The dynamic interplay of the intrinsic mechanisms in oligodendrocytes and axon-derived extrinsic signals are crucial steps for the suitable balance between differentiation and myelination (20). Several extrinsic signals derived from axons impact oligodendrocytes' terminal differentiation (25), promote myelination (9) or regulate myelin thickness (48). Using *in vitro* myelination assays, we identified that only a reduced number of plasmalogen-deficient oligodendrocytes are able to assemble shorter and scarcer myelin sheaths around axons. Using scaffolds of microfibers, we were able to unravel that the defect in assembling myelin sheaths was caused by a compromised intrinsic capacity of plasmalogen-deficient oligodendrocytes to ensheath and assemble myelin segments.

In adult mice, the lack of plasmalogens continued to have a negative impact on myelin content throughout the CNS, as evidenced by reduced g-ratio and the progressive increase in the density of axons lacking myelin sheaths. These myelin defects correlate with the neurological phenotype of Gnpat KO mice. From the age of 9 months, Gnpat KO mice start developing a severe and progressive neurological condition that includes tremors and generalized ataxia. This phenotype worsens after 1 year of age with increased tremor frequency and limb paralysis. This led us to hypothesize that altered myelin composition could contribute to failure in attaining correct myelination and the sustainment of myelin. Differential expression MBP, SEPT7 and MAG was observed in plasmalogen-deficient myelin. Decreased levels of MBP and SEPT7 were observed during initial hypomyelination. MBP is known to be essential in initiating and driving the axonal wrapping process, myelin compaction and the maintenance of the physical stability of the sheaths (45, 57). Interestingly, plasmalogens and MBP are the two major constituents of myelin at the cytoplasmic apposition (1, 28). Thus, the complete absence of plasmalogens, together with the decreased levels of MBP, could be the major cause of inadequate formation of the myelin sheath, and consequently impaired myelination. The enrichment of septins in mature myelin (22, 26, 58), together with the reported importance of septins in myelin disorders, reflects a general association between the abundance of septins and myelin pathology. Recently, it has been described that the presence of myelin outfoldings, a common feature observed in several myelin-related disorders, correlates with a loss of cytoskeletal septins in myelin (40). Septin filaments are localized to the non-compacted adaxonal myelin compartment and were judged to be important for scaffolding the axon/myelin unit at a later stage of myelin maturation (40). Here we reported that plasmalogen-deficient myelin is characterized by reduced levels of SEPT7. The association of septins with phospholipids was found to be crucial for the formation and maintenance of membrane domains (7). Our results underscore a possible role of plasmalogens on correct septin location. Moreover, the intimate relationship between septins and actin cytoskeleton (23, 47), together with the well-known function of actin on myelination (37, 60), may also correlate the decreased levels of SEPT7 and defective myelination.

Whereas MBP and SEPT7 levels were consistently reduced in plasmalogen-deficient myelin, the levels of MAG display an additional differential pattern of expression. During the period of hypomyelination, MAG levels were normal

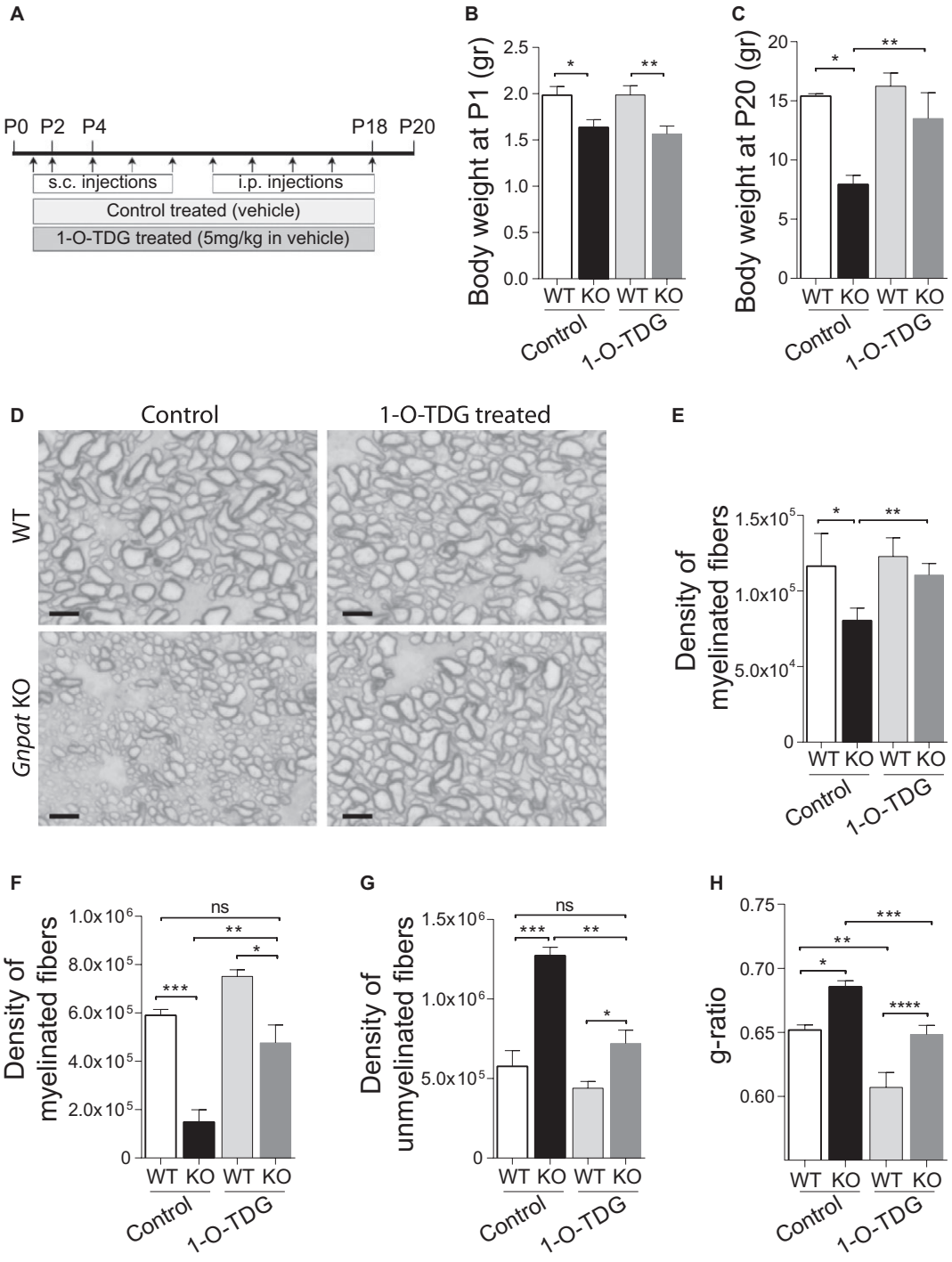

Figure 8. *Treatment with 1-O-tetradecylglycerol rescues* in vivo *myelination defects.* **A.** Schematic representation of *in vivo* treatments. WT and *Gnpat* KO mice were treated from P1 to P18 with 1-O-TDG or control vehicle (n = 3 each genotype and treatment). From postnatal day 1 (P1) to P8, treatments were delivered via subcutaneous (s.c.) injections and from P10 to P18 via intraperitoneal (i.p.) injections. Tissues were collected at P20. **B.** Body weight at the start of treatment. **P* = 0.022, ****P* = 0.012. **C.** Body weight at the end of treatment (P20). **P* = 0.0004, ***P* = 0.0037. **D.** Light microscopy images of dorsal column track stained with PPD from control- and 1-O-TDG-treated WT and *Gnpat* KO mice at P20. *Scale bars* are 5 µm. **E.** Quantification of myelinated fibers in the ventral funiculus, of control- and 1-O-TDG-treated, WT and Gnpat KO spinal cords at P20. **P* = 0.031, ***P* = 0.014. **F.** Quantification of myelinated fibers in optic nerves from of control- and 1-O-TDG-treated WT and *Gnpat* KO mice at P20. **P* = 0.011, ***P* = 0.0083, ****P* = 0.0009. **G.** Quantification of unmyelinated fibers in optic nerves from of control- and 1-O-TDG-treated WT and *Gnpat* KO mice at P20. **P* = 0.040, ***P* = 0.0014, ****P* = 0.0028. **H.** Quantification of myelination by determination of g-ratio in sciatic nerves from of control- and 1-O-TDG-treated WT and *Gnpat* KO mice at P20. **P* = 0.0049, ***P* = 0.0017, ****P* = 0.0066, *****P* = 0.0073.

in myelin from *Gnpat* KO mice but during the period of demyelination MAG levels decreased in plasmalogen-deficient myelin. MAG is a myelin protein preferentially expressed on the innermost myelin wrap, adjacent to the axon (49). Analysis of MAG-null mutants revealed a surprisingly subtle phenotype, which included mild myelin abnormalities and the lack of a periaxonal cytoplasmic collar (8, 35). These observations suggest that MAG plays a role in stabilizing oligodendrocyte-axon contacts in mature myelin sheaths, which may be involved in the long-term stability of axons (43). Therefore, the decreased levels of MAG in plasmalogen-deficient myelin may disturb the myelin-axon stability and lead to the development of axonal outfoldings observed in *Gnpat* KO axons. Combined with the reduced levels of SEPT7, we hypothesize that the abnormal myelin composition observed in aged *Gnpat* KO mice could be the trigger for demyelination and for the engulfment of axonal protrusions that result in the accumulation of vesicle-like structures.

Demyelination was observed throughout the CNS, although different degrees of severity were noted. In addition, we observed that severe demyelination did not cause major axonal loss, suggesting an unaltered trophic support capacity by mutant oligodendrocytes. Notably, whereas the optic nerve was the most severely affected CNS region with regard to myelin content, it completely lacked signs of axonal loss or damage. Therefore, and contrary to previous claims (42), no axon degeneration was observed in optic nerves from plasmalogen-deficient mice. However, axonal damage occurred with an apparent regional specificity since axonal damage was more prominent in other CNS areas (eg, spinal cord, cerebellar white matter and internal capsule). The presence of hallmark signs of axonal damage (eg, axonal swellings with accumulation of organelles) in myelinated axons and in regions with moderate myelin defects (eg, cerebellar white matter) suggests a demyelination-independent contribution to the sustainment of healthy axons. Therefore, we hypothesize that a plasmalogen deficiency may differentially affect different subsets of neurons or that subtle alterations in myelin content or composition may affect these subsets of neurons leading to axonal dysfunction.

Treatment options able to rescue the biochemical or pathologic defects caused by a plasmalogen defect are scarce (14, 19). Although *in vitro* studies have shown that the alkyl glycerols BA or CA are able to restore plasmalogen levels, a previous study showed that their effectiveness *in vivo* excludes the central and peripheral nervous systems (14). Treatment using BA as a plasmalogen precursor proved to be effective on systemic tissues, but inefficient on the nervous system. A possible contribution of the blood-brain barrier (BBB) in the CNS could explain the inability of BA to normalize plasmalogen levels in the brain and spinal cord. Using the *in vitro* myelination system, we assayed the potential of BA and CA to rescue myelination defects in *Gnpat* KO oligodendrocytes. Our results demonstrate that these alkyl glycerols are not capable of restoring myelination even in the absence of a functional BBB. The feasibility of the *in vitro* myelination assays allowed us to test and validate the potential of other alkyl glycerols in rescuing CNS defects. We identified 1-O-TDG as a functional alkyl glycerol capable of rescuing plasmalogen levels in *Gnpat* KO cells and capable of rescuing the differentiation and myelination potential of *Gnpat* KO oligodendrocytes. Although plasmalogens usually contain C16:0, C18:1 and C18:0 moieties at the *sn*-1 position, 1-0-heptadecylglycerol (containing a C17:0 alkyl chain) was also shown to be incorporated into plasmalogens (19). Our results demonstrate that shorter alkyl chains can also be incorporated into plasmalogens. In addition, our results suggest that the synthesis of plasmalogens with their characteristic vinyl-ether bond is more important than the chain length at the *sn*-1 position (13). The ability of 1-O-TDG to rescue myelination *in vivo* represents a novel and valid strategy for the development of translatable approaches to rescue plasmalogen levels in the CNS and treatment of the myelination defects observed in RCDP patients (2, 5).

ACKNOWLEDGEMENTS

We thank Paula Sampaio for microscopy support, Paula Magalhães and Tânia Meireles for genotyping, and Sofia Lamas for excellent animal care. We are grateful to Pedro Abreu for his contribution to the analysis of axonal damage. This work was supported by FEDER Funds through the Operational Competitiveness Program – COMPETE, and by national funds through the FCT – Fundação para a Ciência e a Tecnologia. D. Bessa-Neto was supported by a fellowship under the project E-Rare3/0001/2015. P. Brites is an Investigator FCT, and A.R. Malheiro was supported by the FCT (FRH/BD/93110/2013). P.P. Van Veldhoven was supported by the Flemish Fonds voor Wetenschappelijk Onderzoek (FWO/G0D7915N) under the PERescue project of the ERA-Net for Research Programmes on Rare Diseases.

CONFLICT OF INTEREST

The authors have declared that no conflict of interest exists.

DATA AVAILABILITY STATEMENT

The data that support the findings of this study are available from the corresponding author upon reasonable request.

REFERENCES

1. Aggarwal S, Yurlova L, Simons M (2011) Central nervous system myelin: structure, synthesis and assembly. *Trends Cell Biol* **21**:585–593.
2. Alkan A, Kutlu R, Yakinci C, Sigirci A, Aslan M, Sarac K (2003) Delayed myelination in a rhizomelic chondrodysplasia punctata case: MR spectroscopy findings. *Magn Reson Imaging* **21**:77–80.
3. Baglole CJ, Reddy SY, Pollock SJ, Feldon SE, Sime PJ, Smith TJ, Phipps RP (2005) Isolation and phenotypic characterization of lung fibroblasts. *Methods Mol Med* **117**:115–127.

4. Bams-Mengerink AM, Koelman JH, Waterham H, Barth PG, Poll-The BT (2013) The neurology of rhizomelic chondrodysplasia punctata. *Orphanet J Rare Dis* **8**:174.
5. Bams-Mengerink AM, Majoie CB, Duran M, Wanders RJ, Van Hove J, Scheurer CD *et al* (2006) MRI of the brain and cervical spinal cord in rhizomelic chondrodysplasia punctata. *Neurology* **66**:798–803; discussion 789.
6. Baroy T, Koster J, Stromme P, Ebberink MS, Misceo D, Ferdinandusse S *et al* (2015) A novel type of rhizomelic chondrodysplasia punctata, RCDP5, is caused by loss of the PEX5 long isoform. *Hum Mol Genet* **24**:5845–5854.
7. Barral Y, Mermall V, Mooseker MS, Snyder M (2000) Compartmentalization of the cell cortex by septins is required for maintenance of cell polarity in yeast. *Mol Cell* **5**:841–851.
8. Bartsch U (1996) Myelination and axonal regeneration in the central nervous system of mice deficient in the myelin-associated glycoprotein. *J Neurocytol* **25**:303–313.
9. Bauer NG, Richter-Landsberg C, Ffrench-Constant C (2009) Role of the oligodendroglial cytoskeleton in differentiation and myelination. *Glia* **57**:1691–1705.
10. Bergles DE, Richardson WD (2015) Oligodendrocyte development and plasticity. *Cold Spring Harb Perspect Biol* **8**:a020453.
11. Billon N, Jolicoeur C, Ying QL, Smith A, Raff M (2002) Normal timing of oligodendrocyte development from genetically engineered, lineage-selectable mouse ES cells. *J Cell Sci* **115**:3657–3665.
12. Bin JM, Harris SN, Kennedy TE (2016) The oligodendrocyte-specific antibody 'CC1' binds Quaking 7. *J Neurochem* **139**:181–186.
13. Braverman NE, Moser AB (2012) Functions of plasmalogen lipids in health and disease. *Biochim Biophys Acta* **1822**:1442–1452.
14. Brites P, Ferreira AS, da Silva TF, Sousa VF, Malheiro AR, Duran M *et al* (2011) Alkyl-glycerol rescues plasmalogen levels and pathology of ether-phospholipid deficient mice. *PLoS One* **6**:e28539.
15. Brites P, Mooyer PA, El Mrabet L, Waterham HR, Wanders RJ (2009) Plasmalogens participate in very-long-chain fatty acid-induced pathology. *Brain* **132**(Pt 2):482–492.
16. Buchert R, Tawamie H, Smith C, Uebe S, Innes AM, Al Hallak B *et al* (2014) A peroxisomal disorder of severe intellectual disability, epilepsy, and cataracts due to fatty acyl-CoA reductase 1 deficiency. *Am J Hum Genet* **95**:602–610.
17. da Silva TF, Eira J, Lopes AT, Malheiro AR, Sousa V, Luoma A *et al* (2014) Peripheral nervous system plasmalogens regulate Schwann cell differentiation and myelination. *J Clin Invest* **124**:2560–2570.
18. da Silva TF, Sousa VF, Malheiro AR, Brites P (2012) The importance of ether-phospholipids: a view from the perspective of mouse models. *Biochim Biophys Acta* **1822**:1501–1508.
19. Das AK, Holmes RD, Wilson GN, Hajra AK (1992) Dietary ether lipid incorporation into tissue plasmalogens of humans and rodents. *Lipids* **27**:401–405.
20. Emery B (2010) Regulation of oligodendrocyte differentiation and myelination. *Science* **330**:779–782.
21. Feng G, Mellor RH, Bernstein M, Keller-Peck C, Nguyen QT, Wallace M *et al* (2000) Imaging neuronal subsets in transgenic mice expressing multiple spectral variants of GFP. *Neuron* **28**:41–51.
22. Fewou SN, Fernandes A, Stockdale K, Francone VP, Dupree JL, Rosenbluth J *et al* (2010) Myelin protein composition is altered in mice lacking either sulfated or both sulfated and non-sulfated galactolipids. *J Neurochem* **112**:599–610.
23. Gladfelter AS, Bose I, Zyla TR, Bardes ES, Lew DJ (2002) Septin ring assembly involves cycles of GTP loading and hydrolysis by Cdc42p. *J Cell Biol* **156**:315–326.
24. Grider MH, Chen Q, Shine HD (2006) Semi-automated quantification of axonal densities in labeled CNS tissue. *J Neurosci Methods* **155**:172–179.
25. Ishibashi T, Dakin KA, Stevens B, Lee PR, Kozlov SV, Stewart CL, Fields RD (2006) Astrocytes promote myelination in response to electrical impulses. *Neuron* **49**:823–832.
26. Jahn O, Tenzer S, Werner HB (2009) Myelin proteomics: molecular anatomy of an insulating sheath. *Mol Neurobiol* **40**:55–72.
27. Khanna AJ, Braverman NE, Valle D, Sponseller PD (2001) Cervical stenosis secondary to rhizomelic chondrodysplasia punctata. *Am J Med Genet* **99**:63–66.
28. Kirschner DA, Ganser AL (1982) Myelin labeled with mercuric chloride. Asymmetric localization of phosphatidylethanolamine plasmalogen. *J Mol Biol* **157**:635–658.
29. Lariosa-Willingham KD, Rosler ES, Tung JS, Dugas JC, Collins TL, Leonoudakis D (2016) Development of a central nervous system axonal myelination assay for high throughput screening. *BMC Neurosci* **17**:16.
30. Lee S, Chong SY, Tuck SJ, Corey JM, Chan JR (2013) A rapid and reproducible assay for modeling myelination by oligodendrocytes using engineered nanofibers. *Nat Protoc* **8**:771–782.
31. McCarthy KD, de Vellis J (1980) Preparation of separate astroglial and oligodendroglial cell cultures from rat cerebral tissue. *J Cell Biol* **85**:890–902.
32. Mezzar S, de Schryver E, Van Veldhoven PP (2014) RP-HPLC-fluorescence analysis of aliphatic aldehydes: application to aldehyde-generating enzymes HACL1 and SGPL1. *J Lipid Res* **55**:573–582.
33. Mitew S, Hay CM, Peckham H, Xiao J, Koenning M, Emery B (2014) Mechanisms regulating the development of oligodendrocytes and central nervous system myelin. *Neuroscience* **276**:29–47.
34. Miyamoto N, Maki T, Shindo A, Liang AC, Maeda M, Egawa N *et al* (2015) Astrocytes promote oligodendrogenesis after white matter damage via brain-derived neurotrophic factor. *J Neurosci* **35**:14002–14008.
35. Montag D, Giese KP, Bartsch U, Martini R, Lang Y, Bluthmann H *et al*. (1994) Mice deficient for the myelin-associated glycoprotein show subtle abnormalities in myelin. *Neuron* **13**:229–246.
36. Nave KA, Werner HB (2014) Myelination of the nervous system: mechanisms and functions. *Annu Rev Cell Dev Biol* **30**:503–533.
37. Nawaz S, Sanchez P, Schmitt S, Snaidero N, Mitkovski M, Velte C *et al* (2015) Actin filament turnover drives leading edge growth during myelin sheath formation in the central nervous system. *Dev Cell* **34**:139–151.
38. Norton WT, Poduslo SE (1973) Myelination in rat brain: changes in myelin composition during brain maturation. *J Neurochem* **21**:759–773.

39. Norton WT, Poduslo SE (1973) Myelination in rat brain: method of myelin isolation. *J Neurochem* **21**:749–757.
40. Patzig J, Erwig MS, Tenzer S, Kusch K, Dibaj P, Mobius W *et al* (2016) Septin/anillin filaments scaffold central nervous system myelin to accelerate nerve conduction. *Elife* **5**:e17119.
41. Powers JM, Kenjarski TP, Moser AB, Moser HW (1999) Cerebellar atrophy in chronic rhizomelic chondrodysplasia punctata: a potential role for phytanic acid and calcium in the death of its Purkinje cells. *Acta Neuropathol* **98**:129–134.
42. Rodemer C, Thai TP, Brugger B, Kaercher T, Werner H, Nave KA *et al* (2003) Inactivation of ether lipid biosynthesis causes male infertility, defects in eye development and optic nerve hypoplasia in mice. *Hum Mol Genet* **12**:1881–1895.
43. Schachner M, Bartsch U (2000) Multiple functions of the myelin-associated glycoprotein MAG (siglec-4a) in formation and maintenance of myelin. *Glia* **29**:154–165.
44. Schrakamp G, Schalkwijk CG, Schutgens RB, Wanders RJ, Tager JM, van den Bosch H (1988) Plasmalogen biosynthesis in peroxisomal disorders: fatty alcohol versus alkylglycerol precursors. *J Lipid Res* **29**:325–334.
45. Snaidero N, Velte C, Myllykoski M, Raasakka A, Ignatev A, Werner HB *et al* (2017) Antagonistic functions of MBP and CNP establish cytosolic channels in CNS myelin. *Cell Rep* **18**:314–323.
46. Snyder F (1999) The ether lipid trail: a historical perspective. *Biochim Biophys Acta* **1436**:265–278.
47. Spiliotis ET, Nelson WJ (2006) Here come the septins: novel polymers that coordinate intracellular functions and organization. *J Cell Sci* **119**(Pt 1):4–10.
48. Taveggia C, Thaker P, Petrylak A, Caporaso GL, Toews A, Falls DL *et al* (2008) Type III neuregulin-1 promotes oligodendrocyte myelination. *Glia* **56**:284–293.
49. Trapp BD, Andrews SB, Cootauco C, Quarles R (1989) The myelin-associated glycoprotein is enriched in multivesicular bodies and periaxonal membranes of actively myelinating oligodendrocytes. *J Cell Biol* **109**:2417–2426.
50. Trapp BD, Nishiyama A, Cheng D, Macklin W (1997) Differentiation and death of premyelinating oligodendrocytes in developing rodent brain. *J Cell Biol* **137**:459–468.
51. Trapp BD, Peterson J, Ransohoff RM, Rudick R, Mork S, Bo L (1998) Axonal transection in the lesions of multiple sclerosis. *N Engl J Med* **338**:278–285.
52. Van Veldhoven PP, Bell RM (1988) Effect of harvesting methods, growth conditions and growth phase on diacylglycerol levels in cultured human adherent cells. *Biochim Biophys Acta* **959**:185–196.
53. Van Veldhoven PP, Mannaerts GP (1987) Inorganic and organic phosphate measurements in the nanomolar range. *Anal Biochem* **161**:45–48.
54. Vanderver A, Prust M, Tonduti D, Mochel F, Hussey HM, Helman G *et al* (2015) Case definition and classification of leukodystrophies and leukoencephalopathies. *Mol Genet Metab* **114**:494–500.
55. Wanders RJ, Waterham HR (2006) Biochemistry of mammalian peroxisomes revisited. *Annu Rev Biochem* **75**:295–332.
56. Watkins TA, Emery B, Mulinyawe S, Barres BA (2008) Distinct stages of myelination regulated by gamma-secretase and astrocytes in a rapidly myelinating CNS coculture system. *Neuron* **60**:555–569.
57. Weil MT, Mobius W, Winkler A, Ruhwedel T, Wrzos C, Romanelli E *et al* (2016) Loss of myelin basic protein function triggers myelin breakdown in models of demyelinating diseases. *Cell Rep* **16**:314–322.
58. Werner HB, Kuhlmann K, Shen S, Uecker M, Schardt A, Dimova K *et al* (2007) Proteolipid protein is required for transport of sirtuin 2 into CNS myelin. *J Neurosci* **27**:7717–7730.
59. White AL, Modaff P, Holland-Morris F, Pauli RM (2003) Natural history of rhizomelic chondrodysplasia punctata. *Am J Med Genet A* **118A**:332–342.
60. Zuchero JB, Fu MM, Sloan SA, Ibrahim A, Olson A, Zaremba A *et al* (2015) CNS myelin wrapping is driven by actin disassembly. *Dev Cell* **34**:152–167.

SUPPORTING INFORMATION

Additional supporting information may be found in the online version of this article at the publisher's web site.